Analysis of the Buckling States of an Infinite Plate Conducting Current

Katarina Terzić Conrad

Dissertation submitted to the faculty of the Virginia Polytechnic Institute and State University in partial fulfillment of the requirements for the degree of

Doctor of Philosophy
In
Mathematics

Robert C. Rogers
Peter Haskell
Martin V. Day
Shu Ming Sun

September 9th, 2011
Blacksburg, VA

Keywords: self-forces, bifurcation, buckling, nonlinear continuum mechanics

Analysis of the Buckling States of an Infinite Plate Conducting Current

Katarina Terzić Conrad

Abstract

In this thesis we analyze the buckling behavior of an infinitely long, thin, uniform, inextensible, elastic plate that has a steady current flowing along its length. We are concerned with the derivation of the nonlinear equations of motion using nonlinear continuum mechanics, and subsequent analysis of the buckling behavior of the plate under electromagnetic self-forces. In particular, we concentrate on how the body-forces that result from the applied current determine the buckled configurations. We derive both analytical and numerical results, and in the process develop a novel boundary value problem solver for integro-differential equations in addition to a predictor-corrector algorithm to continue solutions with respect to the control parameters. We take a relatively complex problem in magneto-solid mechanics and elasticity theory and form a realistic model that sheds light on the bifurcation and buckling behavior resulting from the electromagnetic-field- induced self-forces that are derived in their full, exact form using Biot-Savart Law.

Dedication

This dissertation would not have been written if it were not for the unconditional love, support, encouragement, and sacrifice of my family. Most of all I dedicate this dissertation to my husband Emery, whose extreme patience, tolerance, encouragement, help, and advice has enabled me devote myself to this research. For lending me a hand and lifting me up when I felt discouraged, for his advice, suggestions and help in writing this dissertation, I will always be indebted to him.

Also, I want to dedicate this research to my sons, Sasha and Milosh, who kindly tolerated my absence from many play-times, outings and birthday parties, so that I could work. Also, to my parents Petar and Slavka for their love, guidance and the sacrifice they have shown me over the years, especially in the last six months when they took care of my boys, so that I could complete this research.

And last but not least, I dedicate this dissertation to my brother Balša, who has been there for me to look up to since we started school together. His love for science was so infectious that has naturally rubbed on me. His belief in me and my abilities to achieve anything I put my mind and heart into has been the wind beneath my wings.

This research has been fun and rewarding, and I am pleased with the results obtained. I believe that this research opens up other related avenues to expanding the results to include more generality and hope that this can provide impetus for other research by future doctoral students.

Thanks!

Katarina Terzić Conrad

Acknowledgements

My professor and advisor, Dr. Robert Rogers, was the very first math professor I met at Virginia Tech, many years ago when I was still a young and inexperienced student. During that very first encounter, he assured me that I had arrived to a right school. Over the years, our relationship progressed from professor-student to advisor-advisee. He was the advisor for my Master's thesis, and now for my doctoral dissertation as well. His advice and helpful direction throughout my graduate journey has been crucial to my success. And although the road had many obstacles (many moves out of state, birth of two children), Dr. Rogers has shown his patience and understanding throughout. For that I am very grateful.

I would also like to thank Dr. Peter Haskell, a math professor whom I met shortly after returning from the break I took after giving birth to my first child Sasha. That was a challenging time for me and my family, and Dr. Haskell helped me to regain the confidence to successfully continue my graduate journey. He has taught me many valuable lessons both in- and outside the classroom and has been more than a mentor to me. For this I will always be indebted to him.

To the rest of my committee, Dr. Martin Day and Dr. Shu Ming Sun, thank you for donating your valuable time to reviewing and judging my dissertation.

Contents

List of Figures

List of Algorithms

Chapter 1

Introduction

In the past half century, problems involving the motion and deformation of solid structures in high magnetic fields and currents have become important due to the development of superconducting magnets, lasers, magnetically levitated trains, fusion reactors, high-energy particle accelerators, electromagnetic rail guns, aerospace vehicles, etc [10]. However, these problems are not easy to study, and very few analytic solutions for nonlinear coupled problems are found in today's literature. This is due to the fact that geometries that lead to simple solutions in mechanics do not often lead to simple electromagnetic problems and vice versa. Thus the first papers that investigated problems for elastic current-carrying structures such as rods and plates subjected to magnetic fields were linear, concerned only with small deformations, and focused mostly on finding total force and moment, as well as the internal stresses. The linear analysis is not complete because the equations of motion are considered in the undeformed geometry where small deformations do not significantly affect the magnitude or the direction of the magnetic field (i.e., the magnetic field and body-forces are independent of the induced deformation). More interesting problems arise from studying large deformations that require the full nonlinear system which leads to complex integro-differential equations. These equations are hard to solve due to the non-local nature of the electromagnetic self-forces because the deformation itself leads to a change in the magnetic forces, introducing a feedback loop between the structure and the source of the magnetic field. These nonlinear problems are more realistic and are important in predicting the load-deflection behavior of structures under both magnetic and mechanical forces. [10]

In this paper we study buckling of an eletrically conducting plate under electromagnetic self-forces. Leontovich and Shafranov [9] were the first researchers to show theoretically that an elastic rod carrying current is inherently unstable, and thus prone to buckling. Dolbin and Morozov [3] extended this research by introducing the idea of a critical current at which the current-carrying

rod buckles—analogous to the buckling of a column under critical axial load first described by Euler—and studying its instability. They concluded that a periodically supported rod could buckle under high-enough static current when no tension forces or other constraints were placed on the rod. Chattepadhyay and Moon [2] reexamined this problem and obtained experimental evidence for this instability.

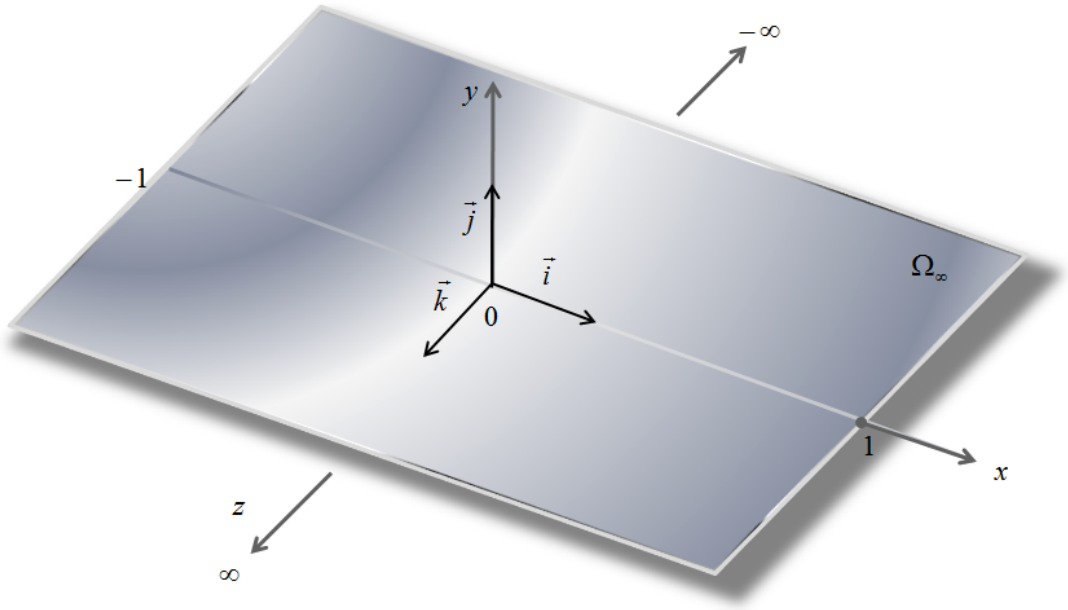

Figure 1.1: Here we see a thin, uniform, inextensible, elastic, infinite plate extending in the z direction with a steady current flowing along its length, represented in its reference configuration by Ω_∞. The physical beam, B, is depicted along with its axis in the center.

Moon generalized this to two dimensions in an experiment in which he ran several kiloampers of uniform current through a sheet of aluminum foil. This current induces a magnetic field that produces compressive stresses that lead to buckling of the sheet. Thus he concluded that for large enough currents the plate will collapse under in-plane compressive stresses analogous to the Euler-buckling of a column. Such buckling failures in thin plates have been observed in lightning-strike damage to structures such as aircraft wings. In his investigation, Moon was primarily interested in finding the so-called self-field and self-stress of the current on the conductor. He carries out integration of the electromagnetic body-forces for the case of constant current distribution across a strip and shows the resulting stresses. He then calculates the self-force based on the fact that, for any structural beam, there is a critical load at which the beam will buckle [13]. He makes the

assumption that the net force and moments of these self-fields are zero, meaning that there is no bending in the plate due to the planar equilibrium stress system. Moon's initial stress problem without bending is therefore a precursor to the stability problem of large deformations.

To date, there has only been one investigation regarding the behavior of a thin plate subjected to an applied current that couples the geometric and electromagnetic nonlinearities. Hasanyan *et. al.* [6] start out with a general problem by considering a current-carrying ferromagnetic plate exposed to a magnetic field of arbitrary orientation. Their approach follows the engineering literature in which approximations are made on the forces (terms of order δ^3 and above are neglected, where δ is the thickness of the plate). Their primary goal is to study the current-induced buckling instabilities and the current's role in post-buckling behavior. In particular, although they include non-linearities in the governing equations, they focus their study on the near-equllibrium behavior that leads to instability that can cause buckling (and the after effects). They are not concerned with the exact geometry of the deformed, non-trivial solutions, nor does their analysis include the exact expression of the force terms.

In this thesis we extend Moon's work by considering an infinitely long, thin, uniform, inextensible, elastic plate that has a steady current flowing along its length. We are concerned with the derivation of the nonlinear equations of motion, and subsequent analysis of the buckling behavior of the plate. Unlike Hasanyan *et. al.*, we will focus on the exact geometry of the deformed, non-trivial solutions. We will see that the derivation of the mechanical equations is straightforward but that the determination of the electromagnetic field and non-local body-forces is more involved, and leads to a complex set of integro-differential equations that we explore both numerically and analytically. Following Antman, we use nonlinear continuum vector mechanics and the axiomatic method to cast the set of governing equations in a classical form. Our theory naturally includes large deformations by formulating the exact equations of motion in the deformed configuration in their full nonlinear form. We calculate exact magnetic body-forces as described by the Biot-Sawart Law, and use them to complete our classical equations of motion. To achieve this goal, we will need to develop a set of numerical algorithms specifically tailored to the derived set of equations. We extract the full geometric implications of the buckling problem by focusing on an exact expression of the non-local self-forces and the feedback loop between the induced electromagnetic field and the deformation of the plate.

Overview of Chapters

In Chapter 2, we derive mechanical nonlinear equations governing the motion of the plate that are constrained to depend on only one spatial dimension. This derivation is divided into a description of the geometry of deformation relating displacements to strains, a generalization of Newton's

Second Law to continua relating the contact and body-forces to stresses and constitutive equations relating stresses to strains. In order to complete the set up of our boundary value problem, we supplement the above domain equations with the boundary conditions. Once we make our boundary value problem well-posed we further derive the body forces resulting from the electromagnetic field induced by the current.

The nonlinear system of partial differential equations we encounter in Chapter 2 is complex, and we therefore first address a simplified case in Chapter 3 in which we consider an applied mechanical compressive load at the ends of the beam instead of an applied current. After some calculation our system reduces to a two-point boundary value problem of the Duffing equation. We first find the general solutions of our Duffing equation in terms of the level sets of an energy function which are closed periodic orbits. Then we look for the non-trivial solutions that satisfy our boundary values. This allows us to investigate a mild static version of the equations in order to build intuition about how to attack the more complicated system.

In Chapter 4, we extend the results of Chapter 3 to the full system of equations. Here we consider the full non-linear system with an applied current and with no applied compressive load or other mechanical constraints. This more complicated integro-differential system can also be viewed as a forced Duffing equation, where the "forcing" term is expressed as a non-local integral operator on the solution function. In particular, in Chapter 4 we concentrate on how the body-forces that result from the applied current determine the buckled configurations.

The exact geometrical shapes of the beam are found using the numerical methods that we develop in Chapter 5. These numerical algorithms were designed to solve the boundary value problem with and without an applied current and to continue these solutions while varying parameters (either the magnitude of the contact force at the boundary or the magnitude of the applied current). The core algorithm is a boundary-value problem solver that takes the form of a shooting method that repeatedly solves initial value problems to hone in on the correct initial values that reproduce the boundary conditions. Layered on top of this is a predictor-corrector continuation method that allows us to extend our knowledge of solutions through parameter space.

In Chapter 6, we conclude by summarizing results and indicating improvements and potential future work.

Chapter 2

Governing Equations

In this chapter we derive a system of nonlinear differential equations describing the motion of a thin, inextensible, infinite plate conducting a current along its length. The basic strategy is to derive equations that are constrained to depend on only one spatial variable by using nonlinear continuum vector mechanics and the axiomatic method as described in [11]. Our theory naturally includes large deformations by formulating the exact equations of motion in the deformed configuration in their full nonlinear classical form. This is accomplished by making a number of reasonable assumptions about the known symmetries and behavior of the plate, ultimately reducing a three dimensional mathematical model, which is too hard to solve on today's computers, into a planar one that describes the deformation of a transverse segment of the plate. The deformation of this "beam" is sufficient to describe the behavior of the entire plate.

We start by describing the geometry of the plate in the reference configuration, and then move on to a description of the deformed configuration along with the associated physical quantities. Next, we describe the forces and couples acting on the plate governed by Newton's laws of conservation of linear and angular momentum. We use a generalization of Newton's second law to continua to derive balance laws that form the basis of the equations of motion. We describe properties of the material by means of constitutive equations which relate force to deformation. These complete the governing equations.

2.1 Geometry of Deformation

The primary focus of this section is to describe the geometry of the plate in two different configurations. We begin with a description of the plate and its characteristics in a known, reference configuration, that is, the initial unstressed and unstrained state of the plate. And then move on to describing the deformed configuration. It is important to notice, since we are not interested in the sequence of configurations between undeformed and deformed configurations, we don't consider time when analyzing deformation.

2.1.1 Undeformed Configuration of the Plate

We begin with the description of a reference configuration, which all subsequent configurations are referenced from. We name this configuration *undeformed* configuration, describing the natural state of the plate before any forces are applied. We imagine the plate to be a thin, uniform, elastic nonferromagnetic sheet of finite width and infinite extent. For our purposes we assume that the plate is a continuous body located in three-dimensional space. More precisely, let $\{\boldsymbol{i},\boldsymbol{j},\boldsymbol{k}\}$ be a fixed right-hand orthonormal basis for $\mathbb{R}^3$. And let the **reference configuration**, Ω_∞ be defined as

$$\Omega_\infty := \{(x,y,z) \in \mathbb{R}^3 \;\big|\; x \in [-1,1], y \in [-\delta,\delta], z \in [-\infty,\infty]\}$$

for some $\delta > 0$. We identify a *material point*, P, within the plate by its coordinates $\{x,y,z\}$ relative to the origin of the coordinate system. We identify a *position vector*,

$$\boldsymbol{x} = (x,y,z) = x\boldsymbol{i} + y\boldsymbol{j} + z\boldsymbol{k},$$

as a vector pointing from the origin to the point P.

We assume that the plate extends infinitely along the z-axis and is symmetric with respect to $(\boldsymbol{i},\boldsymbol{j})$-plane. This assumption ensures that we do not have to worry about boundary conditions at the ends. Our study can thus be limited to deformations that preserve symmetry about the $(\boldsymbol{i},\boldsymbol{j})$-plane. Consequently, the deformation of the entire plate is characteristic of the deformation of any transverse segment.

Accordingly, we define such a segment as a **beam** and, since each segment will behave the same, we focus our attention on the beam of length two units laying along the $x-axis$ from -1 to 1, denoted by

$$B := \{(x,y,z) \in \mathbb{R}^3 \;\big|\; x \in [-1,1], y \in [-\delta,\delta], z \in [-\delta,\delta]\}$$

where δ is a very small positive number. We define the **cross-section** of the beam at $x \in [-1,1]$ by

$$A(x) := \{(x,y,z) \in \mathbb{R}^3 \;\big|\; y \in [-\delta,\delta], z \in [-\delta,\delta]\}.$$

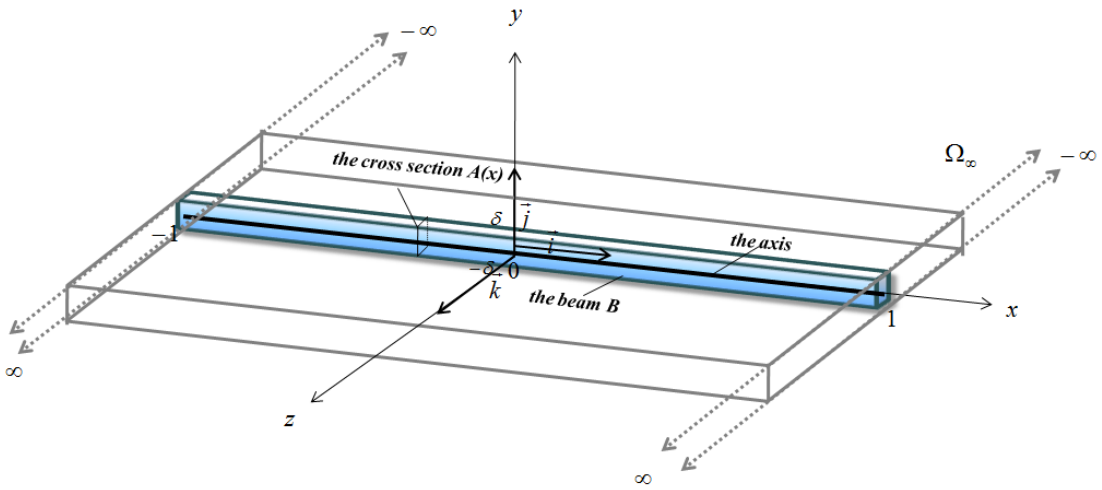

Figure 2.1: Here we see an infinite plate extending in the z direction, represented in its reference configuration by Ω_∞. The physical beam, B, is depicted along with its axis in the center.

Further, we define the **axis** of the beam to be its centerline, given by the set of material points, (or centroids), $(x, 0, 0)$, $x \in [-1, 1]$ (see Figure 2.1). Note: a straight cross-section would typically deform into a plane curve, however, the exact description of deformation with curved cross-sections would require partial differential equations with two independent spatial variables (see Antman [1]). Now, the assumption about the thinness of the plate helps us formulate a coherent mathematical model of the planar deformation of the plate, a model that is governed by ordinary differential equations that depend only on one spatial variable. We realize that this assumption is somewhat restrictive, however it enables us to reduce the dimensionality of the model. And since the plate is thin enough we realize that if we know what the axis deforms into we know the gross shape of the plate. And to know the shape of the curved cross-sections one needs to introduce a unit vector that will characterize some average orientation of the deformed cross-section. However, we need not worry about curved cross-section anyway since we assume that the plate is thin and consequently we further assume that the cross-sections move rigidly, meaning that the cross-sections remain straight and unchanged during the deformation, depending only on transverse variables. Thus, to describe the motion of the beam it is sufficient to describe the motion of the axis and the orientation of the cross-sections $A(x)$. In the next section we use more precise mathematical language to describe this motion.

Remark: Later in Section 2.3.3, we shell go as far as to assume that during the deformation, the cross-sections are not only rigid, but they remain orthogonal to the axis during the deformation. This assumption is commonly known in structural mechanics as Kirchhoff assumption (see [5]).

2.1.2 Deformed (Planar) Configuration of the Beam

Now that we have characterized the geometry of the beam in its reference configuration, we are ready to construct a simple model that describes the motion of our plate. This motion is characterized by describing the current position of each material point in the beam relative to the position that point occupied in the reference configuration. Since the motion naturally includes deformation, we call this mathematical description of the motion a **deformation map**, $\boldsymbol{p}(\boldsymbol{x}, t)$ (see [4]). More precisely, the three-dimensional motion of the beam, $\boldsymbol{p}(\boldsymbol{x}, t)$, can be fully described by the motion of the axis represented by $\boldsymbol{r}(x, t)$ and the relative deformation of the cross-sections spanned by $\boldsymbol{d}_2(x, t)$ and $\boldsymbol{d}_3$, i.e.,

$$\boldsymbol{p}(x, y, z, t) := \boldsymbol{r}(x, t) + y\boldsymbol{d}_2(x, t) + z\boldsymbol{d}_3, \tag{2.1}$$

where $\boldsymbol{r}(x, t)$, and $\boldsymbol{d}_2(x, t)$, are vector-valued functions

$$[-1, 1] \times [0, \infty) \ni (x, t) \longmapsto \boldsymbol{r}(x, t), \boldsymbol{d}_2(x, t) \in \mathbb{R}^3.$$

We define the vector $\boldsymbol{d}_1 := \boldsymbol{d}_2 \times \boldsymbol{d}_3$ so that $\{\boldsymbol{d}_1, \boldsymbol{d}_2, \boldsymbol{d}_3\}$ form an orthonormal basis for $\mathbb{R}^3$. These vectors are called *directors.* In particular, $\boldsymbol{d}_2$ is a unit vector that indicates the orientation of the cross-section in the deformed configuration. $\boldsymbol{d}_3$ is the unit vector in the $\boldsymbol{k}$ direction and does not depend on x since we assumed symmetry of the plate about the ($\boldsymbol{i}$,$\boldsymbol{j}$)-plane. Therfore, $\boldsymbol{d}_1$ and $\boldsymbol{d}_2$ are confined to the ($\boldsymbol{i}$,$\boldsymbol{j}$)-plane and along with $\boldsymbol{d}_3$ are defined as

$$\begin{aligned} \boldsymbol{d}_1(x, t) &:= \cos\theta(x, t)\boldsymbol{i} + \sin\theta(x, t)\boldsymbol{j}, \\ \boldsymbol{d}_2(x, t) &:= -\sin\theta(x, t)\boldsymbol{i} + \cos\theta(x, t)\boldsymbol{j}, \\ \boldsymbol{d}_3 &:= \boldsymbol{k}, \end{aligned}$$

where θ is the angle from the x-axis to $\boldsymbol{d}_1$. Note that we could therefore alternatively define the configuration of the beam by $\boldsymbol{r}$ and θ. We also assume that the function $\boldsymbol{r}$ is smooth and that, as a result of our assumption about the symmetry, its motion is confined to the ($\boldsymbol{i}$,$\boldsymbol{j}$)-plane:

$$\boldsymbol{r} \cdot \boldsymbol{k} \equiv 0 \tag{2.2}$$

$$\boldsymbol{r}_x \cdot \boldsymbol{k} \equiv 0. \tag{2.3}$$

Some of the most important results from the analysis of deformation are the *strain* characteristic and they shall prove useful for the development of the constitutive equations for the material.

2.1.3 The Strains: Stretch, Shear, and Bending

Loosly speaking, strain is a description of deformation in terms of relative displacement of material points in the beam. In structural mechanics, there are three basic types of deformation a beam can

undergo. And, although we shall describe and characterize each one of them in great detail, for the purposes of deriving the equations of motion of the inextensible and unshearable beam that this thesis deals with, we mostly focus on the last one. Before we move on to the definitions for these characteristics, we need to define a vector that will help us measure and describe deformation in terms of relative displacement of particles within the beam. Let $\boldsymbol{r}_x$ be a vector tangent to the deformed axis. We choose to express $\boldsymbol{r}_x$ in terms of the basis $\{\boldsymbol{d}_1, \boldsymbol{d}_2\}$ since it is a natural choice for the intrinsic description of deformation, i.e.

$$\boldsymbol{r}_x \quad = \quad \nu(x,t)\boldsymbol{d}_1(x,t) + \eta(x,t)\boldsymbol{d}_2(x,t), \tag{2.4}$$

where the functions ν, η and

$$\mu := \theta_x \tag{2.5}$$

are the *strain* variables corresponding to the configuration (2.1). And although the concepts of stretch, shear and bending are related to these variables, we shall not confuse the pairs as strictly equivalent.

First, notice that in the length of the tangent vector $\boldsymbol{r}_x$ in the reference configuration is unity, since the axis in the reference configuration is unstreched and unsheared, i.e.

$$\boldsymbol{r}_x(x,t) = \boldsymbol{d}_1(x,t) = \cos\theta\boldsymbol{i} + \sin\theta\boldsymbol{j} = \boldsymbol{i}, \nu(x,t) = 1, \eta(x,t) = 0.$$

Then the **stretch** of the axis of the beam is defined as the local ratio of deformed to reference length, or simply the length of the tangent vector $\boldsymbol{r}_x$ in the deformed configuration, i.e.

$$|\boldsymbol{r}_x(x,t)| \quad = \quad \sqrt{\nu(x,t)^2 + \eta(x,t)^2} \tag{2.6}$$

The strain ν represents the local ratio of deformed to reference area of the parallelogram whose sides are the vectors $\boldsymbol{r}_x$ and $\boldsymbol{d}_2$. Only in the case of pure elongation of the axis does the stretch $|\boldsymbol{r}_x|$ reduce to ν, (see [1]). We shall later observe in Section 2.3.3 this exact result as a consequence of assuming that the beam does not shear, i.e. $\eta = 0$.

The **shearing** of the beam is measured with the *shearing angle* β and represents the angle of the cross-section $A(x)$ from its nominal position perpendicular to $\boldsymbol{r}_x$ in the reference configuration, or simply put the reduction in the right angle. The angle β can be derived from the projection of $\boldsymbol{d}_2$ onto the unit vector $\boldsymbol{r}_x/|\boldsymbol{r}_x|$, i.e.

$$\boldsymbol{d}_2 \cdot \frac{\boldsymbol{r}_x}{|\boldsymbol{r}_x|} = \frac{\eta}{\sqrt{\nu^2 + \eta^2}} =: \sin(\beta) \tag{2.7}$$

See Figure 2.2.

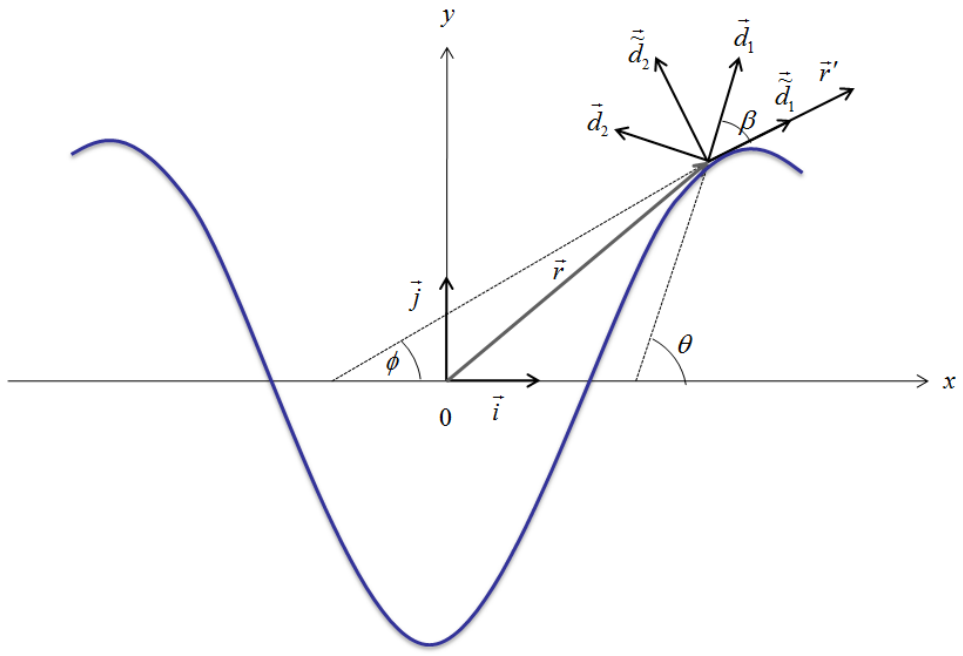

Figure 2.2: Deformed planar configuration of beam axis along with the relevant defining vectors.

As in [1], we impose the following constraint,

$$\boldsymbol{r}_x(x,t)\cdot\boldsymbol{d}_1(x,t) = \nu(x,t) > 0, \tag{2.8}$$

or equivalently, $|\beta| < \frac{\pi}{2}$, which ensures that the deformation of the axis is never so compressed that the stretch, $|\boldsymbol{r}_x|$, is ever reduced to zero, and that the cross-section $A(x)$ never shears so much that it becomes tangent to the axis in the deformed configuration.

Before we move to a description of the last strain variable, let us define ϕ as the angle that the tangent vector $\boldsymbol{r}_x$ makes with the $x-axis$, since in general this need not be the same as θ. Thus,

$$\phi := \theta + \beta.$$

We then define the *curvature* of the axis as the ratio of its derivative, ϕ_x and the stretch, $|\boldsymbol{r}_x|$, i.e.

$$\frac{\phi_x}{|\boldsymbol{r}_x|}.$$

(See [1]). In general, as we can observe from its definition, changes in curvature are associated with streching whereas the effect of bending is associated with the **bending** strain μ which we

earlier defined as θ_x. Only in the case of an inextensible and unshearable beam, where $|\boldsymbol{r}_x| = 1$, $\beta = 0$ and $\phi = \theta$, does the curvature becomes the same as μ.

2.1.4 Formulation of Density and Momentum

As we have seen, a purely geometric argument led us to the definitions of strain, whereas the concept of balance of momentum, which we are now ready to introduce will lead us to the definition of stress, and hence the concept of force. But before we dive into a description of Newton's laws of conservation of linear and angular momentum, we first introduce and define the physical quantities associated with these laws, such as the density, linear and angular momentum. Recall that the goal is to have these quantities depend on only one spatial dimension, x, by taking into consideration some of the previously disscused constraints.

Density

We assume that there is a positive, Riemann integrable **mass density** function $\rho : B \to (0, \infty)$ that describes the mass of the beam per unit reference volume at $\boldsymbol{x} = (x, y, z)$. Assume that the *center of mass* of each cross-section, $A(x)$, is the point $(x, 0, 0)$ where the axis intersects the cross-section. This implies that

$$\begin{aligned} &\frac{1}{M_{A(x)}} \int_{A(x)} \rho(x, y, z)(y\boldsymbol{d}_2 + z\boldsymbol{d}_3)\, dA =< 0, 0 > \\ &\Rightarrow \int_{A(x)} y\rho(x, y, z)\, dy\, dz = \int_{A(x)} z\rho(x, y, z)\, dy\, dz = 0 \end{aligned} \tag{2.9}$$

as described in [11]. Traditionally, these integrants are denoted as ρI and represent the first mass moment of inertia per unit reference length of cross-section, $A(x)$, about the y- and z-axis respectively in the reference configuration. They measure the beam's resistance to changes to its rotation. See [1].

Remark: Since we assumed that the plate is uniform, it follows that the beam is uniform and that the mass density is uniform and therefore constant. This implies that the *center of mass* of the beam is along the axis. However, we will still treat $\rho(x, y, z)$ as a function in our derivations and only equate it with a constant when it becomes relevant to our problem.

Linear Momentum

Now recall from mechanics that the linear momentum of a mass point is its mass times velocity and is therefore linear in the velocity. Accordingly, we could think of the linear momentum of the material of $[a, b] \subset (-1, 1)$ at time t as an integral of a linear combination of the 'velocities' $\boldsymbol{r}_t$ and $\boldsymbol{d}_{2,t}$. Note that $\boldsymbol{d}_{3,t} = 0$ since $\boldsymbol{d}_3$ does not depend on t.

Formally, the **linear momentum** of a segment of beam

$$S_{[a,b]} := \bigcup_{x \in [a,b]} A(x), \quad [a, b] \subset (-1, 1)$$

at time t is given by the integral:

$$\int_{S_{[a,b]}} \rho(x, y, z) \boldsymbol{p}_t(x, y, z, t)\, dx\, dy\, dz.$$

Using (2.9), we further simplify to get (dropping explicit dependence on (x, y, z), (x, y, z, t) and (x, t) where appropriate to simplify the notation)

$$\begin{aligned}
\int_{S_{[a,b]}} \rho\, \boldsymbol{p}_t\, dx\, dy\, dz &= \int_{S_{[a,b]}} \rho\, (\boldsymbol{r}_t + y\boldsymbol{d}_{2,t})\, dx\, dy\, dz \\
&= \int_{S_{[a,b]}} (\rho \boldsymbol{r}_t + \rho y \boldsymbol{d}_{2,t})\, dx\, dy\, dz \\
&= \int_a^b \boldsymbol{r}_t \left(\int_{A(x)} \rho\, dy\, dz \right) dx + \int_a^b \boldsymbol{d}_{2,t} \left(\int_{A(x)} y\rho\, dy\, dz \right) dx \\
&= \int_a^b \rho A \boldsymbol{r}_t\, dx \qquad (2.10)
\end{aligned}$$

where

$$\rho A(x) = \int_{A(x)} \rho(x, y, z)\, dy\, dz,$$

is defined as *the mass density per unit reference length* at x, and it is equivalent to the integral of the density per unit reference volume, $\rho(\boldsymbol{x})$, over the cross-section $A(x)$ as adopted from Antman [1]. We take ρA to be everywhere positive on (a, b).

Angular Momentum

Likewise, we recall that the angular momentum of a mass point about the origin is the cross product of its position with its linear momentum. Accordingly, we could think of the angular momentum of

the material of $[a, b]$ at time t as an integral of a linear combination of cross products of 'positions' $\boldsymbol{r}$, $\boldsymbol{d}_2$ and $\boldsymbol{d}_3$ with the 'velocities' $\boldsymbol{r}_t$ and $\boldsymbol{d}_{2,t}$.

Formally, the **angular momentum** of the segment of beam $S_{[a,b]}$ at time t is given by

$$\int_{S_{[a,b]}} \rho(x, y, z)\boldsymbol{p}(x, y, z, t) \times \boldsymbol{p}_t(x, y, z, t)\, dx\, dy\, dz.$$

Again, using (2.9) and the identity $\boldsymbol{d}_2 \times \boldsymbol{d}_{2,t} \equiv \theta_t \boldsymbol{d}_3$, we can further simplify to get

$$\begin{aligned}
\int_{S_{[a,b]}} \rho \boldsymbol{p} \times \boldsymbol{p}_t\, dx\, dy\, dz &= \int_{S_{[a,b]}} \rho(\boldsymbol{r} + y\boldsymbol{d}_2 + z\boldsymbol{d}_3) \times (\boldsymbol{r}_t + y\boldsymbol{d}_{2,t})\, dx\, dy\, dz \\
&= \int_a^b \boldsymbol{r} \times \boldsymbol{r}_t \left(\int_{A(x)} \rho\, dy\, dz \right) dx \\
&\quad + \int_a^b \boldsymbol{r} \times \boldsymbol{d}_{2,t} \left(\int_{A(x)} y\rho\, dy\, dz \right) dx \\
&\quad + \int_a^b \boldsymbol{d}_2 \times \boldsymbol{r}_t \left(\int_{A(x)} y\rho\, dy\, dz \right) dx \\
&\quad + \int_a^b \boldsymbol{d}_2 \times \boldsymbol{d}_{2,t} \left(\int_{A(x)} y^2\rho\, dy\, dz \right) dx \\
&\quad + \int_a^b \boldsymbol{d}_3 \times \boldsymbol{r}_t \left(\int_{A(x)} z\rho\, dy\, dz \right) dx \\
&\quad + \int_a^b \boldsymbol{d}_3 \times \boldsymbol{d}_{2,t} \left(\int_{A(x)} yz\rho\, dy\, dz \right) dx.
\end{aligned}$$

Consistent with our assumption that the motion of the axis is confined to the $(\boldsymbol{i},\boldsymbol{j})$-plane we require that all components of the angular momentum act perpendicular to $(\boldsymbol{i},\boldsymbol{j})$-plane so that

$$\int_{A(x)} yz\rho(x, y, z)\, dy\, dz = 0. \tag{2.11}$$

See [11]. Although not a great assumption in some beams it is traditional in the type of the equation we are about to derive and it simplifies our discussion quite a bit later.

After substituting (2.11) into the above calculations, the angular momentum about the origin

reduces to

$$\begin{aligned}\int_{S_{[a,b]}} \rho\, \boldsymbol{p} \times \boldsymbol{p}_t \, dx\, dy\, dz &= \int_a^b \boldsymbol{r} \times \boldsymbol{r}_t \left(\int_{A(x)} \rho \, dy\, dz \right) dx \\ &\quad + \int_a^b \boldsymbol{d}_2 \times \boldsymbol{d}_{2,t} \left(\int_{A(x)} y^2 \rho \, dy\, dz \right) dx \\ &= \int_a^b \left[\rho A \boldsymbol{r} \times \boldsymbol{r}_t + \rho J \theta_t \boldsymbol{d}_3 \right] \, dx, \end{aligned} \tag{2.12}$$

where

$$\rho J(x) = \int_{A(x)} y^2 \rho(x, y, z) \, dy\, dz$$

is defined as *the second mass moment of inertia per unit reference length* of $A(x)$ about the y-axis in the reference configuration, and it predicts the resistance of cross-sections to bending and deflection. We take $\rho J(x)$ to be everywhere positive on (a, b). Note that when the plate is very thin $\rho J(x)$ is approximatly zero. We will now put these formulas to good use in the balance laws.

Note: The integration over the cross-section eliminates the dependance on y and z coordinates and leaves the linear and angular momentum as functions of only the axial coordinate x.

2.2 Mechanics

2.2.1 Forces Acting on the System

Before we dive into the derivation of balance laws we take some time to describe all the forces and torques that arise in the mechanics of the beam which is assumed to be a continuous body. Newton's laws of conservation of linear and angular momentum basically governs the transmition of force in the plate. But, unlike Newton, we are interested in continuous body and not system of particles. Therefore, we must find an apropriate way to model force transmission throughout the plate. Here is where Cauchy notion of *stress* becomes essential to the mechanics of our continuous body. It measures the state of force transmission in the interior of the body. We assume that there are basically two types of forces that we deal with in our contiuous model: *body-force* (force per unit volume) and *surface forces* (force per unit area.) As defined in [7].

Body-Force and Couple

In our case, the body-force is a force caused by an electromagnetic field, and does not require contact to be transmitted, it rather acts at a distance. This force is by nature non-local and therefore complicates our differential equation quite a bit by adding an integral term. The interesting thing about this body-force is that it is a self-force, meaning that it arises as a result of an internally generated magnetic field produced by the current. Its intensity depends on the strength of the applied current. And as the current, and therefore the strength of the electromagnetic field, increases, the beam may deform. This deformation, in turn, causes changes in the body-force, forming a feedback loop.

Suppose that $\bar{\boldsymbol{f}}(\boldsymbol{x}, t)$ is the *body-force per unit reference volume*. And since the beam is a continuous body, $\bar{\boldsymbol{f}}$ is distributed continuously throughout the volume of the beam and thus expressed as a piecewise function of space and time. Then the *body-force* on the segment $S_{[a,b]}$ of the beam is

$$\int_a^b \boldsymbol{f}(x, t)\, dx \tag{2.13}$$

where

$$\boldsymbol{f}(x, t) = \int_{A(x)} \bar{\boldsymbol{f}}(\boldsymbol{x}, t)\, dy\, dz \tag{2.14}$$

is the *body-force per unit reference length*, which we assume that takes values in $span\{\boldsymbol{i}, \boldsymbol{j}\}$. In our case, $\boldsymbol{f}(x, t)$ is prescribed as the result of the current applied transverse to the beam. This will be explored in section (2.5.4). In general, however, we might derive many different versions of such a force depending on the specific context of a problem.

The sum of all *couples* of the body-force are given by

$$\begin{aligned}
\int_{S_{[a,b]}} \boldsymbol{p} \times \bar{\boldsymbol{f}}\, dy\, dz\, dx &= \int_a^b \int_{A(x)} (\boldsymbol{r}(x,t) + y\boldsymbol{d}_2(x,t) + z\boldsymbol{d}_3) \times \bar{\boldsymbol{f}}(\boldsymbol{x},t)\, dy\, dz\, dx \\
&= \int_a^b \int_{A(x)} \left(\boldsymbol{r} \times \bar{\boldsymbol{f}} + y\boldsymbol{d}_2 \times \bar{\boldsymbol{f}} + z\boldsymbol{d}_3 \times \bar{\boldsymbol{f}}\right)\, dy\, dz\, dx \\
&= \int_a^b \left(\int_{A(x)} \boldsymbol{r} \times \bar{\boldsymbol{f}}\, dy\, dz + \int_{A(x)} \left(y\boldsymbol{d}_2 \times \bar{\boldsymbol{f}} + z\boldsymbol{d}_3 \times \bar{\boldsymbol{f}}\right)\, dy\, dz\right)\, dx \\
&= \int_a^b \left(\boldsymbol{r} \times \int_{A(x)} \bar{\boldsymbol{f}}\, dy\, dz + \int_{A(x)} \left(y\boldsymbol{d}_2 \times \bar{\boldsymbol{f}} + z\boldsymbol{d}_3 \times \bar{\boldsymbol{f}}\right)\, dy\, dz\right)\, dx \\
&= \int_a^b \left(\boldsymbol{r} \times \boldsymbol{f} + \int_{A(x)} \left(y\boldsymbol{d}_2 \times \bar{\boldsymbol{f}}\right)\, dy\, dz\right)\, dx \\
&= \int_a^b \boldsymbol{r} \times \boldsymbol{f} + \boldsymbol{l}\, dx,
\end{aligned}$$

where $\boldsymbol{l}(x,t)$ is the *body-couple per unit reference length* defined as

$$\boldsymbol{l}(x,t) := \boldsymbol{d}_2(x,t) \times \int_{-\delta}^{\delta} \int_{-\delta}^{\delta} y\bar{\boldsymbol{f}}(\boldsymbol{x},t)\, dy\, dz. \tag{2.15}$$

Since we assume that the motion of the axis is planar, i.e., confined to the $(\boldsymbol{i},\boldsymbol{j})$-plane, $\boldsymbol{l}$ then takes values in $span\{\boldsymbol{k}\}$, and thus we require that all components of the body-couple act perpendicular to $(\boldsymbol{i},\boldsymbol{j})$-plane so that

$$\int_{A(x)} \left(z\boldsymbol{d}_3 \times \bar{\boldsymbol{f}}\right)\, dy\, dz = 0.$$

Note, by couple we mean the resulting torque force caused by coupling forces.

Surface Forces and Torques

Surface forces, as their name suggests, are forces that act across both the external and internal surfaces of the beam. And although both types of surface forces are worth mentioning, we are only going to deal with the internal ones.

The former ones, often referred to as *surface tractions*, are forces that act on the external surface of the beam. These arise as a result of mechanical contact with other surounding material. Since the plate is isolated, we assume that all surface tractions but those at the ends of the beam are zero.

At the ends of the beam, we equate the traction forces with the internal contact forces and include them in the boundary conditions, as suggested in [7].

The later ones, on the other hand, are forces internal to the beam that arise as a result of the mechanical interaction between the segments of the beam to either side of the cross-section $A(x)$. They are measured as the force per unit area on the surface of cross-section $A(x)$. In other words, they represent *stress*, the state of force transmission in the interior of the beam. These forces exist in equal and opposite pairs, by Newton's third law. In general, these pairs are denoted as

$$\boldsymbol{t}_{\pm \boldsymbol{i}}(\boldsymbol{x}, t) := \sum_{n=1}^{3} \tau_n(\boldsymbol{x}, t)\boldsymbol{d}_n(x, t), \tag{2.16}$$

and are defined as the *contact force per unit reference area* on the surface of $A(x)$ as in Hjelmstad [7]. The subscript + corresponds to the force that the material from the right of $A(x)$ exerts on the material to the left of $A(x)$ and vice versa for the subscript $-$. These subscripts are somewhat artificial and we can drop them due to the *Cauchy reciprocal theorem* $\boldsymbol{t}_{+\boldsymbol{i}}(\boldsymbol{x}, t) = -\boldsymbol{t}_{-\boldsymbol{i}}(\boldsymbol{x}, t)$, whose proof can be found in Hjelmsted [7].

$\boldsymbol{t}_{\boldsymbol{i}}$ is given by the *Cauchy stress formula*:

$$\boldsymbol{t}_{\boldsymbol{i}} = \boldsymbol{S}\boldsymbol{i}.$$

Here, $\boldsymbol{S}$ is the *first Piola-Kirchhoff stress tensor*, and $\boldsymbol{i}$ is outward unit normal to A. The *resultant contact force* of the segment $S_{[-1,x)}$ on the segment $S_{[x,a]}$, or equivalently (equal and opposite of that) of the segment $S_{(x,1]}$ on the segment $S_{[a,x]}$, can be computed by integrating the contact force $\boldsymbol{t}$ over the cross-sectional area A, i.e,

$$\boldsymbol{n}(x, t) := \int_{A(x)} \boldsymbol{t}_{\boldsymbol{i}}(x, y, z, t)\, dy\, dz. \tag{2.17}$$

In a way you can think of the stress resultant $\boldsymbol{n}(x, t)$ as representing the combined effect of all the contact forces acting on the cross section $A(x)$ in which we have adopted the sign convention that the right of the beam acts on the left of the beam in the positive sense (and vice versa). We assume that $\boldsymbol{n}$ takes values in $span\{\boldsymbol{i}, \boldsymbol{j}\}$, which means that $\boldsymbol{t}_{\boldsymbol{i}}$ has no component in the $\boldsymbol{d}_3$ direction, i.e. $\boldsymbol{t}_{\boldsymbol{i}} = \tau_1\boldsymbol{d}_1 + \tau_2\boldsymbol{d}_2$. Notice that the integration over the cross-section eliminates the dependence on y and z coordinates and leaves the resultants as functions of only spatial variable x.

Now we derive the corresponding *resultant contact torques* generally:

$$\begin{aligned}\int_{A(x)} \boldsymbol{p}(\boldsymbol{x},t)\times\boldsymbol{t_i}(\boldsymbol{x},t)\,dy\,dz &= \int_{A(x)} (\boldsymbol{r}+y\boldsymbol{d}_2+z\boldsymbol{d}_3)\times\boldsymbol{t_i}\,dy\,dz\\ &= \boldsymbol{r}\times\int_{A(x)}\boldsymbol{t_i}\,dy\,dz+\int_{A(x)} y(\boldsymbol{d}_2\times\boldsymbol{t_i})\,dy\,dz\\ &= \boldsymbol{r}(x,t)\times\boldsymbol{n}(x,t)+\boldsymbol{m}(x,t). \end{aligned} \tag{2.18}$$

Since we assumed earlier that the motion of the axis is confined to the ($\boldsymbol{i}$,$\boldsymbol{j}$)-plane, we require that all components of the resultant contact couple act perpendicular to ($\boldsymbol{i}$,$\boldsymbol{j}$)-plane so that

$$\int_{A(x)} z(\boldsymbol{d}_3\times\boldsymbol{t_i})\,dy\,dz = 0.$$

Thus, we define the *resultant contact couple* as

$$\boldsymbol{m}(x,t) := \int_{A(x)} y(\boldsymbol{d}_2\times\boldsymbol{t_i}(\boldsymbol{x},t))\,dy\,dz, \tag{2.19}$$

and the *resultant moment* of contact force on $A(x)$ as $\boldsymbol{r}(x,t)\times\boldsymbol{n}(x,t)$. Thus, the corresponding *resulting contact torque* of the resultant contact force $\boldsymbol{n}$ is

$$\boldsymbol{r}(x,t)\times\boldsymbol{n}(x,t)+\boldsymbol{m}(x,t). \tag{2.20}$$

2.2.2 Balance Laws

We now assume that all segments of the beam obey the following generalizations of Newton's second law.

Hypothesis 2.1. (Balance of Linear Momentum). *For a segment of the beam, $S_{[a,b]}$, the time rate of change of its linear momentum is equal to the sum of all forces on the segment, $\hat{\boldsymbol{f}}(S_{[a,b]})$, i.e.*

$$\frac{\partial}{\partial t}\int_a^b \rho A(x)\boldsymbol{r}_t(x,t)\,dx = \hat{\boldsymbol{f}}(S_{[a,b]}). \tag{2.21}$$

Hypothesis 2.2. (Balance of Angular Momentum). *For a segment of the beam, $S_{[a,b]}$, the time rate of change of its angular momentum is equal to the sum of all torques on the segment, $\hat{\boldsymbol{l}}(S_{[a,b]})$, i.e.*

$$\frac{\partial}{\partial t}\int_a^b \left[\rho A(x)\boldsymbol{r}(x,t)\times\boldsymbol{r}_t(x,t)+\rho J(x)\theta_t(x,t)\boldsymbol{d}_3\right]\,dx = \hat{\boldsymbol{l}}(S_{[a,b]}). \tag{2.22}$$

Notice that we have previously defined linear and angular momentum relative to $\boldsymbol{r}(x,t)$ in the equations (2.10) and (2.12) respectively. Now we equate the time rate of change of linear and angular momentum with the sum of all forces and torques of the system, respectively.

Hypothesis 2.3. *The sum of all forces on the segment of the beam $S_{[a,b]}$ at time t is given by*

$$\hat{\boldsymbol{f}}(S_{[a,b]}) := \boldsymbol{n}(b,t) - \boldsymbol{n}(a,t) + \int_a^b \boldsymbol{f}(x,t)\, dx, \tag{2.23}$$

Hypothesis 2.4. *The sum of all the torques on the segment of the beam $S_{[a,b]}$ at time t is given by*

$$\begin{aligned} \hat{\boldsymbol{l}}(S_{[a,b]}) : \quad &= \quad \boldsymbol{m}(b,t) + \boldsymbol{r}(b,t) \times \boldsymbol{n}(b,t) - \boldsymbol{m}(a,t) - \boldsymbol{r}(a,t) \times \boldsymbol{n}(a,t) \\ &\quad + \int_a^b (\boldsymbol{r}(x,t) \times \boldsymbol{f}(x,t) + \boldsymbol{l}(x,t))\ dx, \end{aligned} \tag{2.24}$$

Using (2.23), the balance of linear momentum (2.21) becomes

$$\begin{aligned} \int_a^b \rho A(x) \boldsymbol{r}_{tt}(x,t)\, dx \quad &= \quad \boldsymbol{n}(b,t) - \boldsymbol{n}(a,t) + \int_a^b \boldsymbol{f}(x,t)\, dx. \\ &= \quad \int_a^b (\boldsymbol{n}_x(x,t) + \boldsymbol{f}(x,t))\, dx, \end{aligned} \tag{2.25}$$

Assuming that all of the above functions are sufficiently regular, we differentiate (2.25) with respect to x to obtain the *differential form* of the balance of linear momentum

$$\rho A(x) \boldsymbol{r}_{tt} = \boldsymbol{n}_x + \boldsymbol{f}. \tag{2.26}$$

Similarly, applying (2.24), the balance of angular momentum (2.22) yields the integral equation

$$\begin{aligned} \int_a^b (\rho A \boldsymbol{r} \times \boldsymbol{r}_{tt} + \rho J \theta_{tt} \boldsymbol{d}_3)\ dx \quad &= \quad \boldsymbol{m}(b,t) - \boldsymbol{m}(a,t) + \boldsymbol{r}(b,t) \times \boldsymbol{n}(b,t) - \boldsymbol{r}(a,t) \times \boldsymbol{n}(a,t) \\ &\quad + \int_a^b (\boldsymbol{r}(x,t) \times \boldsymbol{f}(x,t) + \boldsymbol{l}(x,t))\ dx \\ &= \quad \int_a^b (\boldsymbol{m}_x + \boldsymbol{r} \times \boldsymbol{n}_x + \boldsymbol{r}_x \times \boldsymbol{n} + \boldsymbol{r} \times \boldsymbol{f} + \boldsymbol{l})\ dx \end{aligned}$$

which after using (2.26) further reduces to

$$\int_a^b (\boldsymbol{r} \times\ (\boldsymbol{n}_x + \boldsymbol{f}) + \rho J \theta_{tt} \boldsymbol{d}_3)\ dx = \int_a^b (\boldsymbol{m}_x + \boldsymbol{r} \times \boldsymbol{n}_x + \boldsymbol{r}_x \times \boldsymbol{n} + \boldsymbol{r} \times \boldsymbol{f} + \boldsymbol{l})\ dx,$$

or simply

$$\int_a^b \rho J\theta_{tt}\boldsymbol{d}_3 \, dx = \int_a^b (\boldsymbol{m}_x + \boldsymbol{r}_x \times \boldsymbol{n} + \boldsymbol{l}) \, dx. \tag{2.27}$$

As in Antman [1], equations (2.25) and (2.27) represent the *integral* version of the balance of linear and angular momentum, respectively.

Again, we differentiate (2.27) with respect to x, to get the *differential form* of the balance of angular momentum

$$\rho J\theta_{tt}(x)\boldsymbol{d}_3 = \boldsymbol{m}_x + \boldsymbol{r}_x \times \boldsymbol{n} + \boldsymbol{l}. \tag{2.28}$$

We have now obtained the *classical form of the equations of motion*:

$$\begin{aligned} \rho A(x)\boldsymbol{r}_{tt} &= \boldsymbol{n}_x + \boldsymbol{f}, \\ \rho J\theta_{tt}(x)\boldsymbol{d}_3 &= \boldsymbol{m}_x + \boldsymbol{r}_x \times \boldsymbol{n} + \boldsymbol{l}. \end{aligned}$$

In order to get *componential* form of these equations, we make the following assumptions about forces and couples in accord with our assumption of planarity. As we mentioned earlier, the basis $\{\boldsymbol{d}_1, \boldsymbol{d}_2, \boldsymbol{d}_3\}$ is natural for the intrinsic desctiption of deformation and we therefore decompose the following vector-valued functions with respect to it. We will show that for an electrically conducting plate, the *body-force per unit reference length*, *body couple per unit reference length*, *resultant contact force*, and *resultant contact couple* respectively, take the following forms:

$$\boldsymbol{f}(x,t) =: -\gamma^2(f_1(x,t)\boldsymbol{d}_1(x,t) + f_2(x,t)\boldsymbol{d}_2(x,t)), \tag{2.29}$$

$$\boldsymbol{l}(x,t) =: \gamma^2 l(x,t)\boldsymbol{d}_3, \tag{2.30}$$

$$\boldsymbol{n}(x,t) =: N(x,t)\boldsymbol{d}_1(x,t) + H(x,t)\boldsymbol{d}_2(x,t), \text{ and} \tag{2.31}$$

$$\boldsymbol{m}(x,t) =: M(x,t)\boldsymbol{d}_3, \tag{2.32}$$

where $\gamma > 0$ is a given constant whose meaning will become clear in Section 2.5.2. We may think of H as the *shear force* and M as the *bending couple*. N can be thought of as the *tension* only if $\eta = 0$. Otherwise, there is no standard name for N and the tension is expressed as $\boldsymbol{n} \cdot \frac{\boldsymbol{r}_x}{|\boldsymbol{r}_x|}$.

Substituting (2.29) and (2.31) into (2.26) we get

$$\begin{aligned} \rho A\boldsymbol{r}_{tt} &= \boldsymbol{n}_x + \boldsymbol{f} \\ &= N_x\boldsymbol{d}_1 + N\boldsymbol{d}_{1,x} + H_x\boldsymbol{d}_2 + H\boldsymbol{d}_{2,x} - \gamma^2(f_1\boldsymbol{d}_1 + f_2\boldsymbol{d}_2) \\ &= N_x\boldsymbol{d}_1 + N\theta_x\boldsymbol{d}_2 + H_x\boldsymbol{d}_2 - H\theta_x\boldsymbol{d}_1 - \gamma^2 f_1\boldsymbol{d}_1 - \gamma^2 f_2\boldsymbol{d}_2 \\ &= \left[N_x - \theta_x H - \gamma^2 f_1\right]\boldsymbol{d}_1 + \left[H_x + \theta_x N - \gamma^2 f_2\right]\boldsymbol{d}_2. \end{aligned}$$

This gives us our first two equations of motions (along the axes of the deformed beam):

$$\begin{aligned}\rho A \boldsymbol{r}_{tt} \cdot \boldsymbol{d}_1 &= N_x - \theta_x H - \gamma^2 f_1, \text{ and} \\ \rho A \boldsymbol{r}_{tt} \cdot \boldsymbol{d}_2 &= H_x + \theta_x N - \gamma^2 f_2.\end{aligned}$$

Similarly, we substitute (2.30), (2.31), and (2.32) into (2.28) to get

$$\begin{aligned}\rho J \theta_{tt} \boldsymbol{d}_3 &= \boldsymbol{m}_x + \boldsymbol{r}_x \times \boldsymbol{n} + \boldsymbol{l} \\ &= M_x \boldsymbol{d}_3 + (\nu \boldsymbol{d}_1 + \eta \boldsymbol{d}_2) \times (N \boldsymbol{d}_1 + H \boldsymbol{d}_2) + \gamma^2 l \boldsymbol{d}_3 \\ &= M_x \boldsymbol{d}_3 + (\nu H - \eta N) \boldsymbol{d}_3 + \gamma^2 l \boldsymbol{d}_3 \\ &= \left[M_x + \nu H - \eta N + \gamma^2 l \right] \boldsymbol{d}_3.\end{aligned}$$

This gives us a third equation of motion:

$$\rho J \theta_{tt} = M_x + \nu H - \eta N + \gamma^2 l.$$

Thus, the componential forms of the balance law equations are

$$\begin{aligned}\rho A \boldsymbol{r}_{tt} \cdot \boldsymbol{d}_1 &= N_x - \theta_x H - \gamma^2 f_1 \\ \rho A \boldsymbol{r}_{tt} \cdot \boldsymbol{d}_2 &= H_x + \theta_x N - \gamma^2 f_2 \\ \rho J \theta_{tt} &= M_x + \nu H - \eta N + \gamma^2 l,\end{aligned} \tag{2.33}$$

in which there are more unknowns than equations. On the right-hand-side we have 6 unknowns, three resultants N, H and M and three strain variables θ_x, η, and ν. Recall that forces and couple are prescribed. Given that our focus is on static configurations including buckled states, we will concentrate on the following static versions of (2.33):

$$\begin{aligned}0 &= N_x - \theta_x H - \gamma^2 f_1, \\ 0 &= H_x + \theta_x N - \gamma^2 f_2, \text{ and} \\ 0 &= M_x + \nu H - \eta N + \gamma^2 l.\end{aligned} \tag{2.34}$$

But, this still leaves us with more unknowns than equations and leads us to conclude that the equations of kinematics and balance laws are insufficient in fully characterizing the behavior of the beam because they do not distinguish between different types of materials. We thus introduce constitutive assumptions which serve to distinguish between different types of material.

2.3 Material Properties

So far we have seen that the two types of equations: the equations of *kinematics* (relating displacement to strains), and the *balance laws* (relating contact and body-forces to stresses) are not sufficient in setting up our problem. These equations do not destinguish between the responses of different types of materials the plate is made of. We need to know how forces are related to the change of shape suffered by the beam in every motion. Thus, we supplement our system with a new set of equations relating stress to strain which we call *constitutive* equations. This new relation between forces and deformation is intuitive and physically reasonable. For example, if a rubber band is pulled on, it tends to stretch, and the more it is pulled on the more it stretches.

2.3.1 Constitutive Equations

In general, constitutive equations express constraints specific to the material being investigated and are helpful in approximating the material's response to external forces. Constitutive equations in our study relate the resultants N, H, and M to the strain variables ν, η, and μ and are thus helpful in simplifying the nonlinear equations.

As in [11] for a uniform *elastic* beam, we assume that N, H, and M are given as functions of the strains as

$$\begin{aligned} N(x,t) &= \tilde{N}(\nu(x,t), \eta(x,t), \mu(x,t)), \\ H(x,t) &= \tilde{H}(\nu(x,t), \eta(x,t), \mu(x,t)), \\ M(x,t) &= \tilde{M}(\nu(x,t), \eta(x,t), \mu(x,t)) \end{aligned} \tag{2.35}$$

with the common domain consisting of those ν, η and μ satisfying the condition:

$$\boldsymbol{r}_x \cdot \boldsymbol{d}_1 = \nu > 0 \quad \forall x \in [a,b]. \tag{2.36}$$

This condition ensures that the deformation is never so severe that the stretch of $\boldsymbol{r}$, the local ratio of deformed to reference length, is ever reduced to zero, or that the shear is so large that $\boldsymbol{r}$ and $\boldsymbol{d}_2$ ever coincide. See [1].

These equations are invariant under rigid motions, which means that the material response should be unaffected by rigid motions and by time translations. This is known as the Principle of Frame Indifference [1].

2.3.2 Constitutive Assumptions

As in Antman [1], we assume that $\tilde{N}, \tilde{H}$, and $\tilde{M}$ are continuously differentiable and note that not every choice of the constitutive functions $\tilde{N}, \tilde{H}$, and $\tilde{M}$ is physically reasonable. For example, when we tug on the beam, we do not expect it to shorten, so that we can reasonably suppose that an increase in the tension $\boldsymbol{n} \cdot \frac{\boldsymbol{r}_x}{|\boldsymbol{r}_x|}$ accompanies an increase in the stretch $|\boldsymbol{r}_x|$. Likewise, an increase in the shear force H accompanies an increase in the shear strain η and finally, an increase in the bending couple M accompanies an increase in the bending strain μ. This is conveniently characterized by requiring that the matrix

$$\frac{\partial(\tilde{N}, \tilde{H}, \tilde{M})}{\partial(\nu, \eta, \mu)} \tag{2.37}$$

be positive-definite at any value of the strains. We refer to (2.37) as the *monotonicity condition*, a condition necessary to establish a reasonable existence theory for solutions of our nonlinear system of partial differential equations.

We assume that extreme values of the resultants accompany the extreme values of the strains so that is in accord with the monotonicity condition. We assume that N and M are unaffected by the sense of shearing. We assume that there are "primary" couplings between N and ν, H and η, and M and μ and that all other pairings are considered "secondary."

2.3.3 Material Constraints Specific To Our Problem

The material constraints commonly imposed in structural mechanics, and the ones that will help us simplify the governing equations are the kind of restrictions that prevent the plate from extending and shearing regardless of what values are assumed by resultant contact force and couple, i.e.

$$\nu(x,t) \equiv 1 \text{ and} \tag{2.38}$$

$$\eta(x,t) \equiv 0, \tag{2.39}$$

respectively. Physically, this means that cross-sections remain undeformed and perpendicular to the deformed axis of the beam. As a consequence of the above constraints (2.38) and (2.39) we have only one constitutive equation, which we assume has the form known as Bernoulli-Euler constitutive equation

$$M(x,t) = EI\mu(x,t). \tag{2.40}$$

This moment-curvature relation (2.40) assumes linear distribution of strain μ and resultant M across the cross-section $A(x)$, that is, it tells us that the bending force M is a function of only the bending strain μ, which now represents the curvature since $|\boldsymbol{r}_x| = 1$ and $\phi = \theta$ (from $\phi_x/|\boldsymbol{r}_x|$),

and is linear in the change in μ. The constants E and I are, respectively, Young's modulus (i.e., the measure of stiffness of an isotropic elastic material) and the second moment of area (i.e. the property of a cross-section used to predict the resistance of the shape to bending and deflection). Together, they represent the beam's bending stiffness. Note that when we linearize the system about the equilibrium this relationship arises naturally.

Note that N and H are no longer defined constitutively, rather they assume whatever form necessary to ensure the imposed material constraints are met. In particular, N represents the tension at (x, t) related to the stretch constraint $\nu = 1$ and is enough to preserve the inextensibility of the beam. H is related to the no-shear constraint $\eta = 0$. (Alternatively, one can think of N and H as Lagrange multipliers for their respective constraint equations.)

With these extra assumptions, we got rid of M, η, and ν, and consequently ensured that our system (2.34) has the same number of equations and unknowns. Thus, reducing it to

$$\begin{aligned} 0 &= N_x - \mu H - \gamma^2 f_1, \\ 0 &= H_x + \mu N - \gamma^2 f_2, \text{ and} \\ 0 &= EI\mu_x + H + \gamma^2 l, \end{aligned} \tag{2.41}$$

in which we have three equations and three unknowns. Recall that $\mu = \theta_x$. In the remainder of this thesis, we will concentrate on this set of equations, first in a simplified context (see Chapter 3) and then in a more general setting (see Chapter 4).

The equations of kinematics, balance laws and constitution alone are not sufficient to solve our boundary value problem. In order to have a well-posed boundary value problem we must supplement the field equations with boundary conditions, which we do in the next section.

2.4 Boundary Conditions

Ultimately, our system has no dependence on z, and it may therefore be treated as a beam. To that end, we assume reasonable forms for the boundary conditions to complete the picture. We will briefly mention several options but focus only on the one we are going to use. For a detailed discussion of the boundary conditions we refer to Antman [1].

Case 1: Prescribed Position

We could impose kinematic boundary condition such as prescribing the position vector $\boldsymbol{r}(-1, t)$ at the left-hand end (the right-hand end is analogues), and letting the resultant forces assume whatever

values necessary to maintain the kinematic constrains. More precisely, suppose that the left-hand end of the axis is fixed at $x = -1$, that is we require that

$$\boldsymbol{r}(-1,t) = \boldsymbol{r}_*$$

or equivalently

$$u(-1,t) = u_* \quad \textit{and} \quad v(-1,t) = v_*. \tag{2.42}$$

This condition assures that there is no translation in space.

Case 2: Prescribed Resultant Force

Alternatively, we could prescribe the resultant force, in which case we do not prescribe the position vector $\boldsymbol{r}(-1,t)$. At the left-hand end we require that there be a given vector $\boldsymbol{n}_*$ such that

$$\boldsymbol{n}(-1,t) = \boldsymbol{n}_*$$

or equivalently

$$N(-1,t) = N_* \quad \text{and} \quad H(-1,t) = H_*. \tag{2.43}$$

In either case we would have to choose another set of conditions to complete the boundary values. Thus, we could choose welded, clamped, hinged or free end.

Welded End

In this case we prescribe the angle $\theta(-1)$, i.e.,

$$\theta(-1,t) = \theta_* \tag{2.44}$$

where $\theta(x,t)$ is as defined earlier the angle between $\boldsymbol{i}$ and $\boldsymbol{d}_1$. In this situation we are prescribing the orientation $\boldsymbol{d}_2(-1)$ of the left-hand cross section. This condition in conjunction with prescribed position (2.42) physically represents *welding* of the left-hand end of the beam to some given surface, and it is known as Dirichlet condition.

Clamped End

Alternatively, we could prescribe the angle $\phi(-1)$, i.e.,

$$\phi(-1, t) = \phi_* \tag{2.45}$$

where $\phi(x, t)$ is as defined earlier an angle between $\boldsymbol{i}$ and $\boldsymbol{r}_x$. Note that $\theta(x, t)$ and $\phi(x, t)$ are the same when we assume that the beam is unstreached and unsheared. This condition in conjunction with prescribed position (2.42) physically represents *clamping* of the left-hand end of the beam to some given surface.

Hinged

We could also prescribe the bending couple at the left-hand end, i.e.

$$M(-1, t) = M_*. \tag{2.46}$$

This condition if combined with prescribed position (2.42), is known as a Neumann condition and represents the physical situation of a *hinged* beam that is free to rotate.

Free-end

And last but not least, we could prescribe resultant force (2.43) and bending couple (2.46) to obtain the *free-end* boundary condition which we are going to use to complete our boundary value problem. Note that in the case of the equilibrium problem we are not allowed to prescribe the resultant forces arbitrarily, in which case the boundary conditions must be consistent with the requirement that the resultant forces and couple on the beam must vanish. This is important because such conditions are necessary for the existence of solutions to equilibrium problems. See Antman for details [1]. Also worth mentioning here is that in the case of an inextensible and unshearable beam, i.e. its cross-sections remain plane and orthogonal, we are not able to determine shear and axial force from the constitutive equations, they must be determined from the equilibrium equation.

For the problems we consider in this thesis, in order to get a well-posed boundary value problem, we will prescribe resultant forces at the ends of the beam as well as fix rotation by specifying a value for θ along the beam.

Let us now move on to a derivation of the body-forces resulting from a current conducted along the length of our infinite plate.

2.5 Derivation of the Body-Forces

We now complete the set of equations (2.34) by deriving the body-forces associated with an applied current traveling along the body of our plate. This current is assumed to be conducted transversely to the beam (i.e., in the $\boldsymbol{k}$ direction). Note also that these forces are by nature non-local, and complicate analysis of equations (2.34), forcing us to consider the entire beam (as a proxy for the plate) in our discussion. To derive the forces, we can make one of two assumptions about the current: either it is constant per unit deformed volume or it is constant per unit reference volume. We will stick to the former even though it involves more difficult calculations because it is more realistic.

2.5.1 Deformation Gradient

Because we need to transform an integration from one configuration to another, we are first going to introduce a very important second-order tensor called the *deformation gradient*, defined as

$$\boldsymbol{F}(\boldsymbol{x}) = \nabla \boldsymbol{p}(\boldsymbol{x}) = \frac{\partial \boldsymbol{p}}{\partial \boldsymbol{x}}(x, y, z).$$

This tensor represents the gradient of the mapping function $\boldsymbol{p}(\boldsymbol{x})$ ($\boldsymbol{p}$ as in (2.1), where we ignore the time dependence for these geometric derivations). Assuming continuity in the mapping function $\boldsymbol{p}(\boldsymbol{x})$ implies that any material line in the reference configuration is transformed to another in the deformed configuration according to $\boldsymbol{F}$, implying that no cracks form during the deformation. Calculation of $\boldsymbol{F}$ affords us the convenience of deriving the system forces in the reference body and then transforming to the deformed frame.

First, note that the identity matrix,

$$\boldsymbol{I} = \frac{\partial \boldsymbol{x}}{\partial \boldsymbol{x}} = \frac{\partial \boldsymbol{x}}{\partial x}\frac{\partial x}{\partial \boldsymbol{x}} + \frac{\partial \boldsymbol{x}}{\partial y}\frac{\partial y}{\partial \boldsymbol{x}} + \frac{\partial \boldsymbol{x}}{\partial z}\frac{\partial z}{\partial \boldsymbol{x}} = \boldsymbol{i}\frac{\partial x}{\partial \boldsymbol{x}} + \boldsymbol{j}\frac{\partial y}{\partial \boldsymbol{x}} + \boldsymbol{k}\frac{\partial z}{\partial \boldsymbol{x}},$$

so that

$$\frac{\partial x}{\partial \boldsymbol{x}} = \boldsymbol{i}^T, \quad \frac{\partial y}{\partial \boldsymbol{x}} = \boldsymbol{j}^T, \quad \frac{\partial z}{\partial \boldsymbol{x}} = \boldsymbol{k}^T.$$

However, we drop the transpose notation since there can be no confusion if we adopt the *dyadic* product $\boldsymbol{ab} = \boldsymbol{ab}^T$ for $\boldsymbol{a}, \boldsymbol{b} \in \mathbb{R}^3$ (where it naturally follows that the dot product, $\boldsymbol{a} \cdot \boldsymbol{b} = \boldsymbol{a}^T\boldsymbol{b}$, is distinct). Note that the dyadic product is simply represented as the square matrix obtained by

multiplying $\boldsymbol{a}$ as a column vector by $\boldsymbol{b}$ as a row vector. Since

$$\begin{aligned}\frac{\partial}{\partial x}\boldsymbol{p}(\boldsymbol{x}) &= \boldsymbol{r}_x + y\boldsymbol{d}_{2,x} \\ &= (\nu\boldsymbol{d}_1 + \eta\boldsymbol{d}_2) - y\mu\boldsymbol{d}_1 \\ &= (\nu - y\mu)\boldsymbol{d}_1 + \eta\boldsymbol{d}_2\end{aligned}$$

the deformation gradient can be calculated and simplified as follows:

$$\begin{aligned}\boldsymbol{F}(\boldsymbol{x}) &= \frac{\partial \boldsymbol{p}}{\partial \boldsymbol{x}}(x, y, z) \\ &= \frac{\partial \boldsymbol{p}}{\partial x}\frac{\partial x}{\partial \boldsymbol{x}} + \frac{\partial \boldsymbol{p}}{\partial y}\frac{\partial y}{\partial \boldsymbol{x}} + \frac{\partial \boldsymbol{p}}{\partial z}\frac{\partial z}{\partial \boldsymbol{x}} \\ &= ((\nu - y\mu)\boldsymbol{d}_1 + \eta\boldsymbol{d}_2)\boldsymbol{i} + \boldsymbol{d}_2\boldsymbol{j} + \boldsymbol{d}_3\boldsymbol{k} \\ &= ((\nu - y\mu)(\cos\theta\boldsymbol{i} + \sin\theta\boldsymbol{j}) + \eta(-\sin\theta\boldsymbol{i} + \cos\theta\boldsymbol{j}))\boldsymbol{i} + (-\sin\theta\boldsymbol{i} + \cos\theta\boldsymbol{j})\boldsymbol{j} + \boldsymbol{k}\boldsymbol{k} \\ &= (\nu - y\mu)(\cos\theta\boldsymbol{i} + \sin\theta\boldsymbol{j})\boldsymbol{i} + \eta(-\sin\theta\boldsymbol{i} + \cos\theta\boldsymbol{j})\boldsymbol{i} + (-\sin\theta\boldsymbol{i} + \cos\theta\boldsymbol{j})\boldsymbol{j} + \boldsymbol{k}\boldsymbol{k} \\ &= ((\nu - y\mu)\cos\theta - \eta\sin\theta)\boldsymbol{i}\boldsymbol{i} + ((\nu - y\mu)\sin\theta + \eta\cos\theta)\boldsymbol{j}\boldsymbol{i} - \sin\theta\boldsymbol{i}\boldsymbol{j} + \cos\theta\boldsymbol{j}\boldsymbol{j} + \boldsymbol{k}\boldsymbol{k}\end{aligned}$$

or more compactly in matrix-form,

$$\boldsymbol{F}(\boldsymbol{x}) = \begin{pmatrix}(\nu - y\mu)\cos\theta - \eta\sin\theta & -\sin\theta & 0 \\ (\nu - y\mu)\sin\theta + \eta\cos\theta & \cos\theta & 0 \\ 0 & 0 & 1\end{pmatrix}.$$

The *change in volume* from reference to deformed configurations is described by the *determinant* of $\boldsymbol{F}$, so we define

$$\alpha(x, y) := \det \boldsymbol{F}(\boldsymbol{x}) = \nu - y\mu. \tag{2.47}$$

Note that in a thin plate under small deformations, α is very close to 1. Since it is physically impossible to annihilate volumes, or even to deform them to negative volumes, we require that at any point in the domain of deformation map

$$\alpha(x, y) > 0.$$

Since $\det \boldsymbol{F}(\boldsymbol{x}) > 0$ everywhere, we are guarantied by the implicit function theorem that $\boldsymbol{F}$ has an inverse function, $\boldsymbol{F}^{-1}$. As we shall later see the inverse function $\boldsymbol{F}^{-T}$ will prove useful in transforming the body-force from the deformed back to the reference frame. Thus, we first compute $\boldsymbol{F}^{-1}$:

$$\boldsymbol{F}^{-1}(x, y) = \begin{pmatrix}\frac{1}{\alpha}\cos\theta & \frac{1}{\alpha}\sin\theta & 0 \\ -\sin\theta - \frac{\eta}{\alpha}\cos\theta & \cos\theta - \frac{\eta}{\alpha}\sin\theta & 0 \\ 0 & 0 & 1\end{pmatrix}$$

and its transpose, which we give in simplified form

$$\begin{aligned}
\boldsymbol{F}^{-T} &= \frac{1}{\alpha}\cos\theta \boldsymbol{ii} - (\sin\theta + \frac{\eta}{\alpha}\cos\theta)\boldsymbol{ij} + \frac{1}{\alpha}\sin\theta \boldsymbol{ji} + (\cos\theta - \frac{\eta}{\alpha}\sin\theta)\boldsymbol{jj} + \boldsymbol{kk} \\
&= \frac{1}{\alpha}(\cos\theta \boldsymbol{i} + \sin\theta \boldsymbol{j})\boldsymbol{i} + (-\sin\theta \boldsymbol{i} + \cos\theta \boldsymbol{j})\boldsymbol{j} - \frac{\eta}{\alpha}(\cos\theta \boldsymbol{i} + \sin\theta \boldsymbol{j})\boldsymbol{j} + \boldsymbol{kk} \\
&= \frac{1}{\alpha}\boldsymbol{d}_1\boldsymbol{i} + \boldsymbol{d}_2\boldsymbol{j} - \frac{\eta}{\alpha}\boldsymbol{d}_1\boldsymbol{j} + \boldsymbol{kk} \\
&= \frac{1}{\alpha}\boldsymbol{d}_1\boldsymbol{i} + (\boldsymbol{d}_2 - \frac{\eta}{\alpha}\boldsymbol{d}_1)\boldsymbol{j} + \boldsymbol{d}_3\boldsymbol{k}.
\end{aligned}$$

We are now prepared to calculate the forces due to the applied current.

2.5.2 Constant Current Per Unit Volume

Let us assume that the plate carries a steady, constant conduction current per unit deformed volume mantained by a power supply external to the plate. As a result of this current there is a magnetic body-force density function given by $j(\boldsymbol{x}) \times \boldsymbol{b}(\boldsymbol{x})$, (as described in [10]) where j is the current density vector and $\boldsymbol{b}$ is the resultant magnetic field.

Let us define *constant current per unit deformed volume* as

$$\bar{j}(\boldsymbol{p}(\boldsymbol{x})) = \bar{\gamma}\boldsymbol{d}_3, \tag{2.48}$$

where $\bar{\gamma}$ is a non-dimensional parameter. The material version of the current (*current per unit reference volume*) is given by

$$\begin{aligned}
j(\boldsymbol{x}) &= \det \boldsymbol{F}(\boldsymbol{x})\boldsymbol{F}^{-T}(\boldsymbol{x})\bar{j}(\boldsymbol{p}(\boldsymbol{x})) \\
&= \alpha(x,y)\left[\left(\frac{1}{\alpha(x,y)}\right)\boldsymbol{d}_1(x)\boldsymbol{i} - \frac{\eta(x)}{\alpha(x,y)}\boldsymbol{d}_1\boldsymbol{j} + \boldsymbol{d}_2(x)\boldsymbol{j} + \boldsymbol{d}_3\boldsymbol{k}\right]\bar{\gamma}\boldsymbol{d}_3 \\
&= \bar{\gamma}\alpha(x,y)\boldsymbol{k} \\
&\equiv j(x,y).
\end{aligned} \tag{2.49}$$

2.5.3 Magnetic Field

Although simple force distributions lead to simple stress patterns in the plate, a uniform current distribution can be shown to lead to a highly nonuniform magnetic field density in and around the

vicinity of the plate [10]. The uniform current flow in the plate generates its own magnetic field $\boldsymbol{b}$ which can be calculated by the *Biot-Savart Law* (see [4], p. 186)

$$\begin{aligned}
\boldsymbol{b}(\boldsymbol{x}) &= \frac{\mu_0}{4\pi}\int_{\Omega_\infty}\frac{j(\tilde{\boldsymbol{x}})\times(\boldsymbol{x}-\tilde{\boldsymbol{x}})}{|\boldsymbol{x}-\tilde{\boldsymbol{x}}|^3}\,d\tilde{\boldsymbol{x}}\\
&= \frac{\mu_0}{4\pi}\int_{\Omega_\infty}\frac{[\bar{\gamma}\alpha(\tilde{x},\tilde{y})\boldsymbol{k}]\times[(x-\tilde{x})\boldsymbol{i}+(y-\tilde{y})\boldsymbol{j}+(z-\tilde{z})\boldsymbol{k}]}{[(x-\tilde{x})^2+(y-\tilde{y})^2+(z-\tilde{z})^2]^{\frac{3}{2}}}\,d\tilde{\boldsymbol{x}}\\
&= \hat{\gamma}\int_{\Omega_\infty}\frac{\alpha(\tilde{x},\tilde{y})[(x-\tilde{x})\boldsymbol{k}\times\boldsymbol{i}+(y-\tilde{y})\boldsymbol{k}\times\boldsymbol{j}+(z-\tilde{z})\boldsymbol{k}\times\boldsymbol{k}]}{[(x-\tilde{x})^2+(y-\tilde{y})^2+(z-\tilde{z})^2]^{\frac{3}{2}}}\,d\tilde{\boldsymbol{x}}\\
&= \hat{\gamma}\int_{\Omega_\infty}\frac{\alpha(\tilde{x},\tilde{y})[(x-\tilde{x})\boldsymbol{j}-(y-\tilde{y})\boldsymbol{i}]}{[(x-\tilde{x})^2+(y-\tilde{y})^2+(z-\tilde{z})^2]^{\frac{3}{2}}}\,d\tilde{\boldsymbol{x}}\\
&= \hat{\gamma}\int_{-1}^{1}\int_{-\delta}^{\delta}\int_{-\infty}^{\infty}\frac{\alpha(\tilde{x},\tilde{y})(x-\tilde{x})\boldsymbol{j}}{[(x-\tilde{x})^2+(y-\tilde{y})^2+(z-\tilde{z})^2]^{\frac{3}{2}}}\,d\tilde{z}\,d\tilde{y}\,d\tilde{x}\\
&\quad -\hat{\gamma}\int_{-1}^{1}\int_{-\delta}^{\delta}\int_{-\infty}^{\infty}\frac{\alpha(\tilde{x},\tilde{y})(y-\tilde{y})\boldsymbol{i}}{[(x-\tilde{x})^2+(y-\tilde{y})^2+(z-\tilde{z})^2]^{\frac{3}{2}}}\,d\tilde{z}\,d\tilde{y}\,d\tilde{x}, \qquad (2.50)
\end{aligned}$$

where $\hat{\gamma} = \bar{\gamma}\mu_0/4\pi$ and μ_0 is the permeability of free space measuring the ability of a material to support the formation of a magnetic field within itself. Simplifying, we get

$$\begin{aligned}
\boldsymbol{b}(x,y) := \boldsymbol{b}(\boldsymbol{x}) &= -2\hat{\gamma}\left(\int_{-1}^{1}\int_{-\delta}^{\delta}\frac{\alpha(\tilde{x},\tilde{y})(y-\tilde{y})}{(x-\tilde{x})^2+(y-\tilde{y})^2}\,d\tilde{y}\,d\tilde{x}\right)\boldsymbol{i}\\
&\quad +2\hat{\gamma}\left(\int_{-1}^{1}\int_{-\delta}^{\delta}\frac{\alpha(\tilde{x},\tilde{y})(x-\tilde{x})}{(x-\tilde{x})^2+(y-\tilde{y})^2}\,d\tilde{y}\,d\tilde{x}\right)\boldsymbol{j}. \qquad (2.51)
\end{aligned}$$

2.5.4 Forces

The goal in this section is to find the destabilizing magnetic self-forces (as a function of the deformation expressed as the curvature, μ, of the plate) that arise as a result of the electromagnetic self-field induced by the current per unit deformed volume. After we find them they are equilibrated with the elastic constraining forces, or contact forces under the given geometric constraints. As mentioned in [10] our body-force density function is given by $j(x)\times\boldsymbol{b}(x)$. However, we want to use the gradient $\boldsymbol{F}$ and its inverse transpose $\boldsymbol{F}^{-T}$ to transform the body-force from the reference to the deformed and from the deformed to the reference frame, respectively. Thus, we express the *body-force per unit reference volume* in the conducting plate as

$$\bar{\boldsymbol{f}}(\boldsymbol{x}) := (\boldsymbol{F}(\boldsymbol{x})j(x,y))\times(\boldsymbol{F}^{-T}(\boldsymbol{x})\boldsymbol{b}(x,y)). \qquad (2.52)$$

In our case, we compute $\boldsymbol{F}(\boldsymbol{x})\, j(x,y)$ to be

$$\begin{aligned}\boldsymbol{F}(\boldsymbol{x})\, j(x,y) &= (((\nu - y\mu)\boldsymbol{d}_1 + \eta\boldsymbol{d}_2)\boldsymbol{i} + \boldsymbol{d}_2\boldsymbol{j} + \boldsymbol{d}_3\boldsymbol{k})\, \bar{\gamma}\alpha(x,y)\boldsymbol{k} \\ &= \bar{\gamma}\alpha(x,y)\boldsymbol{d}_3. \end{aligned} \tag{2.53}$$

Using the results for $\boldsymbol{b}(x,y)$ in equation (2.51) and dotting it with $\boldsymbol{F}^{-T}(\boldsymbol{x})$ we get

$$\begin{aligned}\boldsymbol{F}^{-T}(\boldsymbol{x})\boldsymbol{b}(x,y) &= -2\hat{\gamma}\left(\int_{-1}^{1}\int_{-\delta}^{\delta} \frac{\alpha(\tilde{x},\tilde{y})\,(\eta(x)(x-\tilde{x}) + (y-\tilde{y}))}{\alpha(x,y)((x-\tilde{x})^2 + (y-\tilde{y})^2)}\, d\tilde{y}\, d\tilde{x}\right)\boldsymbol{d}_1 \\ &\quad +2\hat{\gamma}\left(\int_{-1}^{1}\int_{-\delta}^{\delta} \frac{\alpha(\tilde{x},\tilde{y})(x-\tilde{x})}{(x-\tilde{x})^2 + (y-\tilde{y})^2}\, d\tilde{y}\, d\tilde{x}\right)\boldsymbol{d}_2. \end{aligned} \tag{2.54}$$

Crossing equation (2.53) with equation (2.54) we find that

$$\begin{aligned}\bar{\boldsymbol{f}}(\boldsymbol{x}) &= 2\gamma^2\left(\int_{-1}^{1}\int_{-\delta}^{\delta} \frac{\alpha(x,y)\alpha(\tilde{x},\tilde{y})(x-\tilde{x})}{(x-\tilde{x})^2 + (y-\tilde{y})^2}\, d\tilde{y}\, d\tilde{x}\right)\boldsymbol{d}_3 \times \boldsymbol{d}_2 \\ &\quad -2\gamma^2\left(\int_{-1}^{1}\int_{-\delta}^{\delta} \frac{\alpha(\tilde{x},\tilde{y})\,(\eta(x)(x-\tilde{x}) + (y-\tilde{y}))}{(x-\tilde{x})^2 + (y-\tilde{y})^2}\, d\tilde{y}\, d\tilde{x}\right)\boldsymbol{d}_3 \times \boldsymbol{d}_1 \\ &= -2\gamma^2\left(\int_{-1}^{1}\int_{-\delta}^{\delta} \frac{\alpha(x,y)\alpha(\tilde{x},\tilde{y})(x-\tilde{x})}{(x-\tilde{x})^2 + (y-\tilde{y})^2}\, d\tilde{y}\, d\tilde{x}\right)\boldsymbol{d}_1 \\ &\quad -2\gamma^2\left(\int_{-1}^{1}\int_{-\delta}^{\delta} \frac{\alpha(\tilde{x},\tilde{y})\,(\eta(x)(x-\tilde{x}) + (y-\tilde{y}))}{(x-\tilde{x})^2 + (y-\tilde{y})^2}\, d\tilde{y}\, d\tilde{x}\right)\boldsymbol{d}_2, \end{aligned} \tag{2.55}$$

where $\gamma^2 = \bar{\gamma}^2\frac{\mu_0}{4\pi}$. Integrating over the cross-section $A(x)$ we get the *body-force per unit reference length*

$$\begin{aligned}\boldsymbol{f}(x,t) := \boldsymbol{f}(\boldsymbol{x}) &= \int_{-\delta}^{\delta}\int_{-\delta}^{\delta} \bar{\boldsymbol{f}}(\boldsymbol{x})\, dy\, dz \\ &= 2\delta\int_{-\delta}^{\delta} \bar{\boldsymbol{f}}(\boldsymbol{x})\, dy \\ &= -4\delta\gamma^2\int_{-1}^{1}\left(\int_{-\delta}^{\delta}\int_{-\delta}^{\delta} \frac{\alpha(x,y)\alpha(\tilde{x},\tilde{y})(x-\tilde{x})}{(x-\tilde{x})^2 + (y-\tilde{y})^2}\, d\tilde{y}\, dy\right) d\tilde{x}\boldsymbol{d}_1(x) \\ &\quad -4\delta\gamma^2\int_{-1}^{1}\left(\int_{-\delta}^{\delta}\int_{-\delta}^{\delta} \frac{\alpha(\tilde{x},\tilde{y})\,(\eta(x)(x-\tilde{x}) + (y-\tilde{y}))}{(x-\tilde{x})^2 + (y-\tilde{y})^2}\, d\tilde{y}\, dy\right) d\tilde{x}\boldsymbol{d}_2(x). \end{aligned}$$

After noting some symmetries in y and $\tilde{y}$, this reduces to

$$\begin{aligned}
\boldsymbol{f}(x,t) &= -4\delta\gamma^2 \int_{-1}^{1} (\nu(x)\nu(\tilde{x})k_1(x-\tilde{x}) + \mu(x)\mu(\tilde{x})k_3(x-\tilde{x}))\ d\tilde{x}\boldsymbol{d}_1(x) \\
&\quad -4\delta\gamma^2 \int_{-1}^{1} [\eta(x)\nu(\tilde{x})k_1(x-\tilde{x}) - \mu(\tilde{x})k_2(x-\tilde{x})]\ d\tilde{x}\boldsymbol{d}_2(x) \\
&=: -\gamma^2[f_1(x,t)\boldsymbol{d}_1(x,t) + f_2(x,t)\boldsymbol{d}_2(x,t)], \qquad (2.56)
\end{aligned}$$

where

$$\begin{aligned}
k_1(x-\tilde{x}) &= (x-\tilde{x}) \int_{-\delta}^{\delta}\int_{-\delta}^{\delta} \frac{1}{(x-\tilde{x})^2 + (y-\tilde{y})^2}\, d\tilde{y}\, dy \\
&= 4\delta \arctan\left(\frac{2\delta}{x-\tilde{x}}\right) - (x-\tilde{x}) \ln\left(1 + \frac{4\delta^2}{(x-\tilde{x})^2}\right), \\
k_2(x-\tilde{x}) &= \int_{-\delta}^{\delta}\int_{-\delta}^{\delta} \frac{\tilde{y}(\tilde{y}-y)}{(x-\tilde{x})^2 + (y-\tilde{y})^2}\, d\tilde{y}\, dy \\
&= 2\delta^2 - 2\delta(x-\tilde{x}) \arctan\left(\frac{2\delta}{x-\tilde{x}}\right) \\
&\quad + \frac{(x-\tilde{x})^2}{2} \ln\left(1 + \frac{4\delta^2}{(x-\tilde{x})^2}\right), \\
k_3(x-\tilde{x}) &= (x-\tilde{x}) \int_{-\delta}^{\delta}\int_{-\delta}^{\delta} \frac{y\tilde{y}}{(x-\tilde{x})^2 + (y-\tilde{y})^2}\, d\tilde{y}\, dy \\
&= \frac{4}{3}\delta^3 \arctan\left(\frac{2\delta}{x-\tilde{x}}\right) \\
&\quad + \frac{(x-\tilde{x})}{6}\left[4\delta^2 - (6\delta^2 + (x-\tilde{x})^2) \ln\left(1 + \frac{4\delta^2}{(x-\tilde{x})^2}\right)\right].
\end{aligned}$$

Similarly, we compute the *body-couple per unit reference length*, $\boldsymbol{l}(x)$, to be

$$\begin{aligned}
\boldsymbol{l}(x) &:= \boldsymbol{d}_2 \times \left(\int_{-\delta}^{\delta} \int_{-\delta}^{\delta} y \bar{\boldsymbol{f}}(\boldsymbol{x})\, dy\, dz \right) && (2.57)\\
&= 4\delta\gamma^2 \int_{-1}^{1} \left(\int_{-\delta}^{\delta} \int_{-\delta}^{\delta} \frac{\alpha(x,y)\alpha(\tilde{x},\tilde{y}) y (x-\tilde{x})}{(x-\tilde{x})^2 + (y-\tilde{y})^2}\, d\tilde{y}\, dy \right) d\tilde{x} \boldsymbol{d}_3 \\
&= 4\delta\gamma^2 \int_{-1}^{1} \left(\int_{-\delta}^{\delta} \int_{-\delta}^{\delta} \frac{(\nu(x) - y\mu(x))(\nu(\tilde{x}) - \tilde{y}\mu(\tilde{x})) y (x-\tilde{x})}{(x-\tilde{x})^2 + (y-\tilde{y})^2}\, d\tilde{y}\, dy \right) d\tilde{x} \boldsymbol{d}_3 \\
&= -4\delta\gamma^2 \int_{-1}^{1} (\nu(x)\mu(\tilde{x}) k_3(x-\tilde{x}) + \nu(\tilde{x})\mu(x) k_4(x-\tilde{x}))\, d\tilde{x} \boldsymbol{d}_3 \\
&=: \gamma^2 l(x,t) \boldsymbol{d}_3, && (2.58)
\end{aligned}$$

where

$$\begin{aligned}
k_4(x-\tilde{x}) &= (x-\tilde{x}) \int_{-\delta}^{\delta} \int_{-\delta}^{\delta} \frac{\tilde{y}^2}{(x-\tilde{x})^2 + (y-\tilde{y})^2}\, d\tilde{y}\, dy \\
&= \frac{2}{3}\delta \left(2\delta^2 - 3(x-\tilde{x})^2\right) \arctan\left(\frac{2\delta}{x-\tilde{x}}\right) \\
&\quad + \frac{(x-\tilde{x})}{3} \left[8\delta^2 - (3\delta^2 - (x-\tilde{x})^2) \ln\left(1 + \frac{4\delta^2}{(x-\tilde{x})^2}\right)\right].
\end{aligned}$$

For the purpose of later computations we take the derivative of $l(x,t)$ with respect to x, and get

$$\begin{aligned}
l_x(x) &= -4\delta \int_{-1}^{1} (\mu(\tilde{x})(\nu_x(x) k_3(x-\tilde{x}) + \nu(x) k_{3,x}(x-\tilde{x})) \\
&\quad + \nu(\tilde{x})(\mu_x(x) k_4(x-\tilde{x}) + \mu(x) k_{4,x}(x-\tilde{x}))\, d\tilde{x},
\end{aligned}$$

where $\boldsymbol{k}_{3,x}(x-\tilde{x})$ and $\boldsymbol{k}_{4,x}(x-\tilde{x})$ are, respectively,

$$\begin{aligned}
k_{3,x}(x-\tilde{x}) &= 2\delta^2 - \frac{1}{2}(2\delta^2 + (x-\tilde{x})^2) \ln\left(1 + \frac{4\delta^2}{(x-\tilde{x})^2}\right), \\
k_{4,x}(x-\tilde{x}) &= 4\delta^2 - 4\delta(x-\tilde{x}) \arctan\left(\frac{2\delta}{x-\tilde{x}}\right) + ((x-\tilde{x})^2 - \delta^2) \ln\left(1 + \frac{4\delta^2}{(x-\tilde{x})^2}\right).
\end{aligned}$$

Plots of these kernel functions can be found in Figures 2.3- 2.8. Note that the kernel function

are well behaved with respect to $x = \tilde{x}$ in the following sense:

$$\begin{aligned}
\lim_{x->\tilde{x}^{\pm}} k_1(x-\tilde{x}) &= \pm 2\delta\pi \\
\lim_{x->\tilde{x}} k_2(x-\tilde{x}) &= 2\delta^2 \\
\lim_{x->\tilde{x}^{\pm}} k_3(x-\tilde{x}) &= \pm\frac{2}{3}\delta^3\pi \\
\lim_{x->\tilde{x}^{\pm}} k_4(x-\tilde{x}) &= \pm\frac{2}{3}\delta^3\pi
\end{aligned}$$

Furthermore, although

$$\begin{aligned}
\lim_{x->\tilde{x}} k_{3,x}(x-\tilde{x}) &= -\infty, \quad \text{and} \\
\lim_{x->\tilde{x}} k_{4,x}(x-\tilde{x}) &= -\infty,
\end{aligned}$$

we can easily see that the integrals through the singularity are finite, so that they pose no problem to numerical calculations.

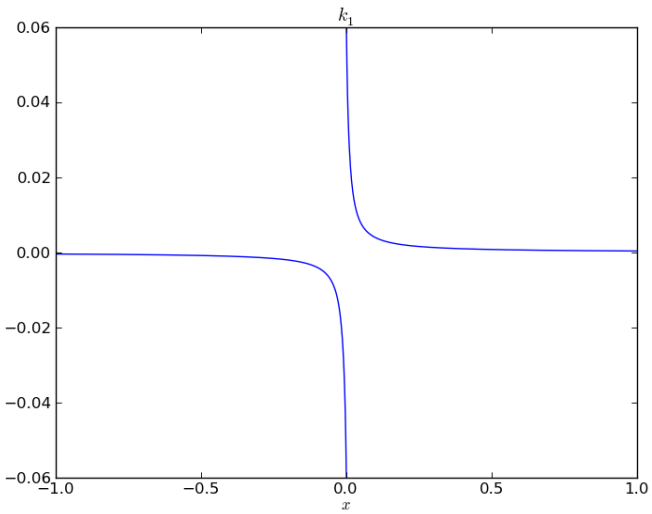

Figure 2.3: k_1

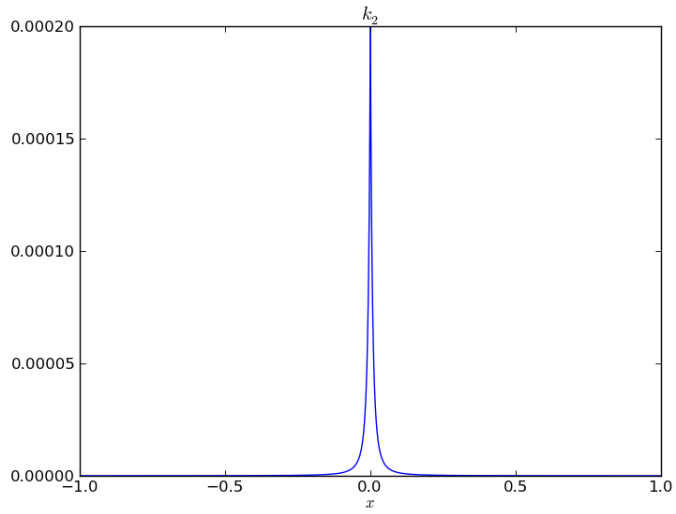

Figure 2.4: k_2

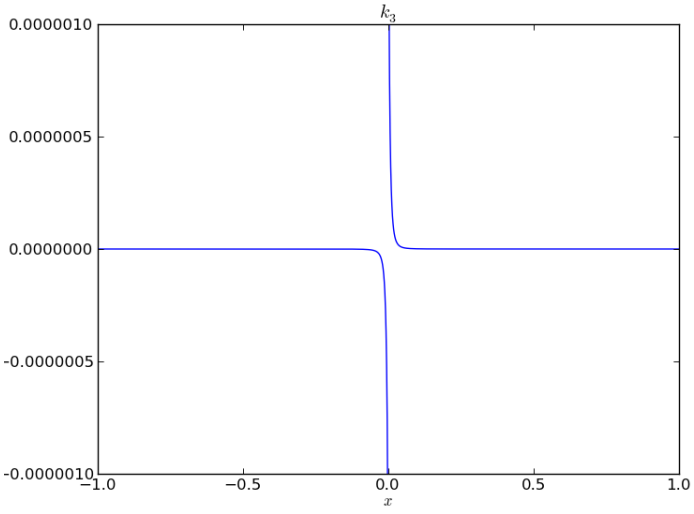

Figure 2.5: k_3

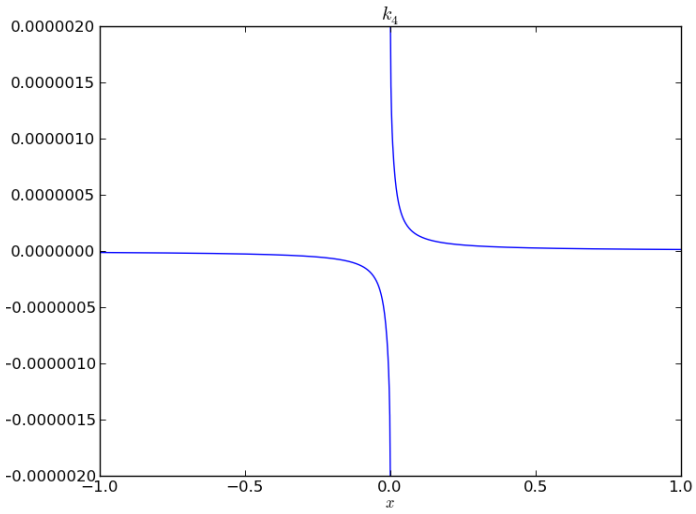

Figure 2.6: k_4

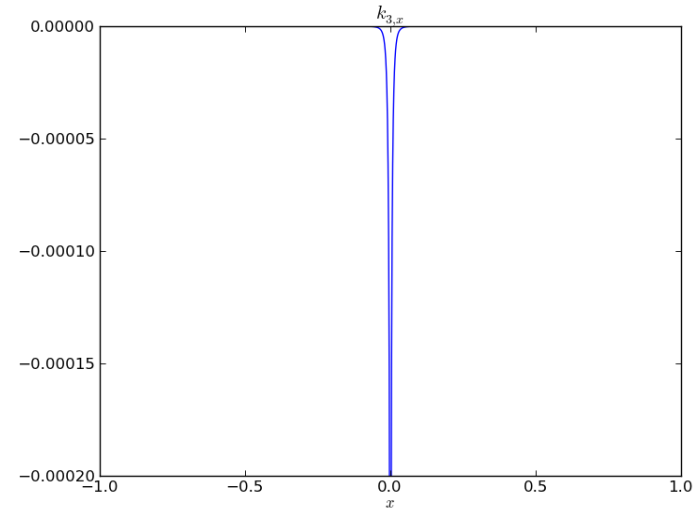

Figure 2.7: $k_{3,x}$

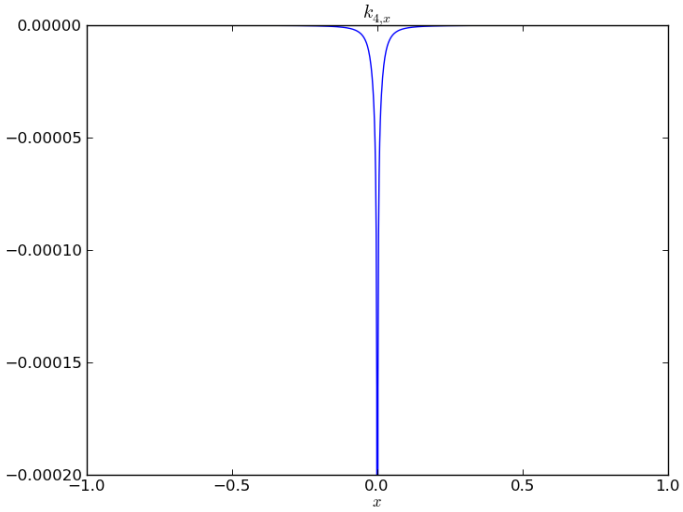

Figure 2.8: $k_{4,x}$

Chapter 3

A Duffing Equation

In this chapter we consider (2.34) in simplified form with $\gamma = 0$. That is, we consider the plate without an applied current. After some calculation our system reduces to a two-point boundary value problem of a Duffing equation. We first find the general solutions of our Duffing equation in terms of energy level sets which are depicted as closed periodic orbits. Then we look for the non-trivial solutions that satisfy our boundary values. As it turns out, there are two qualitatively different types of solutions given the boundary conditions: the "natural" buckled solutions that represent the obvious geometric deformation under load (see Figure 3.5), and the "inverted" solutions that represent a beam whose tangent vector at the ends (i.e. $\boldsymbol{d}_1(x)$) has the opposite orientation. Equivalently, one can understand this as a shift of θ by π. It is possible to define the exact analytical condition separating these two distinct solution sets, and in fact find an analytical expression for the exact initial conditions sufficient to solve the boundary value problem. This is acheived by computing the return "time" around a closed orbit for a fixed energy that we derive.

3.1 Derivation

If we assume that there are no body forces in system (2.41) then we are left with the following system of three equations in three unknowns:

$$N_x - \mu H = 0, \tag{3.1}$$

$$H_x + \mu N = 0, \tag{3.2}$$

$$EI\mu_x + H = 0. \tag{3.3}$$

Recall that N, H and μ are components of the contact force and couple in the $\boldsymbol{d}_1$, $\boldsymbol{d}_2$ and $\boldsymbol{d}_3$ directions, respectively. These equations describe the classical beam system [1]. An interesting physical problem to consider is the buckling behavior that results from an applied compressive load at both ends (i.e., $N(-1) = N(1) < 0$). This is in contrast to the usual buckling problem that assumes a vertical beam fixed to a surface at one end (e.g., $\theta(-1) = 0$) with a load applied at the other (e.g., $N(1) < 0$), which is well studied in the literature (e.g., [13]). As we will see later, this assumption is much more similar to the case when we apply current, and this is our motivation for studying the problem in this form.

Substituting (3.3) into (3.1) and integrating the resulting equation we get $N(x)$, i.e.

$$\begin{aligned} & N_x(x) = -EI\mu(x)\mu_x(x) = -\frac{EI}{2}\Big(\mu^2(x)\Big)_x \\ \Rightarrow \quad & N(x) - N(-1) = -\frac{EI}{2}\left(\mu^2(x) - \mu^2(-1)\right) \\ \Rightarrow \quad & N(x) = -\frac{EI}{2}\left(\mu^2(x) - \mu^2(-1)\right) + N(-1) \end{aligned} \tag{3.4}$$

Differentiating (3.3) with respect to x and solving it for $H_x(x)$ we get

$$H_x(x) = -EI\mu_{xx}(x) \tag{3.5}$$

Substituting (3.5) into (3.2) we get,

$$\begin{aligned} -EI\mu_{xx}(x) + \mu(x)\left(-\frac{EI}{2}\left(\mu^2(x) - \mu^2(-1)\right) + N(-1)\right) &= 0 \\ \Rightarrow -EI\mu_{xx}(x) - \frac{EI}{2}\mu^3(x) + (EI\,k)\,\mu(x) &= 0 \\ \Rightarrow \mu_{xx}(x) - k\mu(x) + \frac{1}{2}\mu^3(x) &= 0, \end{aligned} \tag{3.6}$$

where $k = -\lambda + \frac{1}{2}\mu^2(-1)$, $\lambda = -\frac{N(-1)}{EI}$. In this case, we think of positive λ as the applied load at $N(-1)$ (and negative λ as a tensile force), normalized by the constant EI (which we take as = 1 in the following for simplicity, keeping in mind that λ would need to be scaled appropriately in any real context). To complete the expression of the boundary value problem, we prescribe the contact force and couple acting at the ends of the beam by requiring the following boundary conditions, which describe a compressive load acting along the beam:

$$N(-1) = N(1) = -\lambda, \tag{3.7}$$

$$H(-1) = H(1) = 0. \tag{3.8}$$

In light of (3.4), it must be that $\mu^2(1) = \mu^2(-1)$. For reasons that will become clear in Chapter 4, we restrict our attention to the case where $\mu(x)$ is an even function, so that

$$\mu(-1) = \mu(1) = \mu_*, \tag{3.9}$$

for some fixed μ_*. In addition, we must factor out rotation by fixing $\theta(0) = 0$, so that $\theta(x)$ is an odd function. This completely defines our boundary value problem. A carefule justification of the boundary conditons will be done in Chapter 4.

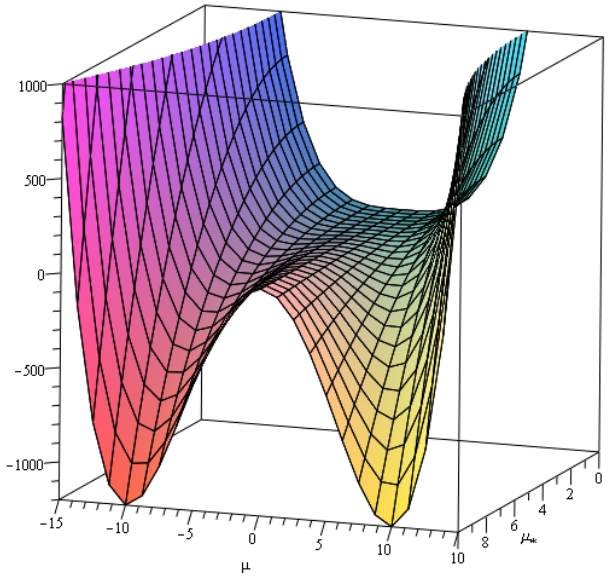

Figure 3.1: The potential function $P_k(\mu) = -\frac{k(\lambda,\mu_*)}{2}\mu^2 + \frac{1}{8}\mu^4$ for a fixed $\lambda = 1$.

3.2 Analysis

Denoting differentiation with respect to x by "$\dot{}$", we rewrite our system as a second-order boundary value problem:

$$\ddot{\mu} - k\mu + \frac{1}{2}\mu^3 = 0, \tag{3.10}$$

with boundary conditions

$$\mu(-1) = \mu(1) = \mu_*, \tag{3.11}$$

$$\dot{\mu}(-1) = \dot{\mu}(1) = 0, \tag{3.12}$$

where (3.12) follows from (3.3). Recall also that k depends on μ_* ($k = -\lambda + \frac{1}{2}\mu_*^2$), so we should think of (3.10) as a family of differential equations parameterized by μ_*. This is a bit different than the usual situation where we think of (3.10) as a fixed equation and we change μ_* to view different solutions. In this case, we must select μ_* first (which is natural because it defines the boundary values) and then consider (3.10) in this context. This, in fact, makes the numerical algorithm we use to solve the boundary value problem more interesting, as we shall see in Chapter 4.

We begin the analysis by recognizing that (3.10) is in the form of a conservative process (because $\dot{\mu}$ is not present), so that multiplying through by $\dot{\mu}$ gives us

$$\begin{aligned} 0 &= \ddot{\mu}\dot{\mu} - k\mu\dot{\mu} + \frac{1}{2}\mu^3\dot{\mu} && (3.13) \\ &= \frac{d}{dx}\left[\frac{1}{2}\dot{\mu}^2 - \frac{k}{2}\mu^2 + \frac{1}{8}\mu^4\right]. && (3.14) \end{aligned}$$

A nice feature of conservative systems is that their behavior is characterized by an "energy" function, in this case $E_k = \frac{1}{2}\dot{\mu}^2 - \frac{k}{2}\mu^2 + \frac{1}{8}\mu^4$, whose level sets define solutions that are closed, periodic orbits. To visualize this, set $\xi = \dot{\mu}$, $p_k(\mu) = -k\mu + \frac{1}{2}\mu^3$ and $P_k(\mu) = \int_0^\mu p(s)\,ds = -\frac{k}{2}\mu^2 + \frac{1}{8}\mu^4$, where P_k is the potential function (see Figure 3.1).

We then rewrite (3.10) as a first order system

$$\begin{cases} \dot{\mu} &= \xi \\ \dot{\xi} &= k\mu - \frac{1}{2}\mu^3 = -p_k(\mu), \end{cases} \tag{3.15}$$

along with our conserved quantity, E_k, which we can rewrite as a kinetic term plus the potential function P_k:

$$E_k(\mu, \xi) = \frac{1}{2}\xi^2 + P_k(\mu). \tag{3.16}$$

In this form, the solutions to (3.15) can be viewed as the level sets

$$\{E_k(\mu, \xi) = E_k^0 |\ E_k^0 \in [0, \infty)\}$$

in the phase plane (see Figure 3.2), except in the case that $\lambda = 0$, which we treat separately below.

Assuming that $\lambda \neq 0$, it is evident from Figure 3.1 that the equilibrium points of (3.15) are the extreme points of the potential energy function. For $k > 0$, i.e. $\sqrt{2\lambda} < |\mu_*|$, there are two centers corresponding to the two nondegenerate minima, found at $(\pm\sqrt{2k}, 0)$, and a saddle point at the origin corresponding to the maximum. The stable and unstable manifolds to the origin

form two homoclinic orbits about each of $(\pm\sqrt{2k}, 0)$, making a figure eight pattern. For $k < 0$, i.e. $\sqrt{2\lambda} \geq |\mu_*|$, the only minimum is at the origin, and all solutions are centers about the origin. In Figure 3.2, we have overlayed these orbits for $\lambda = 1$ for various μ_*. Recall that since the differential equations depend on μ_*, these are solutions to different equations (and hence can overlap). All orbits inside and outside the homoclinic loops are periodic, as noted above, as well as symmetric with respect to the μ-axis. Those orbits that fall outside of the figure eight are also symmetric with respect to the ξ-axis (see Figure 3.2).

Now, for $\lambda = 0$, we have a degeneracy because $k = \frac{1}{2}\mu_*^2$, so that

$$\dot{\xi} = \frac{1}{2}\mu_*^2\mu - \frac{1}{2}\mu^3.$$

At $x = -1$, we then have $\dot{\mu} = 0, \dot{\xi} = 0$ so that $\mu(x) = \mu_*$ and all points $(\mu_*, 0)$ are equilibrium points for (3.15), and μ is constant. Therefore $\theta(x) = \mu_* x$ since we have fixed $\theta(0) = 0$. Recalling that $r(x) = \cos\theta\boldsymbol{i} + \sin\theta\boldsymbol{j}$, we see that these solutions lie on a circle. For $\mu_* = n\pi$, $n \in \mathbb{Z}$, the beam is closed and lies on a circle (making n revolutions), and these are the points at which we "connect" with the $\lambda \neq 0$ solutions discussed above.

Our goal, now, is to find solutions that satisfy (3.11)- (3.12). That is, we need to find any closed orbit starting and ending at the same point on the μ-axis with a "period" $X = 2$. Evidently, there are at least two qualitatively different sets of solutions, since both those solutions inside and outside the figure eight can potentially satisfy these conditions (see Figure 3.2). To ensure $X = 2$, let us compute the return "time" around a closed orbit that encircles the origin for a fixed "energy", $E_{k,*} = \frac{1}{2}\xi_*^2$, so that for simplicity we have "started" our solution at $(0, \xi_*)$. In this case, we need only compute the time it takes to do a quarter of the solution down to $(\mu_*, 0)$:

$$\begin{aligned} X &= 4\int_0^{X/4} dx \\ &= 4\int_0^{\mu_*} \frac{dx}{d\mu} d\mu \\ &= 4\int_0^{\mu_*} \frac{d\mu}{\xi(\mu)} \\ &= 4\int_0^{\mu_*} \left(2E_{k,*} + k\mu^2 - \frac{1}{4}\mu^4\right)^{-1/2} d\mu. \end{aligned}$$

Now, if $k \approx 0$ or $\lambda \approx \frac{1}{2}\mu_*^2$, the above integral simplifies to

$$\begin{aligned} X &\approx \left(\frac{2^9\pi^2}{E_{k,*}}\right)^{1/4} \cdot \frac{\Gamma(\frac{5}{4})}{\Gamma(\frac{3}{4})} \\ &\approx 3.51848\left(\frac{\pi^2}{E_{k,*}}\right)^{1/4} \end{aligned}$$

In this case, solving $X = 2$ gives us that

$$E_{k,*} \approx 9.57853\pi^2.$$

We plug this value in equation $\mu_* = \sqrt{2k + 2\sqrt{2E_{k,*} + k^2}}$, which we derived by solving equation (3.16) for μ_*, to get

$$\mu_* \approx 5.24412.$$

We see that there is a non-trivial solution to the boundary value problem (3.10) with (3.11)- (3.12) given by the contour of the energy function going through $(\mu, \xi) = (5.24412, 0)$. In this case, since our assumption was that $k \approx 0$, we also have that $\lambda \approx (8 \cdot E_{k,*})^{1/4} = 13.7504$. This corresponds to one of the "natural" solutions depicted in Figure 3.5 (for $\lambda = 13.7504$).

The fact that we chose to encircle the origin only once was arbitrary, and we can in fact extend this result to include more solutions by replacing the multiplying factor of 4 with $4n$, where n is the number of revolutions about the origin. In this case, our previous result is extended to

$$X \approx 3.51848 \cdot n\left(\frac{\pi^2}{E_{k,*}}\right)^{1/4}$$

so that for $X = 2$, we have $\mu_* = 5.24412 \cdot n$. These solutions are depicted in the following section in Figure 3.4 where the $k = 0$ curve intersects the natural solutions.

3.3 Bifurcations and Buckling

Having found non-trivial solutions analytically paves the way for a numerical investigation, but first a couple of questions immediately come to mind:

1. Are there branching points from the trivial solution connecting to the solutions found analytically in the previous section?

2. Do we have multiple overlapping solutions corresponding to buckled states of the beam?

To search for branching points, we return to the intergral of the last section. In this case, however, instead of the making the assumption that $k \approx 0$, we suppose that $\mu_* \approx 0$ so that $k \approx -\lambda$ and we can then neglect the higher order terms in μ. We proceed as follows, working with the assumption that μ_*^2 and μ^2 are small but we neglect terms of $O(\mu^4)$:

$$\begin{aligned} X &= 4n \int_0^{\mu_*} \left(2E_{k,*} + k\mu^2 - \frac{1}{4}\mu^4 \right)^{-1/2} d\mu \\ &\approx 4n \int_0^{\mu_*} \left(2E_{k,*} - \lambda\mu^2 \right)^{-1/2} d\mu \end{aligned}$$

Now, if $\xi = 0$, (3.16) gives us that $2E_{k,*} \approx \lambda\mu_*^2$ so that our integral reduces to

$$X \approx 4n \int_0^{\mu_*} \left(\lambda\mu_*^2 - \lambda\mu^2 \right)^{-1/2} d\mu,$$

which is an elementary integral. Solving for λ when $X = 2$ results in

$$\hat{\lambda}_n = n^2\pi^2, \text{ for } n = 1, 2, \ldots \tag{3.17}$$

and we have found the special $\hat{\lambda}_n$ such that there exist non-trivial solutions to the boundary value problem for small μ_* near $\hat{\lambda}_n$. That is, each $\hat{\lambda}_n$ is a bifurcation or branching point for the system corresponding to n revolutions about the origin.

This partially answers question 1) above. To see how these two different sets of solutions connect (the solutions found along $k = 0$ and $\mu_* = 0$), and to answer question 2) above, we move on to numerical methods. Figure 3.4 shows the results of continuing from the branching points (following the numerical procedure defined in Chapter 5). For all λ, there is the trivial solution (i.e., $\mu \equiv 0, \xi \equiv 0$). From each of the branch points, we see that as we increase λ, we do connect to the $k = 0$ solutions found previously, confirming our analytical results. The answer to question 2) is immediately evident from the figure, as we clearly have multiple non-trivial solutions for all λ (including for $\lambda < 0$).

Plotted in Figure 3.4 we see a curve marked "Energy=0". This marks the boundary between the natural and inverted solutions, defined by $E_{k,*} = 0$, and corresponds to the infinite period solutions that form the two homoclinic orbits, as can be seen in Figure 3.2. Substituting $(\mu_*, 0)$ into (3.16)

results in an equation for this boundary in λ and μ_*:

$$\begin{aligned} E_{k,*} = -\frac{k}{2}\mu_*^2 + \frac{1}{8}\mu_*^4 = 0 \quad &\Rightarrow \quad \frac{-(-\lambda + \frac{1}{2}\mu_*^2)}{2}\mu_*^2 + \frac{1}{8}\mu_*^4 = 0 \\ &\Rightarrow \quad \frac{\lambda}{2}\mu_*^2 - \frac{1}{4}\mu_*^4 + \frac{1}{8}\mu_*^4 = 0 \\ &\Rightarrow \quad \lambda = \frac{1}{4}\mu_*^2 \end{aligned} \tag{3.18}$$

The solutions outside the $E_{k,*}$ curve are "inverted" in the sense that $\boldsymbol{d}_1(x)$ has flipped direction along with the sign change of the energy. To better visualize these and other solutions, we plot the resulting beam curves in Figures 3.5-3.6.

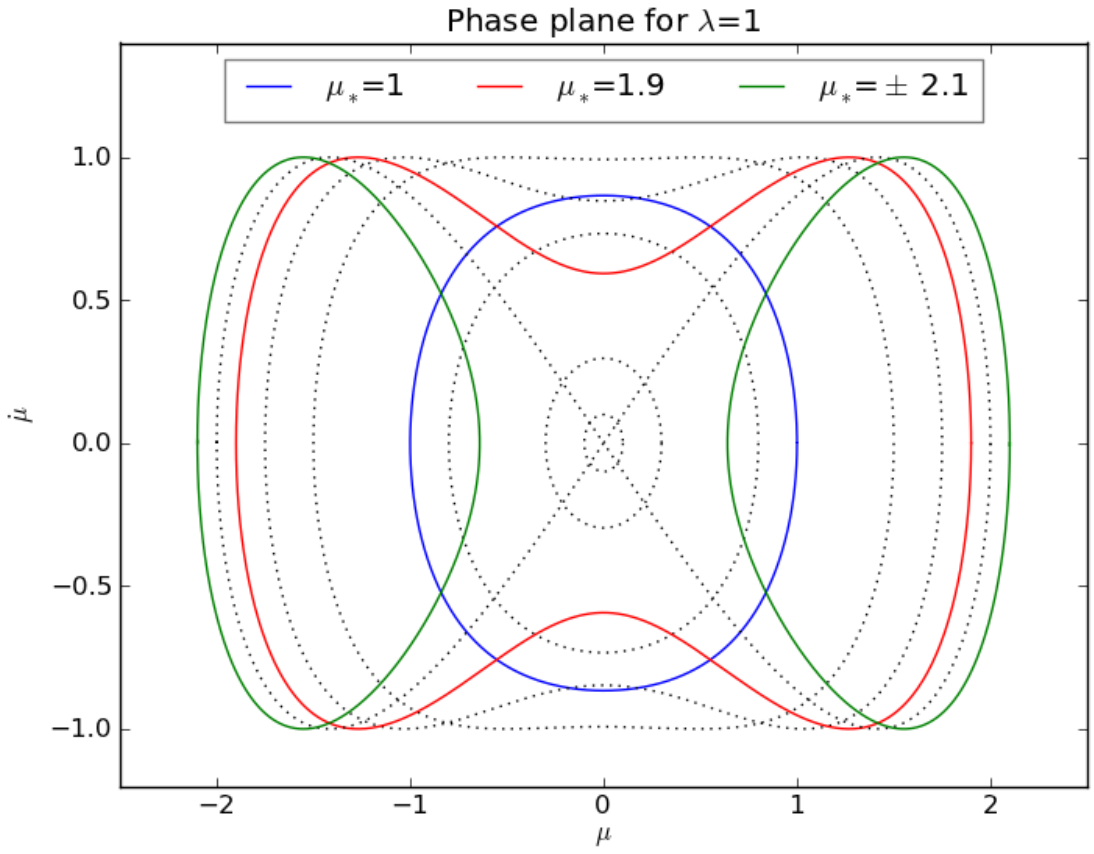

Figure 3.2: For fixed $\lambda = 1$, this plot depicts solutions in the phase plane (μ, μ') to the equation (3.10) for various initial conditions $(\mu_*, 0)$. As we can see, there are at least two qualitatively different types of solutions: those that encircle the origin (blue and red curves), and those that do not (green curve). If we suppose that for each curve, we had alternate boundary conditions $\mu(0) = \mu(x_*) = \mu_*$ and $\dot{\mu}(0) = \dot{\mu}(x_*) = 0$ for some minimal period x_*, then these solutions correspond to different beam shapes (see Figure 3.3). That the green solution is qualitatively different from the blue and red is seems rather obvious in the phase plane, but it is not immediately clear what the consequence on the shape of the beam is. We refer to these two different solution types as "natural" and "inverted", and this terminology is made clear by Figure 3.3. The boundary between the natural and inverted solutions corresponds to the level set $E_{k,*} = 0$, which happens along the curve $\mu_* = 2\sqrt{\lambda}$.

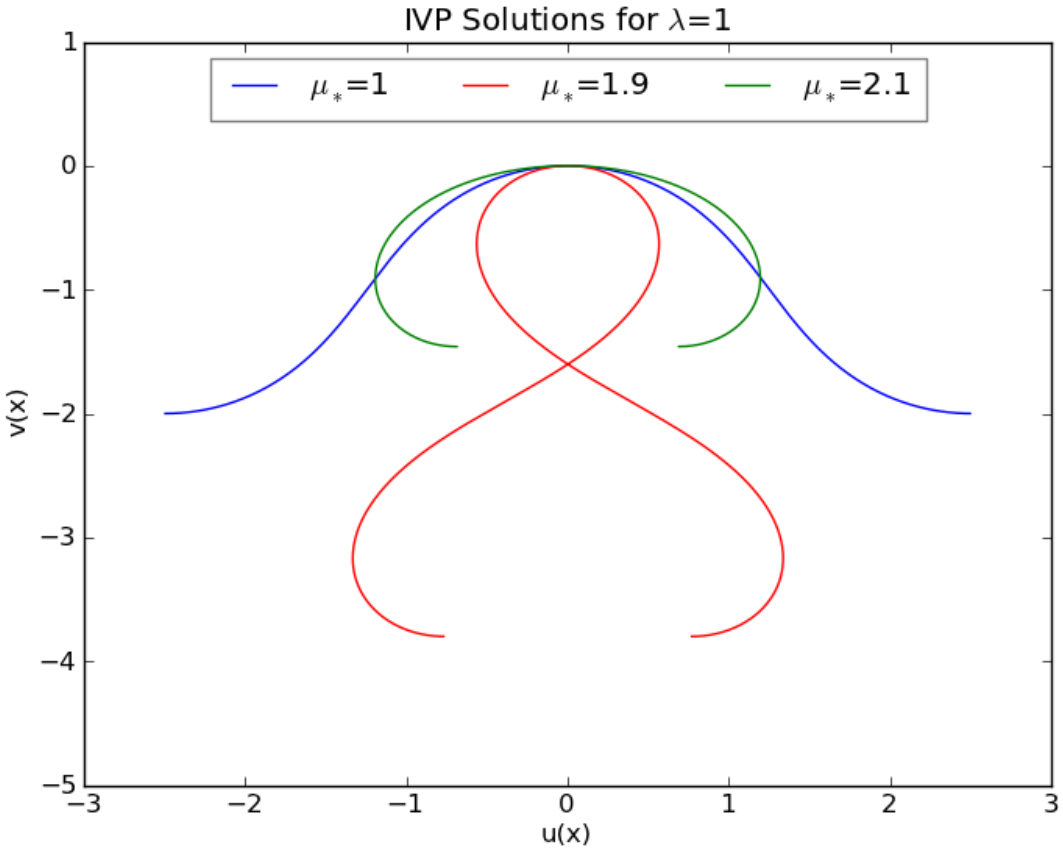

Figure 3.3: For fixed $\lambda = 1$, we have the beam solutions corresponding to those presented in Figure 3.2 where we've anchored $(u(\mu(\frac{x_*}{2})), v(\mu(\frac{x_*}{2})))$ at the origin. When we consider that $\lambda = 1$ represents a compressive load along the beam, we see that the blue and red curved are "natural" in the sense that applying our load to an initially straight beam could produce this deformation (and increasing λ would squeeze the beam more). For the green curve, we have the "inverted" sense where our initial beam is in the shape of a circle (for $\lambda = 0$) and λ decreasing tends to separate this circle (see Figure 3.6). This inversion is due to the fact that for these solutions, $\boldsymbol{d}_1(x)$ has the opposite orientation with respect to the end of the beams. This, in effect, flips the notion of tensile vs. compressive contact force at the beam ends so that a negative lambda active has what appears to be a compressive action (in the sense that compression would be from the end directed in toward the beam).

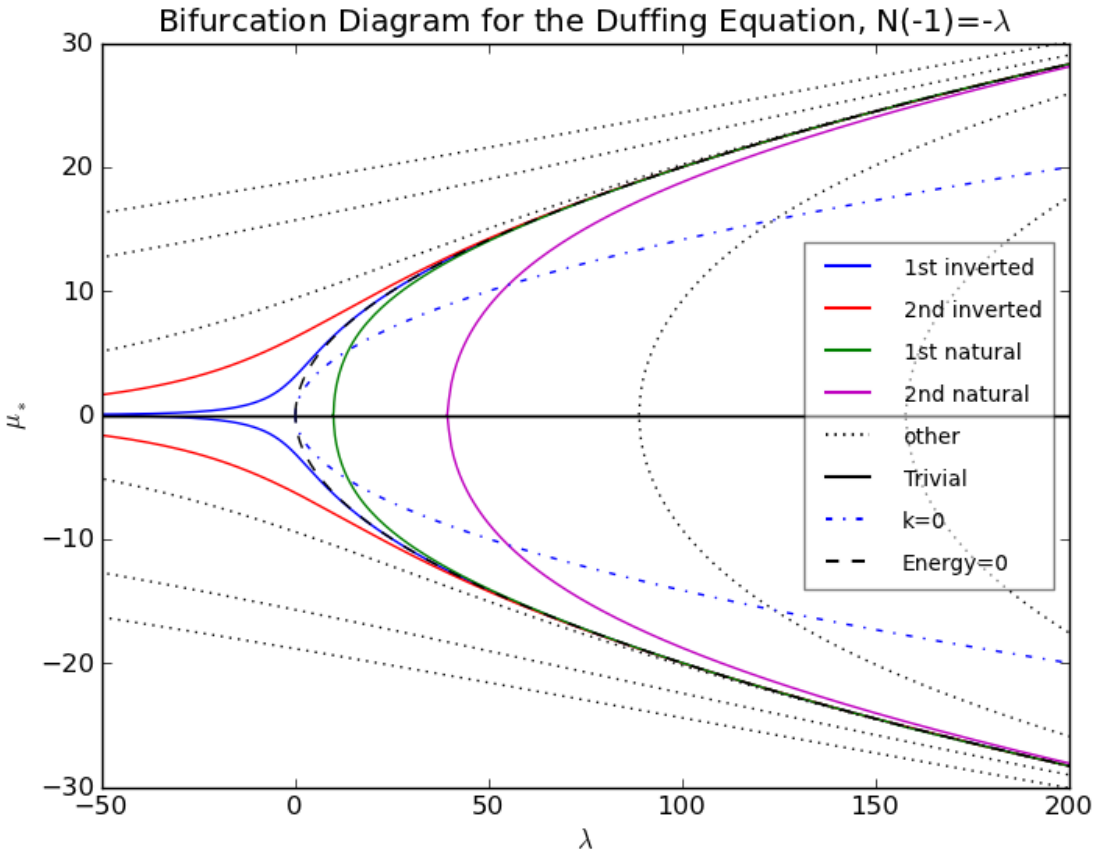

Figure 3.4: Bifurcation diagram for system (3.10)-(3.12) in λ. This diagram is generated by feeding initial points on these curves to a continuation algorithm that is described in Chapter 4. For the natural solution branches (those inside of the *Energy* = 0 curve), we can start the continuation algorithm with either of the analytically found solutions for $\mu_* = 0$ or $k = 0$ (that is, the branching points on the λ-axis or the non-trivial solutions on the $k = 0$ curve). For the inverted solutions, we numerically tested values along the μ_* axis to find starting points. The shape of the beam along the various branches in this diagram are plotted in Figures 3.5 and 3.6.

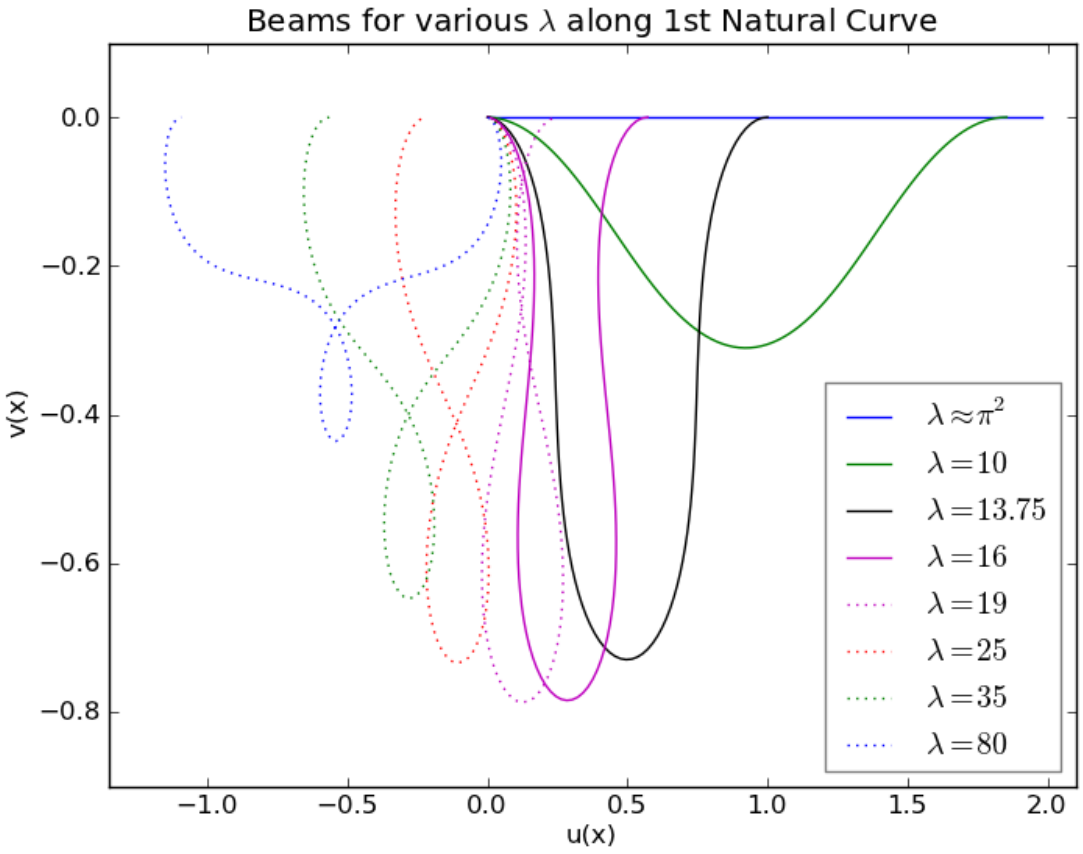

Figure 3.5: Beams for various λ along the 1st natural curve in Figure 3.4, corresponding to a single revolution about the origin. For visual clarity, we have anchored $\boldsymbol{r}(-1) = (0, 0)$ in these plots. Starting with $\lambda \approx \pi^2$, the first bifurcation for $\lambda > 0$, the blue beam is "near" trivial though λ was chosen slightly larger in order to be non-trivial. We then continue along the curve for increasing λ plotting beams as we go. The black curve for $\lambda = 13.75$ corresponds to the intersection of the 1st natural curve with $k = 0$ that we derived analytically in this chapter. For $\lambda > 19$, we see that the curve self-intersects so that we no longer have a physical solution (all dotted curves are non-physical). In the limit as $\lambda \to \infty$, the curve approaches an inverted solution, a fact that can be seen by comparison with Figure 3.6. The 2nd natural branch has similar solutions analogous to the 1st branch except for the fact that there are two, rather than one, bumps. Note that these beams correspond to the lower branch for $\mu_* < 0$. Beams along the upper branch are symmetric with respect to the u-axis in the picture.

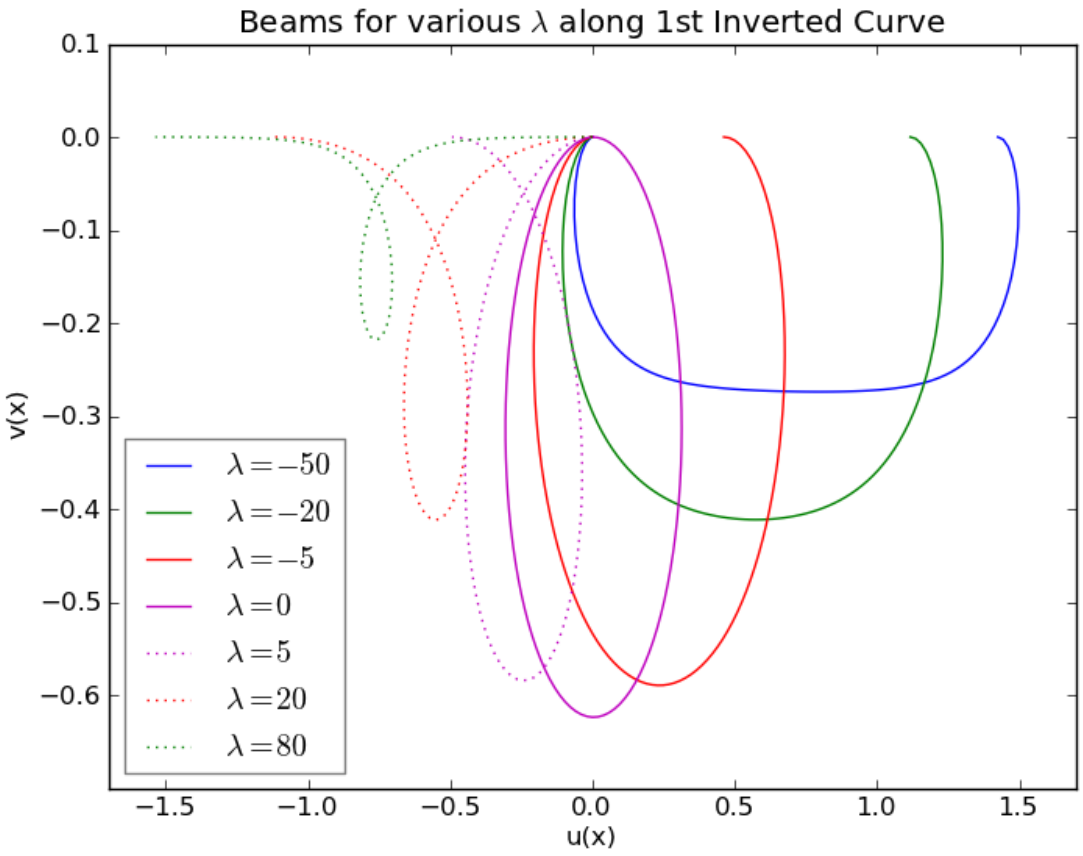

Figure 3.6: Beams for various λ along the 1st inverted curve in Figure 3.4. For visual clarity, we have anchored $\boldsymbol{r}(-1) = (0, 0)$ in these plots. Recall that "inverted" in this context means that $\boldsymbol{d}_1(x)$ has an inverted orientation at the end of the beam and hence the notion of compressive vs. tensile is switched. This is apparent for $\lambda = -50$, where we see that what would normally be called a tensile contact force at the boundary appears to have a compressive action on the beam end. In this case, we see that for $\lambda > 0$ the beam solutions are non-physical.

Chapter 4

Full Nonlinear Static System

In contrast to Chapter 3, we will now consider (2.33) with an applied current, $\gamma \neq 0$. Since our focus is on static equilibrium configurations or buckled states, we pick up after the derivation of the basic equations as given in Chapter 2, and concentrate on the static version of nonlinear system of equations (2.33)

$$N_x - \mu H - \gamma^2 f_1 = 0, \tag{4.1}$$
$$H_x + \mu N - \gamma^2 f_2 = 0, \tag{4.2}$$
$$EI\mu_x + H + \gamma^2 l = 0. \tag{4.3}$$

Before diving into the analysis, we first discuss the boundary conditions (with $\gamma = 0$ as a special case to cover the previous chapter's results).

4.1 Justification of Boundary Conditions

For $\gamma > 0$, we would like to have the contact forces at the ends of the beam vanish because our focus is on the effect of the self-forces generated by an increasing current, γ. When $\gamma = 0$, we achieve the compression by assuming non-zero values for $N(\pm 1)$. However, note we are not free to choose forces and couples at both ends of the beam in an arbitrary fashion because for an equilibrium

problem, the sum of the forces and couples must vanish [1]. That is

$$\begin{aligned} 0 &= \boldsymbol{n}(1) - \boldsymbol{n}(-1) + \int_{-1}^{1} \boldsymbol{f}(x)\, dx \quad \textit{and} \qquad (4.4) \\ 0 &= \boldsymbol{m}(1) - \boldsymbol{m}(-1) + \boldsymbol{r}(1) \times \boldsymbol{n}(1) - \boldsymbol{r}(-1) \times \boldsymbol{n}(-1) \\ &\quad + \int_{-1}^{1} [\boldsymbol{r}(x) \times \boldsymbol{f}(x) + \boldsymbol{l}(x)]\, dx. \qquad (4.5) \end{aligned}$$

Let us consider each of equations (4.4) and (4.5) in terms of their components. In the following to simplify notation, set $c_{\pm 1} = \cos\theta(\pm 1)$ and $s_{\pm 1} = \sin\theta(\pm 1)$. So, for (4.4), we must satisfy

$$\begin{aligned} 0 &= \boldsymbol{n}(1) - \boldsymbol{n}(-1) + \int_{-1}^{1} \boldsymbol{f}(x)\, dx \\ &= (N\boldsymbol{d}_1 + H\boldsymbol{d}_2)(1) - (N\boldsymbol{d}_1 + H\boldsymbol{d}_2)(-1) + \int_{-1}^{1} \boldsymbol{f}(x)\, dx \\ &= N(1)(c_1\boldsymbol{i} + s_1\boldsymbol{j}) + H(1)(-s_1\boldsymbol{i} + c_1\boldsymbol{j}) \\ &\quad -N(-1)(c_{-1}\boldsymbol{i} + s_{-1}\boldsymbol{j}) - H(-1)(-s_{-1}\boldsymbol{i} + c_{-1}\boldsymbol{j})(-1) \\ &\quad + \int_{-1}^{1} \boldsymbol{f}(x)\, dx \\ &= [N(1)c_1 - H(1)s_1 - N(-1)c_{-1} + H(-1)s_{-1}]\ \boldsymbol{i} \\ &\quad + [N(1)s_1 + H(1)c_1 - N(-1)s_{-1} - H(-1)c_{-1}]\ \boldsymbol{j} \\ &\quad + \int_{-1}^{1} \boldsymbol{f}(x)\, dx. \end{aligned} \qquad (4.6)$$

For equation (4.5), we must satisfy

$$
\begin{aligned}
0 &= \boldsymbol{m}(1) - \boldsymbol{m}(-1) + \boldsymbol{r}(1) \times \boldsymbol{n}(1) - \boldsymbol{r}(-1) \times \boldsymbol{n}(-1) \\
&\quad + \int_{-1}^{1} [\boldsymbol{r}(x) \times \boldsymbol{f}(x) + \boldsymbol{l}(x)]\, dx \\
&= (M(1) - M(-1))\boldsymbol{k} \\
&\quad + (r_1(1)\boldsymbol{i} + r_2(1)\boldsymbol{j}) \times (N(1)(c_1\boldsymbol{i} + s_1\boldsymbol{j}) + H(1)(-s_1\boldsymbol{i} + c_1\boldsymbol{j}) \\
&\quad - (r_1(-1)\boldsymbol{i} + r_2(-1)\boldsymbol{j}) \times (N(-1)(c_{-1}\boldsymbol{i} + s_{-1}\boldsymbol{j}) + H(-1)(-s_{-1}\boldsymbol{i} + c_{-1}\boldsymbol{j}) \\
&\quad + \int_{-1}^{1} [\boldsymbol{r}(x) \times \boldsymbol{f}(x) + \boldsymbol{l}(x)]\, dx \\
&= (M(1) - M(-1))\boldsymbol{k} \\
&\quad + (r_1(1)\boldsymbol{i} + r_2(1)\boldsymbol{j}) \times ((N(1)c_1 - H(1)s_1)\boldsymbol{i}) + (N(1)s_1 + H(1)c_1)\boldsymbol{j}) \\
&\quad - (r_1(-1)\boldsymbol{i} + r_2(-1)\boldsymbol{j}) \times ((N(-1)c_{-1} - H(-1)s_{-1})\boldsymbol{i}) + (N(-1)s_{-1} + H(-1)c_{-1})\boldsymbol{j}) \\
&\quad + \int_{-1}^{1} [\boldsymbol{r}(x) \times \boldsymbol{f}(x) + \boldsymbol{l}(x)]\, dx \\
&= (M(1) - M(-1))\boldsymbol{k} \\
&\quad + (r_1(1)(N(1)s_1 + H(1)c_1) - r_2(1)(N(1)c_1 - H(1)s_1) \\
&\quad - r_1(-1)(N(-1)s_{-1} + H(-1)c_{-1}) + r_2(-1)(N(-1)c_{-1} - H(-1)s_{-1})\boldsymbol{k} \\
&\quad + \int_{-1}^{1} [\boldsymbol{r}(x) \times \boldsymbol{f}(x) + \boldsymbol{l}(x)]\, dx \\
&= [M(1) - M(-1) \\
&\quad + r_1(1)N(1)s_1 + r_1(1)H(1)c_1 - r_2(1)N(1)c_1 + r_2(1)H(1)s_1 \\
&\quad - r_1(-1)N(-1)s_{-1} - r_1(-1)H(-1)c_{-1} + r_2(-1)N(-1)c_{-1} - r_2(-1)H(-1)s_{-1}]\boldsymbol{k} \\
&\quad + \int_{-1}^{1} [\boldsymbol{r}(x) \times \boldsymbol{f}(x) + \boldsymbol{l}(x)]\, dx
\end{aligned} \tag{4.7}
$$

Now, given the physics (uniform current) and the expressed forms of the kernels for the problem—namely that k_1, k_3 and k_4 are odd and k_2 is even—it is natural to concentrate on solutions exhibiting symmetry, and we concentrate our attention on the case where μ is even, though the case where μ is odd should exhibit similar characteristics (all results in this thesis focus on even solutions).

When μ is even, θ is odd. Let us first consider when there is no current, i.e. $\gamma = 0$, to cover the results of Chapter 3. In this case, $\boldsymbol{f}(x) = -\gamma(f_1\boldsymbol{d}_1 + f_2\boldsymbol{d}_2) = 0$, and the integral terms vanish. These

assumptions transform equation (4.4) into

$$\begin{aligned} 0 &= [N(1)c_{-1} + H(1)s_{-1} - N(-1)c_{-1} + H(-1)s_{-1}]\ \boldsymbol{i} \\ &\quad + [-N(1)s_{-1} + H(1)c_{-1} - N(-1)s_{-1} - H(-1)c_{-1}]\ \boldsymbol{j} \\ &= [(N(1) - N(-1))c_{-1} + (H(1) + H(-1))s_{-1}]\ \boldsymbol{i} \\ &\quad + [-(N(1) + N(-1))s_{-1} + (H(1) - H(-1))c_{-1}]\ \boldsymbol{j}. \end{aligned}$$

Using the boundary conditions from Chapter 3, $N(1) = N(-1) = -\lambda$ and $H(1) = H(-1) = 0$, we notice that the $\boldsymbol{i}$-terms vanish, and that the $\boldsymbol{j}$-terms reduce to

$$0 = 2\lambda s_{-1} \tag{4.8}$$

which gives us a constraint on θ, i.e.

$$\theta(-1) = n\pi \tag{4.9}$$

As it turns out, this constraint makes sense because, noting that

$$\theta(x) = \int_{-1}^{x} \mu(s)\, ds + \theta(-1) \tag{4.10}$$

we have

$$\begin{aligned} \theta(1) = -\theta(-1) &= \int_{-1}^{1} \mu(s)\, ds + \theta(-1) \\ -2\theta(-1) &= 2\int_{-1}^{0} \mu(s)\, ds \quad \text{half-way around a symmetric solution} \\ &= 2\int_{a}^{b} \mu \frac{ds}{d\mu} d\mu \\ &= 2\int_{a}^{b} \frac{\mu}{\xi(\mu)}\, d\mu \\ &= 2\int_{a}^{b} \frac{\mu}{\left(2E_{k,*} + k\mu^2 - \frac{1}{4}\mu^4\right)^{1/2}} d\mu \\ &= 2\arcsin\left(\frac{\mu^2 - 2k}{\sqrt{8E_{k,*} + 4k^2}} \right)\Bigg|_{a}^{b} \end{aligned}$$

In the natural case,

$$-b = a = \sqrt{2k + 2\sqrt{2E_{k,*} + k^2}},$$

and we get zero. In the inverted case,

$$\begin{aligned} a &= \sqrt{2k + 2\sqrt{2E_{k,*} + k^2}} \\ b &= \sqrt{2k - 2\sqrt{2E_{k,*} + k^2}}, \end{aligned}$$

and the result is $2n\pi$. Therefore, the force constraint is satisfied. Still considering $\gamma = 0$, the couple constraint amounts to (since $M = \mu$ is even)

$$0 = \lambda s_{-1}(r_1(1) + r_1(-1)) + \lambda c_{-1}(r_2(-1) - r_2(1)) \tag{4.11}$$

which is trivially satisfied for even beam solutions. Evidentally, our constraints are met and we have justified our choice of boundary conditions in the case that $\gamma = 0$.

In the case when we have current, $\gamma > 0$, we have chosen $N, H = 0$ at the boundaries and $M(1) = M(-1)$, so that all of the non-integral terms vanish and our constraints reduce to

$$\int_{-1}^{1} \boldsymbol{f} = 0 \tag{4.12}$$

$$\int_{-1}^{1} [\boldsymbol{r} \times \boldsymbol{f} + \boldsymbol{l}] = 0. \tag{4.13}$$

Recall that

$$\boldsymbol{f}(x) = -\gamma^2[f_1(x)\boldsymbol{d}_1(x) + f_2(x)\boldsymbol{d}_2(x)], \tag{4.14}$$

and since we assumed that $\nu = 1$ and $\eta = 0$, $f_1(x)$ and $f_2(x)$ are expressed as

$$\begin{aligned} f_1(x) &= 4\delta \int_{-1}^{1} \left[k_1(x - \tilde{x}) + \mu(x)\mu(\tilde{x})k_3(x - \tilde{x})\right] \, d\tilde{x} \\ f_2(x) &= -4\delta \int_{-1}^{1} \mu(\tilde{x})k_2(x - \tilde{x}) \, d\tilde{x} \end{aligned}$$

Let us examine each of the terms of the integrands. First

$$f_1(-x) = 4\delta \int_{-1}^{1} \left[k_1(-x - \tilde{x}) + \mu(-x)\mu(\tilde{x})k_3(-x - \tilde{x})\right] \, d\tilde{x}.$$

If we make a simple substitution $u = -\tilde{x}$ and $du = -d\tilde{x}$ and recall that $k_1(x-\tilde{x})$ and $k_3(x-\tilde{x})$ are odd functions, then we readily see that

$$\begin{aligned} f_1(-x) &= 4\delta \int_1^{-1} \left[k_1(-x+u) + \mu(-x)\mu(-u)k_3(-x+u)\right](-du) \\ &= -4\delta \int_1^{-1} \left[-k_1(x-u) + \mu(x)\mu(u)(-k_3(x-u))\right]\, du \\ &= -4\delta \int_{-1}^{1} \left[k_1(x-u) + \mu(x)\mu(u)(k_3(x-u))\right]\, du \\ &= -f_1(x) \end{aligned} \tag{4.15}$$

and we have that f_1 is odd. For f_2, recall that k_2 is even so that

$$\begin{aligned} f_2(-x) &= -4\delta \int_{-1}^{1} \mu(\tilde{x})k_2(-x-\tilde{x})\, d\tilde{x} \\ &= -4\delta \int_1^{-1} \mu(-u)k_2(-x+u)(-du) \\ &= -4\delta \left(-\int_{-1}^{1} \mu(u)k_2(x-u)(-du)\right) \\ &= -4\delta \int_{-1}^{1} \mu(u)k_2(x-u)\, du \\ &= f_2(x) \end{aligned} \tag{4.16}$$

so that $f_2(x)$ is even. Now, we have

$$\begin{aligned} \boldsymbol{f}(x) &= -\gamma^2[f_1(x)\boldsymbol{d}_1(x) + f_2(x)\boldsymbol{d}_2(x)] \\ &= -\gamma^2[(f_1(x)\cos\theta(x) - f_2(x)\sin\theta(x))\boldsymbol{i} + (f_1(x)\sin\theta(x) + f_2(x)\cos\theta(x))\boldsymbol{j}]. \end{aligned}$$

When $\mu(x)$ is even, $\theta(x)$ is odd, $\cos\theta(x)$ is even and $\sin\theta(x)$ is odd. Therefore, the $\boldsymbol{i}$-term vanishes when integrated because it is odd. However, the $\boldsymbol{j}$-term is even, meaning that (4.12) is satisfied only if

$$\int_{-1}^{1} f_1(x)\sin\theta(x) + f_2(x)\cos\theta(x)\, dx = 0.$$

Although this was not taken into consideration during solution of the BVP, it was verified numerically after the fact so that we do indeed satisfy the force constraint when μ is even for $\gamma > 0$ for the solutions discussed in this thesis.

Similarly, let us check the terms of (4.13). Recall that the body-couple, $\boldsymbol{l}$, is defined by the following:

$$\boldsymbol{l}(x) \quad = \quad \gamma^2 l(x)\boldsymbol{d}_3 \tag{4.17}$$

where (with $\nu = 1$ and $\eta = 0$) $l(x)$ is defined by

$$l(x) \quad = \quad -4\delta \int_{-1}^{1} (\mu(\tilde{x})k_3(x-\tilde{x}) + \mu(x)k_4(x-\tilde{x}))\ d\tilde{x}$$

For μ even, we see that

$$\begin{aligned} l(-x) &= -4\delta \int_{-1}^{1} (\mu(\tilde{x})k_3(-x-\tilde{x}) + \mu(-x)k_4(-x-\tilde{x}))\ d\tilde{x} \\ &= -4\delta \int_{1}^{-1} (\mu(-u)k_3(-x+u) + \mu(-x)k_4(-x+u))\,(-\,du) \\ &= 4\delta \int_{-1}^{1} (\mu(u)(-k_3(x-u)) + \mu(x)(-k_4(x-u)))\,(-\,du) \\ &= 4\delta \int_{-1}^{1} (\mu(u)(k_3(x-u)) + \mu(x)(k_4(x-u)))\ du \\ &= -l(x) \end{aligned}$$

so that l is odd.

Now, $\boldsymbol{r} \times \boldsymbol{f}$ simplifies to

$$\begin{aligned} (\boldsymbol{r}\times\boldsymbol{f})(x) &= \left[\left(\int_0^x \cos\theta(s)\ ds\right)\boldsymbol{i} + \left(\int_0^x \sin\theta(s)\ ds\right)\boldsymbol{j}\right] \times \left[-\gamma^2\left(f_1(x)\boldsymbol{d}_1(x) + f_2(x)\boldsymbol{d}_2(x)\right)\right] \\ &= -\gamma^2\left[\left(\int_0^x \cos\theta(s)\ ds\right)\boldsymbol{i} + \left(\int_0^x \sin\theta(s)\ ds\right)\boldsymbol{j}\right] \\ &\quad \times \left[(f_1(x)(\cos\theta(x)\boldsymbol{i} + \sin\theta(x)\boldsymbol{j}) + f_2(x)(-\sin\theta(x)\boldsymbol{i} + \cos\theta(x)\boldsymbol{j})\right] \\ &= -\gamma^2\left[\left(\int_0^x \cos\theta(s)\ ds\right)\boldsymbol{i} + \left(\int_0^x \sin\theta(s)\ ds\right)\boldsymbol{j}\right] \\ &\quad \times \left[(f_1(x)\cos\theta(x) - f_2(x)\sin\theta(x))\,\boldsymbol{i} + (f_1(x)\sin\theta(x) + f_2(x)\cos\theta(x))\boldsymbol{j}\right] \end{aligned}$$

$$
\begin{aligned}
&= -\gamma^2 \left(\int_0^x \cos\theta(s)\, ds \right) (f_1(x)\sin\theta(x) + f_2(x)\cos\theta(x))\, \boldsymbol{k} \\
&\quad -\gamma^2 \left(\int_0^x \sin\theta(s)\, ds \right) (f_1(x)\cos\theta(x) - f_2(x)\sin\theta(x))\, (-\boldsymbol{k}) \\
&= -\gamma^2 [\left(\int_0^x \cos\theta(s)\, ds \right) (f_1(x)\sin\theta(x) + f_2(x)\cos\theta(x)) \\
&\quad -\left(\int_0^x \sin\theta(s)\, ds \right) (f_1(x)\cos\theta(x) - f_2(x)\sin\theta(x))]\boldsymbol{k}.
\end{aligned}
$$

Recall that $f_1(x)$ is odd and $f_2(x)$ is even when μ is even and $\theta(x)$ is odd. This gives us that

$$
\begin{aligned}
(\boldsymbol{r}\times\boldsymbol{f})(-x) &= -\gamma^2 [\left(\int_0^{-x} \cos\theta(s)\, ds \right) (f_1(-x)\sin\theta(-x) + f_2(-x)\cos\theta(-x)) \\
&\quad -\left(\int_0^{-x} \sin\theta(s)\, ds \right) (f_1(-x)\cos\theta(-x) - f_2(-x)\sin\theta(-x))]\boldsymbol{k} \\
&= -\gamma^2 [\left(-\int_{-x}^0 \cos\theta(s)\, ds \right) ((-f_1(x))(-\sin\theta(x)) + f_2(x)\cos\theta(x)) \\
&\quad -\left(-\int_{-x}^0 \sin\theta(s)\, ds \right) ((-f_1(x))\cos\theta(x) - f_2(x)(-\sin\theta(x)))]\boldsymbol{k} \\
&= -\gamma^2 [\left(-\int_0^x \cos\theta(s)\, ds \right) (f_1(x)\sin\theta(x) + f_2(x)\cos\theta(x)) \\
&\quad +\left(\int_0^x \sin\theta(s)\, ds \right) ((f_1(x))\cos\theta(x) - f_2(x)\sin\theta(x))]\boldsymbol{k} \\
&= \gamma^2 [\left(\int_0^x \cos\theta(s)\, ds \right) (f_1(x)\sin\theta(x) + f_2(x)\cos\theta(x)) \\
&\quad -\left(\int_0^x \sin\theta(s)\, ds \right) ((f_1(x))\cos\theta(x) - f_2(x)\sin\theta(x))]\boldsymbol{k} \\
&= -(\boldsymbol{r}\times\boldsymbol{f})(x)
\end{aligned}
$$

so that constraint (4.13) is met whenever μ is even. In summary, for μ even, the constraints (4.12) and (4.13) are met.

Another consideration is orientation. Note that any solution can be translated and rotated to another solution—so we should make assumptions on $\boldsymbol{r}$ to factor that out. Put another way, $\boldsymbol{r}$ is only determined up to a constant velocity and rotation. However, since we have already essentially removed $\boldsymbol{r}$ from the equations (i.e., all time derivatives disappear), we only need to consider $\boldsymbol{r}$ once

we have a solution for μ in order to visualize the actual beam. This amounts to fixing $\theta(0) = 0$—which is implied when μ is even but must be recalled if we are to consider μ odd—and also fixing $\boldsymbol{r}(0) = (0, 0)$.

4.2 Derivation of Duffing Form

Now, exactly analogous to the analysis in Chapter 3, we start by substituting (4.3) into (4.1) for H and then we integrate the resulting equation to get $N(x)$, i.e.

$$\begin{aligned} N_x(x) &= -EI\mu(x)\mu_x(x) - \gamma^2 l(x,\mu)\mu(x) + \gamma^2 f_1(x,\mu) \\ &= -\frac{EI}{2}\Big(\mu^2(x)\Big)_x - \gamma^2(l(x,\mu)\mu(x) - f_1(x,\mu)) \\ \Rightarrow N(x) &= N(-1) + \frac{EI}{2}\mu(-1)^2 - \frac{EI}{2}\mu^2(x) - \gamma^2\int_{-1}^{x}(l\mu - f_1)(s,\mu)\,ds \end{aligned} \tag{4.18}$$

Differentiating (4.3) with respect to x and solving it for $H_x(x)$ we get

$$H_x(x) = -EI\mu_{xx}(x) - \gamma^2 l_x(x,\mu,\mu') \tag{4.19}$$

Substituting (4.19) and (4.18) into (4.2) we get

$$\begin{aligned} 0 = &-EI\mu_{xx}(x) - \gamma^2 l_x(x,\mu,\mu') \\ &+\mu(x)\left(N(-1) + \frac{EI}{2}\mu(-1)^2 - \frac{EI}{2}\mu^2(x) - \gamma^2\int_{-1}^{x}(l\mu - f_1)(s,\mu)\,ds\right) \\ &-\gamma^2 f_2(x,\mu). \end{aligned}$$

After some distribution and rearangment we get

$$\begin{aligned} &-EI\mu_{xx}(x) + \left(N(-1) + \frac{EI}{2}\mu(-1)^2\right)\mu(x) - \frac{EI}{2}\mu^3(x) = \\ &\gamma^2\left(f_2(x,\mu) + l_x(x,\mu,\mu') + \mu(x)\int_{-1}^{x}(l\mu - f_1)(s,\mu)\,ds\right). \end{aligned}$$

By dividing both sides with $-EI$ we arrive at

$$\mu_{xx}(x) - k\mu(x) + \frac{1}{2}\mu^3(x) = -\frac{\gamma^2}{EI}\left(f_2(x,\mu) + l_x(x,\mu,\mu') + \mu(x)\int_{-1}^{x}(l\mu - f_1)(s,\mu)\,ds\right).$$

where

$$k = -\lambda + \frac{1}{2}\mu(-1)^2, \lambda = \frac{-N(-1)}{EI}.$$

In the last equation, it is easy to see that the left hand side is the Duffing equation analyzed in the last chapter and that the right hand side can be expressed as a product of the control parameter γ and a "forcing" term Ψ, i.e.

$$\mu_{xx}(x) - k\mu(x) + \frac{1}{2}\mu^3(x) = \gamma^2\Psi(x, \mu, \mu'), \tag{4.20}$$

where

$$\Psi(x, \mu, \mu') = -\frac{1}{EI}\left(f_2(x, \mu) + l_x(x, \mu, \mu') + \mu(x)\int_{-1}^{x}(l\mu - f_1)(s, \mu)\, ds\right).$$

Equation (4.20) is a Duffing-like equation, which we will treat as a two-point boundary value problem in conjunction with

$$N(-1) = N(1) = 0 \tag{4.21}$$

$$H(-1) = H(1) = 0 \tag{4.22}$$

$$\mu(-1) = \mu(1) = \mu_* \tag{4.23}$$

4.3 Analysis

First, our goal is to exhibit that for $\gamma \neq 0$ there exist non-trivial solutions representing buckled states. Because we already have the "inverted" solutions for $\gamma = 0$ near the $\lambda = 0$ boundary (see Figure 3.4), it is natural to ask the question "can we continue these solutions, $\mu(x) = n\pi$ for $\gamma > 0$?" The answer is unfortunately no. As discussed in Chapter 3, there is a degeneracy for $\lambda, \gamma = 0$ and, as it turns out, there is a discontinuity when continuing the solutions with respect to γ in the sense that there are no solutions to the BVP for $\gamma > 0$ near $\mu(x) = n\pi$.

However, points from which to begin a continuation are easily found numerically by solving the BVP with γ small with a range of starting guesses. These curves are depicted in Figure 4.1. As previously described, solutions starting at $\gamma = 0$ lie on a circle in the (u, v)-plane. However, in contrast to those that begin at $\mu_* = n\pi$ for $\gamma = 0$, $\lambda \neq 0$, these solutions do not complete an integral number of revolutions around the circle, as can be seen in Figure 4.2. This "overlap" in the solution, though not physically meaningful, is accounted for by the addition of the integral forcing term Ψ and its application to $\mu(x)$. However, as γ increases, the overlap disappears (at $\gamma \approx 760$) and we have a physically relevant, and rather interesting, buckled shape with increasingly curled ends as γ grows larger (see Figure 4.2).

Figures 4.4 and 4.5 show f_1 and f_2 for a few of the solutions lying along each of the branches depicted in Figure 4.1. As expected, f_1 illustrates a compressive effect resulting from the application of the current, similar to the limiting case of two parallel wires conducting current. Also, f_1 is similar between different branches when γ is small enough, whereas f_2 is qualitatively different between branches. In fact, looking at the form of the body force in the $\boldsymbol{d}_1$ direction, we see that

$$-\gamma^2 f_1 = -4\delta\gamma^2 \int_{-1}^{1} k_1(x-\tilde{x}) + \mu(x)\mu(\tilde{x})k_3(x-\tilde{x})\, d\tilde{x} \tag{4.24}$$

$$\approx -4\delta\gamma^2 \int_{-1}^{1} k_1(x-\tilde{x})\, d\tilde{x} \tag{4.25}$$

when μ is relatively small because $|k_3|$ is four or five orders of magnitude less than $|k_1|$ (see plots of k_i in Chapter 2) and μ remains relatively small for γ in the range we have considered in this thesis. This means that the body force only has γ dependence along curves in the (μ_*, γ)-plane for γ, μ small enough, and this is made clear in Figure 4.4, where both the inverted and natural solutions have practically identical $\boldsymbol{d}_1$ body force at $\gamma = 905$ (almost impossible to distinguish in the plot).

On the other hand, for the body force in the $\boldsymbol{d}_2$ direction, we see that in one case (inverted), $-\gamma^2 f_2$ is strictly postive, corresponding to the uni-directional nature of the deformation, whereas in the other (natural), $-\gamma^2 f_2$ changes sign, corresponding to bending to the left and right of the tangent. One can similarly interpret the couples (not shown).

There are some qualitatively similar features to the solutions found for $\gamma > 0$ near the μ_* or γ axes and those found in Chapter 3. The inverted solutions begin on circles and the initial compressive effects are similar. On the other hand, there are some features that are completely unique for $\gamma > 0$. For example, compare the beams shapes in Figures 3.5 and 4.3. The most striking difference is at the ends, which are no longer fixed by a compressive contact force but can curl freely under the compressive body force.

This tendency to curl at the ends is most clearly expressed by the plot of the body force in the $\boldsymbol{d}_2$ direction in Figure 4.5. Note the peaks in the plots at the end, where the most extreme bending takes place as a result. It would be interesting to see to what extent this effect would be dampened by the inclusion of a non-zero contact force at the end (that is, $\lambda > 0$), even though this does not have physical relevance for the problem as we have stated it.

To summarize, the application of a current induces multiple non-trivial solutions for a given value of the (non-dimensional) current γ, represented in Figure 4.1. Depending on when the trivial solution looses stability (at some value of γ), one of these non-trivial, buckled configurations can be assumed. Using the methods developed here, one can gain insight into the resulting buckled shapes.

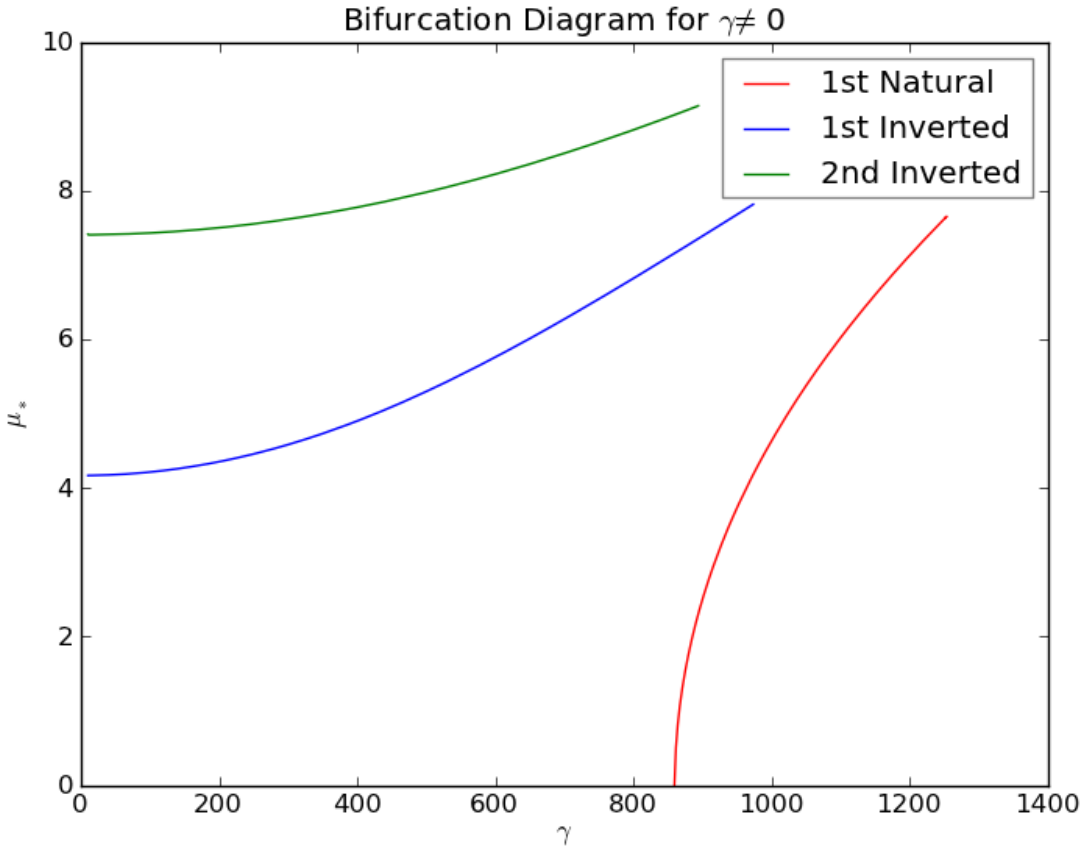

Figure 4.1: Bifurcation diagram displaying μ_* vs. $\gamma > 0$ for branches of even solutions. All curves were generated by continuing from solutions found near the axes by a numerical search. The solutions originating near the vertical axis are curled up beams that start out on a circle (with overlapping ends) for $\gamma = 0$ and are progressively compressed by the effect of an increasing γ, illustrating the compressive nature of the self-forces generated by the current. Those starting on the γ axis bifurcate from the trivial solution and are also compressed in a natural fashion. This meshes well with the results from Chapter 3, which had qualitatively similar solutions, at least in this range of the (μ_*, γ) plane. Note that we do not plot the reflection of these curves across the γ axis although they exist by symmetry.

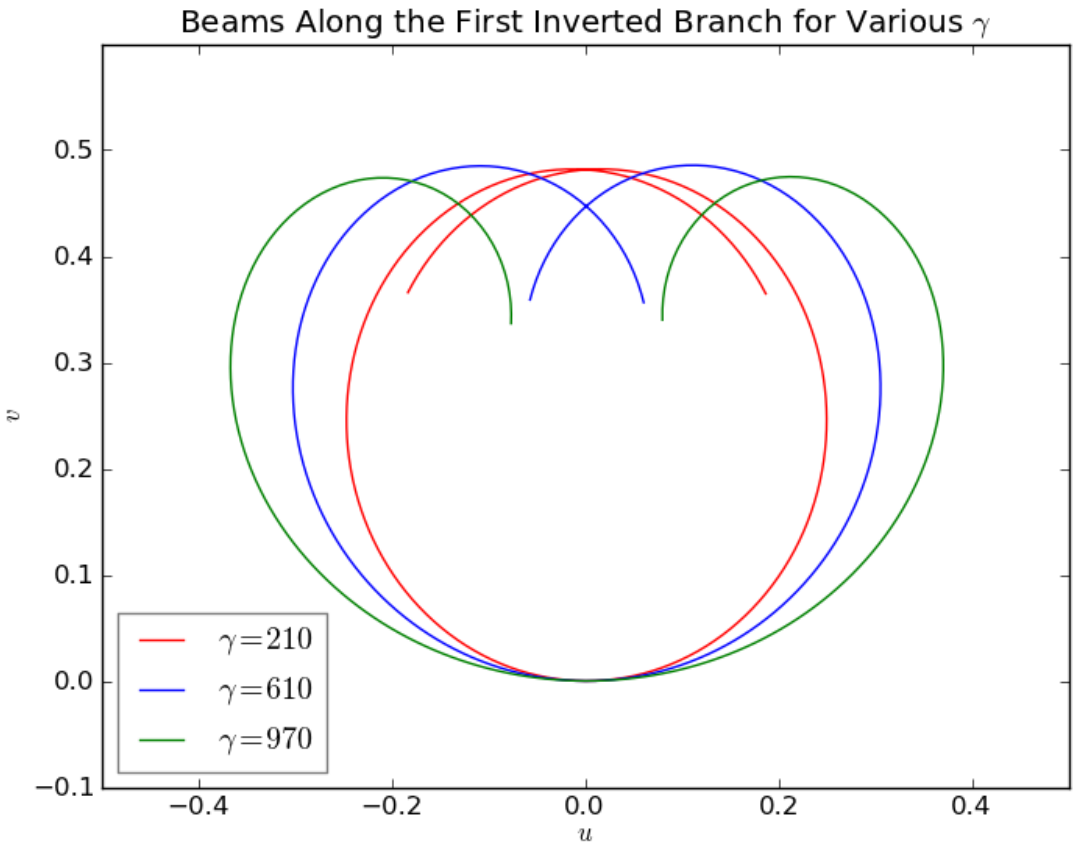

Figure 4.2: Beam shapes for various γ along the first inverted branch, showing increasing curvature at the ends due to the compressive body forces created by the feedback between the body and the electromagnetic field resulting from a transversely conducted current. In this case, the body force orthogonal to the beam always points "inward."

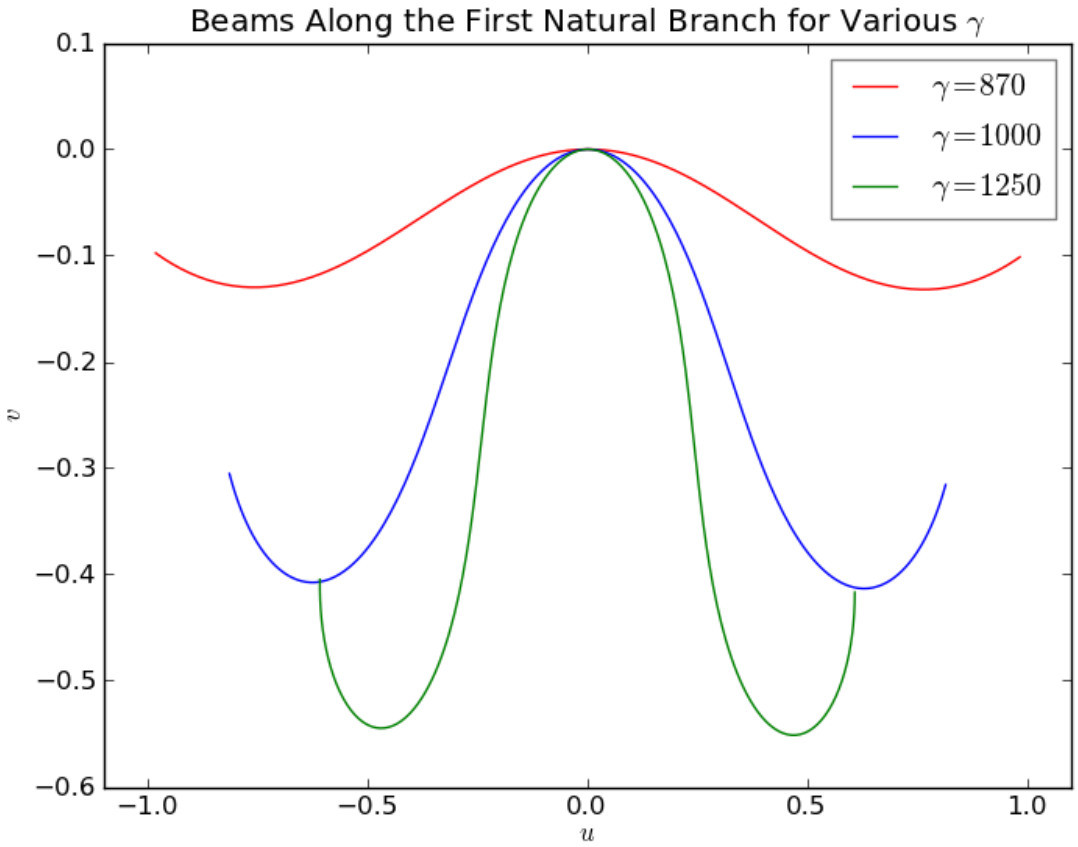

Figure 4.3: Beam shapes for various γ along the first natural branch, also showing increasing curvature at the ends due to the compressive body forces created by the feedback between the body and the electromagnetic field resulting from a transversely conducted current. In this case, we also see that there is bending to both the left and right of the tanget along the beam due to the changing sign of the body force orthogonal to the beam.

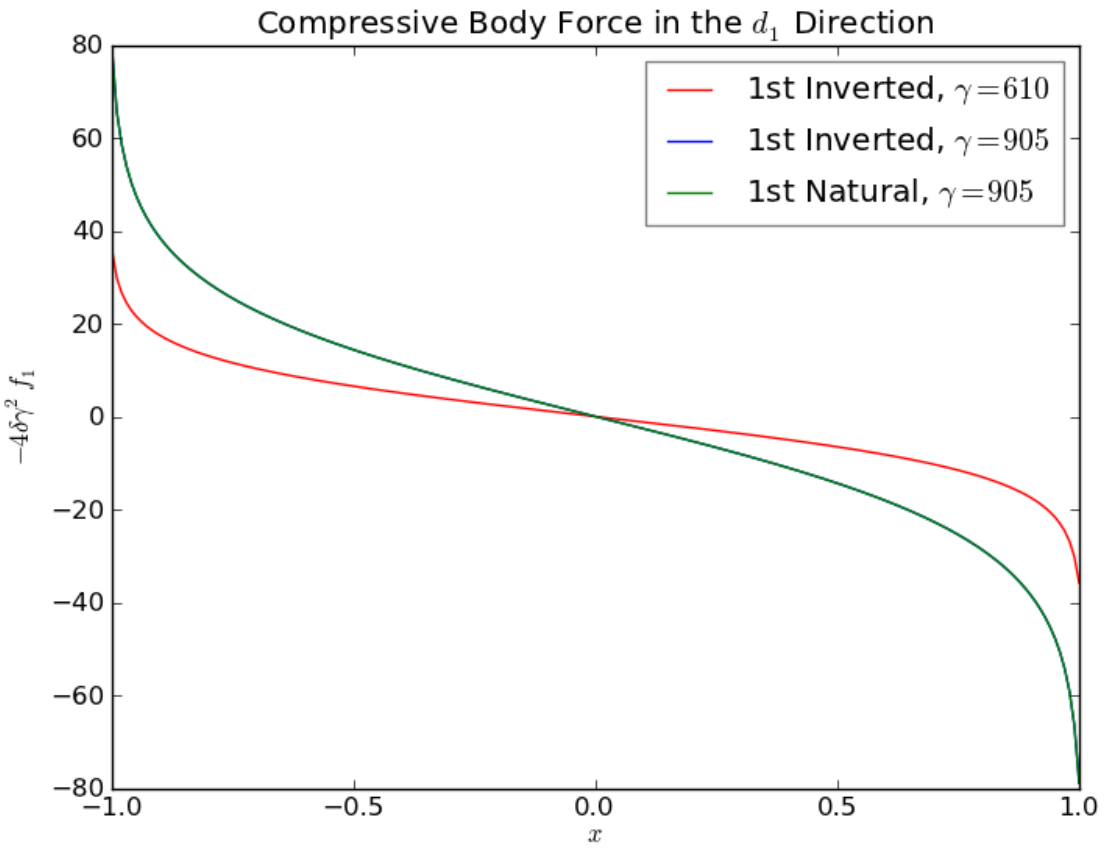

Figure 4.4: Compressive body force in the $\boldsymbol{d}_1$ direction (tangent to the beam). As noted in the text, the 1st inverted and 1st natural curves (in blue and green) overlap here due to the fact that for small enough γ and $\mu(x)$, $\int_{-1}^{1} k_1(x-\tilde{x}) + \mu(x)\mu(\tilde{x})k_3(x-\tilde{x})\, d\tilde{x} \approx \int_{-1}^{1} k_1(x-\tilde{x})\, d\tilde{x}$.

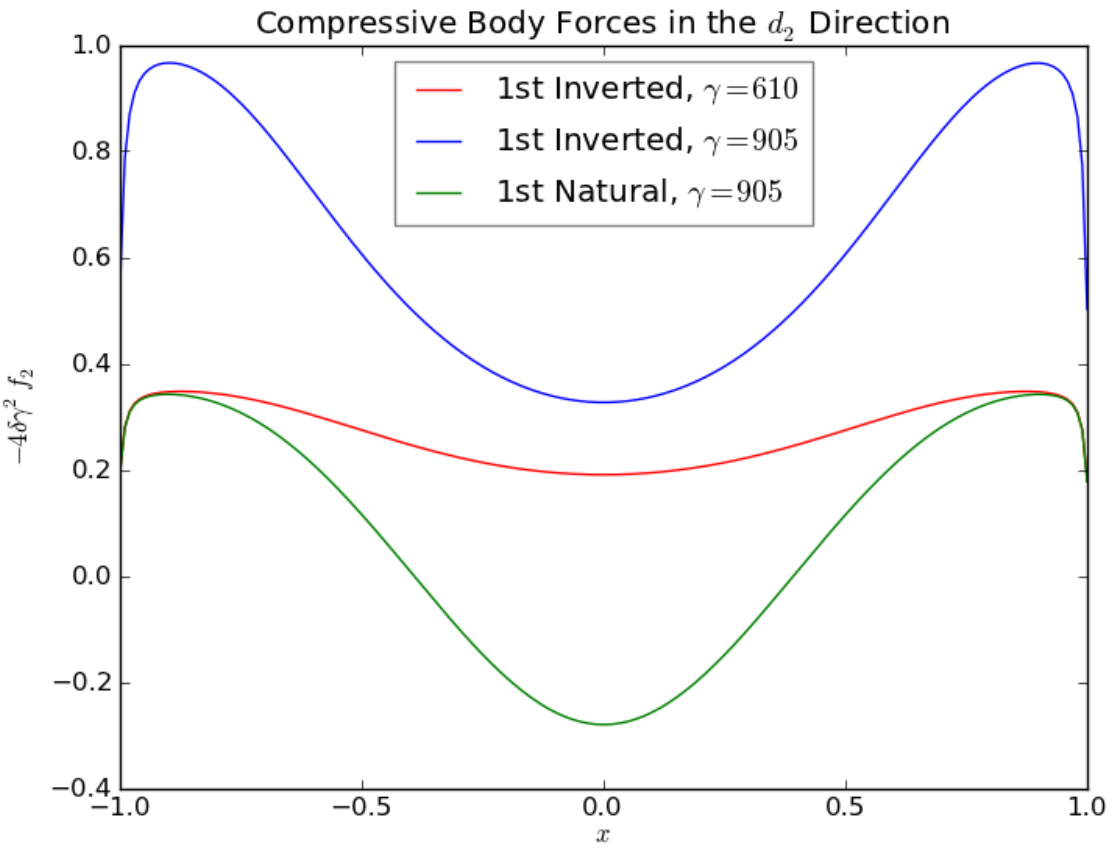

Figure 4.5: Compressive body force in the $\boldsymbol{d}_2$ direction (orthogonal to the beam). Note the difference in sign between the inverted and natural curves. The fact that the natural solutions have this component of the body force with changing signs gives a qualitatively different shape to the beam solutions.

Chapter 5

Numerical Methods

5.1 Shooting Method

To solve the full non-linear system (4.20),

$$\begin{aligned} \mu''(x) - k\mu(x) + \frac{1}{2}\mu^3(x) &= \gamma^2\Psi(x,\mu,\mu'), \\ \mu'(-1) = \mu'(1) &= 0 \\ \mu(-1) &= \mu(1) \end{aligned} \tag{5.1}$$

which is an integro-differential equation (IDE), we attempt to define a robust shooting method specific to (5.1). The basic idea is that we repeatedly solve an initial value problem (IVP) to hone in on the initial values that reproduce the boundary conditions, thereby producing a solution to the boundary value problem (BVP). In particular, we will assume that $\mu'(-1) = \mu'(1) = 0$ in the following argument (noting that the basic algorithm is readily adapted for arbitrary boundary conditions).

5.1.1 $\gamma = 0$

When $\gamma = 0, \lambda \neq 0$ we have a simple ODE system and correctly adjusting initial values to satisfy the boundary conditions is straight forward. The heart of the shooting method assumes that you have two solutions (call them $\mu_+(x), \mu_-(x)$) to the IVP that "almost" satisfy the boundary conditions $\mu(-1) = \mu(1) = \mu_*$ and $\mu'(-1) = \mu'(1) = 0$. We think of $\mu(-1)$ as our adjustable input variable,

whereas $\mu'(-1) = 0$ is fixed, and we shoot for $\mu(1) \to \mu(-1)$ and $\mu'(1) \to 0$. Because our systems are conservative, we know that all solutions are closed curves and we can therefore shoot for only one of $\mu(1)$ or $\mu'(1)$ (since one guarantees the other). We choose to shoot for $\mu'(1) \to 0$ for simplicity. We prove the following Theorem, which is useful:

Theorem 5.1. Contraction Principle for $\gamma = 0$

Suppose that $\mu_\pm$ "almost" satisfy (5.1) *with $\gamma = 0$ in the sense that we replace the boundary conditions with the following, for some small $\delta > 0$:*

$$\mu'_\pm(-1) = 0 \tag{5.2}$$
$$|\mu_\pm(-1) - \mu_\pm(1)| < \delta \tag{5.3}$$
$$0 < \mu'_+(1) < \delta \tag{5.4}$$
$$-\delta < \mu'_-(1) < 0. \tag{5.5}$$

Then there exists a function $\mu_*(x)$ such that

$$\mu'_*(-1) = \mu'_*(1) = 0 \tag{5.6}$$
$$\mu_*(-1) = \mu_*(1) \tag{5.7}$$
$$\mu_-(-1) \le \mu_*(-1) \le \mu_+(-1). \tag{5.8}$$

That is, there is a solution to the BVP (5.1) *with initial $\mu_*(-1)$ in between $\mu_-(-1)$ and $\mu_+(-1)$. In this sense, μ_* is a "contraction" of μ_- and μ_+.*

Proof. This is a simple application of the principle of continuous dependence on initial conditions. In particular, it ensures us that $\mu'(1;\alpha)$ is continuous in α, where $\alpha \in (\mu_-(-1), \mu_+(-1))$ is the relevant initial condition (in this case, also a parameter). But $\mu'_-(1) < 0 < \mu'_+(1)$, so that there exists an $\alpha_* \in (\mu_-(-1), \mu_+(-1))$ such that $\mu'(1;\alpha_*) = 0$, and we choose $\mu_*(x)$ to be the solution with $\mu_*(-1) = \alpha_*$. This completes the proof. □

Now set $\mu^*_+ = \mu_+(-1)$ and $\mu^*_- = \mu_-(-1)$. Due to the Theorem 5.1, we are guaranteed that repeatedly solving the following set of IVPs will converge: continue taking $\mu(-1) = (\mu^*_- + \mu^*_+)/2$ until $\mu'(1)$ is very close to zero (defined by some tolerance $\varepsilon > 0$), updating one of μ^*_- and μ^*_+ on each iteration. The pseudo-code can be found in Algorithm 5.1.

Now, an obvious question is how do we get the initial two solutions that almost satisfy the boundary conditions? Suppose we have a known solution $\mu_{\lambda_*}(x)$ corresponding to $\lambda_* \neq 0$ and we would like to find another solution corresponding to a slight change to λ_*. In this case, we already have a reasonable initial guess, $\mu_{\lambda_*}(x)$ assuming that the change is small enough. This

Algorithm 5.1 ShootInside $(\mu_-^*, \mu_+^*, \varepsilon)$

Set $\mu(x)$ = SolveIVP$(\mu'(-1) = 0, \mu(-1) = (\mu_-^* + \mu_+^*)/2)$
if $|\mu'(1)| > \varepsilon$ **then**
  if $\mu'(1) > 0$ **then**
    Set $\mu_+^* = (\mu_-^* + \mu_+^*)/2$
  else
    Set $\mu_-^* = (\mu_-^* + \mu_+^*)/2$
  end if
  return ShootInside $(\mu_-^*, \mu_+^*, \varepsilon)$
end if
return $(\mu_- + \mu_+)/2$

initial solution may have been found analytically (as in Chapter 3) or may be a solution from a prior iteration during a continuation, as will be described below. In any case, given such a solution with initial $\hat{\mu}_* = \mu_{\lambda_*}(-1)$, we could then attempt to use our knowledge about the geometry to find another bounding guess. However, this makes the search algorithm more parametric than we would like and it turns out not to be useful when we consider the full IDE (we will discuss the issue in detail below). A very simple way to search is to solve the IVP with $\mu(-1) = (1 \pm \sigma)^n \hat{\mu}_*$ for some small $\sigma > 0$ (say ≈ 0.001, for example) for successive values of n until we get a sign change in $\mu'(1)$ (see Algorithm 5.2).

Algorithm 5.2 Shoot $(\hat{\mu}_*, \sigma, \varepsilon)$

Set $n = 0$
repeat
  Set $n = n + 1$
  Set $\mu_\pm^* = \mu'(1)$ from $\mu(x)$ = SolveIVP$(\mu'(-1) = 0, \mu(-1) = (1 \pm \sigma)^n \hat{\mu}_*))$
until $\mu_+'(1)\mu_-'(1) < 0$
Swap μ_+^* and μ_-^* if needed.
return ShootInside$((\mu_-^*, \mu_+^*, \varepsilon))$

5.1.2 $\gamma \neq 0$

Algorithm 5.2 works relatively well when $\gamma = 0$. However, when we consider $\gamma \neq 0$, we now have an integral term involving $\mu(x)$. In the context of the above shooting method, suppose that $\mu_{\gamma_*}(x)$ is a known solution for $\gamma_* > 0$. Then, we change γ slightly to $\hat{\gamma}_*$ and choose $\mu_{\hat{\gamma}_*,0}(x) = \mu_{\gamma_*}(x)$ to be

our first guess for the new solution. To remove the dependence on the integral term, we substitute this guess into Ψ so that it becomes a function of x only:

$$\hat{\Psi}_0(x) = \Psi(x, \mu_{\hat{\gamma}_*,0}(x), \mu'_{\hat{\gamma}_*,0}(x)). \tag{5.9}$$

We now have an ODE problem once again that can be used for this iteration of the shooting method described above. This will produce a new solution, $\mu_{\hat{\gamma}_*,1}(x)$ that satisfies

$$\mu''_{\hat{\gamma}_*,1}(x) - k\mu_{\hat{\gamma}_*,1}(x) + \frac{1}{2}{\mu_{\hat{\gamma}_*,1}}^3(x) = \gamma^2\Psi(x, \mu_{\hat{\gamma}_*,0}, \mu'_{\hat{\gamma}_*,0}),$$

though not yet necessarily meeting the desired boundary conditions. If $\mu_{\hat{\gamma}_*,0} \equiv \mu_{\hat{\gamma}_*,1}$ and $\mu'_{\hat{\gamma}_*,0}(1) = 0$, then we have solved the BVP and we are done. However, we can have no expectation that either is the case. Not meeting the boundary conditions is par for the course in the shooting method, but the equivalence of the $\mu_{\hat{\gamma}_*,i}$ is another matter altogether. On the other hand, the $\mu_{\hat{\gamma}_*,i}$ should be close to each other if $\hat{\gamma}_*$ is close enough to γ_* (assuming that we are sufficiently far from any branching points). In this case, we can have a reasonable expectation that for subsequent iterations, $\mu_{\hat{\gamma}_*}$ will converge.

To be clear, the primary difference in the $\gamma \neq 0$ case is that we have an additional dependence on $\mu(x)$ in the integral term and our method of solution necessitates two levels of convergence, one for the boundary conditions and one for approximations of $\mu(x)$. Although these could be treated orthogonally, this is not necessary nor computationally desirable. Instead, we prefer to allow $\mu_{\hat{\gamma}_*,i}$ to converge naturally as part of the shooting iterative procedure. However, because there is a dependency on $\mu_{\hat{\gamma}_*,i-1}(x)$ during iteration i, we must relax our implicit assumption of a contraction principle, which was self-evident in the case of a simple ODE with $\gamma = 0$ but is not guaranteed for $\gamma \neq 0$. This fact is evident by considering the convergence of $\mu(x)$ in isolation from the shooting method. In this case, we easily see that $\mu'_i(1) > 0$ doesn't guarantee that $\mu'_{i+1}(1) > 0$, so that two solutions for which $\mu'_{\pm,i}(1)$ differ in sign (i.e., bounding solutions) on iteration i does not imply $\mu'_{\pm,i+1}(1)$ differ in sign as well. This is a problem that requires attention, since the contraction principle stated above was necessary for ensuring convergence.

As it turns out, a rather simple refinement fixes this problem. Rather than searching for two points at each iteration with $\mu(-1) = (1 \pm \sigma)^n\hat{\mu}_*$ and assuming there is a contraction principle at work, one can subdivide the range into m test points,

$$\mu_{*,j} = \left(1 + \sigma\frac{2j - (m-1)}{2(m-1)}\right)^n \hat{\mu}_*$$

for $j = 0, \ldots, m-1$ and allow for the case when we may need to widen our range on any subsequent iteration due to the integral dependence on $\mu(x)$ during the iterations. This method has both higher

Algorithm 5.3 GridShootInside $(\mu_-, \mu_+, m, \varepsilon)$

Set $\sigma = \frac{\mu_+ - \mu_-}{m-1}$
Set $\mu_j(x) = \text{SolveIVP}(\mu'(-1) = 0, \mu(-1) = \mu_- + j\sigma)$ for $j = 0, \ldots, m-1$)
Select best j_* where $\mu'_{j_*}(1)\mu'_{j_*+1}(1) < 0$ and j_* is close to $\frac{m}{2}$
if no such j_* exists **then**
  return FAIL
end if
if $j_* = 0$ **then**
  return GridShootInside$((1-\sigma)\mu_0, (1+\sigma)\mu_1, m, \varepsilon)$
else if $j_* = m-1$ **then**
  return GridShootInside$((1-\sigma)\mu_{m-2}, (1+\sigma)\mu_{m-1}, m, \varepsilon)$
else if $|\mu'_{j_*}(1)| > \varepsilon$ and $|\mu'_{j_*+1}(1)| > \varepsilon$ **then**
  return GridShootInside$((1-\sigma)\mu_{j_*}, (1+\sigma)\mu_{j_*+1}, m, \varepsilon)$
end if
Compute max-norm: $\epsilon = \max_{0 \le j < N} |\mu_i(x_j) - \mu_{i-1}(x_j)|$
if $\epsilon > 0.0001$ **then**
  GridShootInside$(\mu_{j_*}, \mu_{j_*+1}, m, \varepsilon)$
end if
if $|\mu'_{j_*}(1)| < |\mu'_{j_*+1}(1)|$ **then**
  return μ_{j_*}
else
  return μ_{j_*+1}
end if

resolution (which increases the rate of convergence, especially with increasing n) and is easily parallelized. The modified logic for this can be found in Algorithms 5.3 and 5.4.

Note that in Algorithm 5.3, we no longer assume that there is a solution in between the two initial guesses. This is done so that the logic for subdividing the interval need only be done in one of GridShoot and GridShootInside, and GridShoot is basically a wrapper algorithm to specify the increasing search range. Also, Algorithm 5.3 handles a few special cases especially relevant when $\gamma \neq 0$ that deserve clarification: in the extreme case where the algorithm has found a sign change at the boundary of the search range, rather than using the two edge values for $\mu(-1)$, we require a slight widening of the range to catch the bulk of the cases where successive iterations of $\mu_i(x)$ have not yet converged (and therefore are most likely to violate the tendency to contract and converge).

Another important difference in the algorithm is that we must include another stopping criterion that measures the difference between successive $\mu_i(x)$, and only terminates when this difference

Algorithm 5.4 GridShoot ($\hat{\mu}_*, m, n_{max}, \sigma, \varepsilon$)

```
n = 0
repeat
  n = n + 1
  if n > n_max then
    return FAIL
  end if
  Set μ_± = (1 ± σ)^n μ̂_*
  Set r = GridShootInside(μ_−, μ_+, m, ε)
until r not FAIL
return r
```

becomes small. We can use any norm on the difference, but a simple max-norm suffices and is computationally efficient. In practice, we ensure

$$\max_{0 \le j < N} |\mu_i(x_j) - \mu_{i-1}(x_j)| < 0.0001$$

before considering that we have solved the BVP.

To visualize the shooting method, Figure 5.1 depicts the procedure starting with an initial guess of $\mu_* = 7$, with $\lambda = 15, \gamma = 0$ using $m = 5$. For the purposes of illustration, we have chosen a rather inaccurate initial guess of $\mu_* = 7$, and there are two nearby solutions to the BVP: one at $\mu_* \approx 7.77$ (which is inverted) and one at $\mu_* \approx 5.6$ (which is natural). After several iterations (about 20, in this pathalogical case), we find the solution $\mu_* \approx 7.77$. With a slightly different choice of initial μ_*, we would have converged to the other, natural solution.

5.2 Continuation Method

In (4.20), we have two control paramters λ and γ. λ represents the compressive contact force at the end of the beam, and it is relevant primarily in the case when $\gamma = 0$. γ is the magnitude of a current running through our plate, and given the expected results that $\gamma \neq 0$ would act to some extent in a manner similar to the compressive force of λ, we designed a continuation algorithm to explore solutions to the BVP for changing λ or γ.

Our continuation algorithm uses a simple predictor-corrector methodology. The basic idea is to start with a known solution to (4.20), $\mu_0(x)$ for p_0, where p means parameter and refers to either λ or γ. We then proceed to extend this knowledge to another nearby solution by adjusting p by

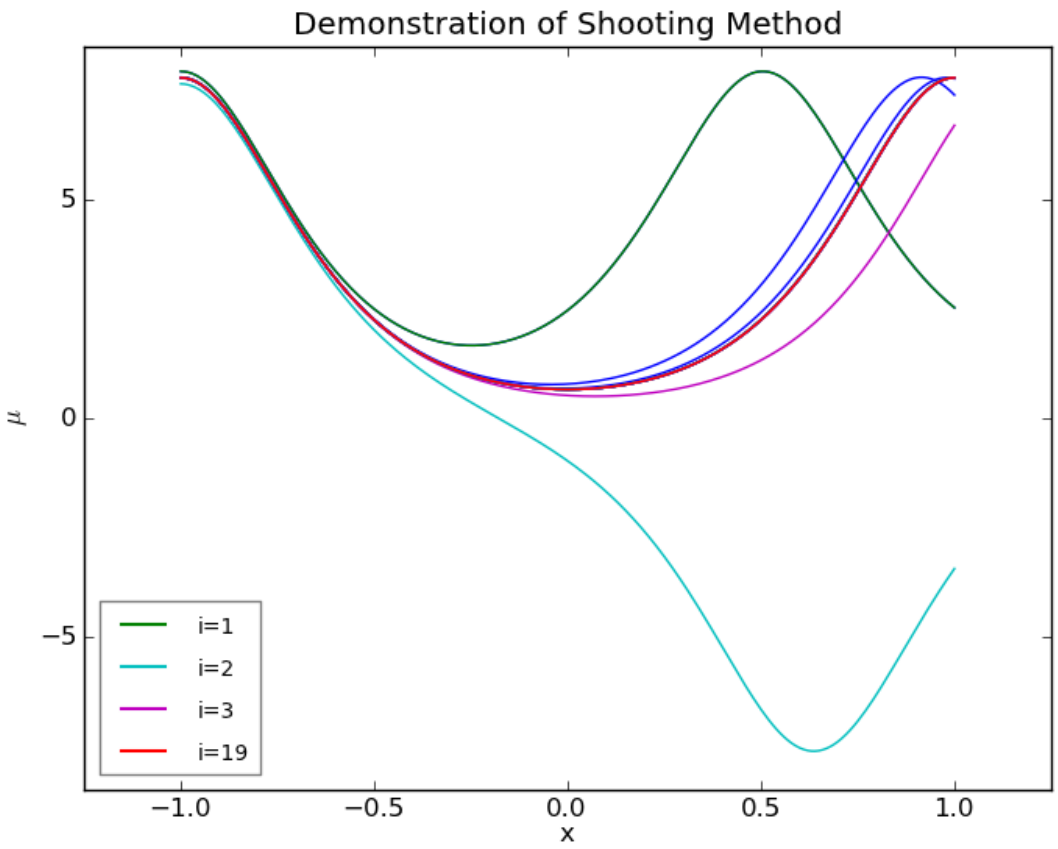

Figure 5.1: Illustration of iterations of the Shooting Method: The curves represent different $\mu(x)$s as the initial $\mu(-1)$ is being adjusted to satisfy the BCs.

a small amount, Δp (a signed quantity), making a prediction about how the solution will change given $p_1 = p_0 + \Delta p$, and finally refining our prediction to find $\mu_1(x)$. In this way, we numerically discover a manifold $(p, \mu(x))$. Because $\mu(x)$ lives in an infinite dimensional space, to visualize this manifold we must define a metric of $\mu(x)$ to plot against p. In our case, we generally used $\mu(-1)$ since this was the main degree of freedom. Alternatively, we also used the L^2-norm to get a better sense of the shape. However, $\mu(-1)$ gives a cleaner, easier to interpret diagram because there is no overlap in the curves produced for different branches.

Although simple in concept, a robust continuation algorithm is an exercise in trade-offs. For example, the smaller Δp, the less sophisticated the prediction needs to be. On the other hand, the

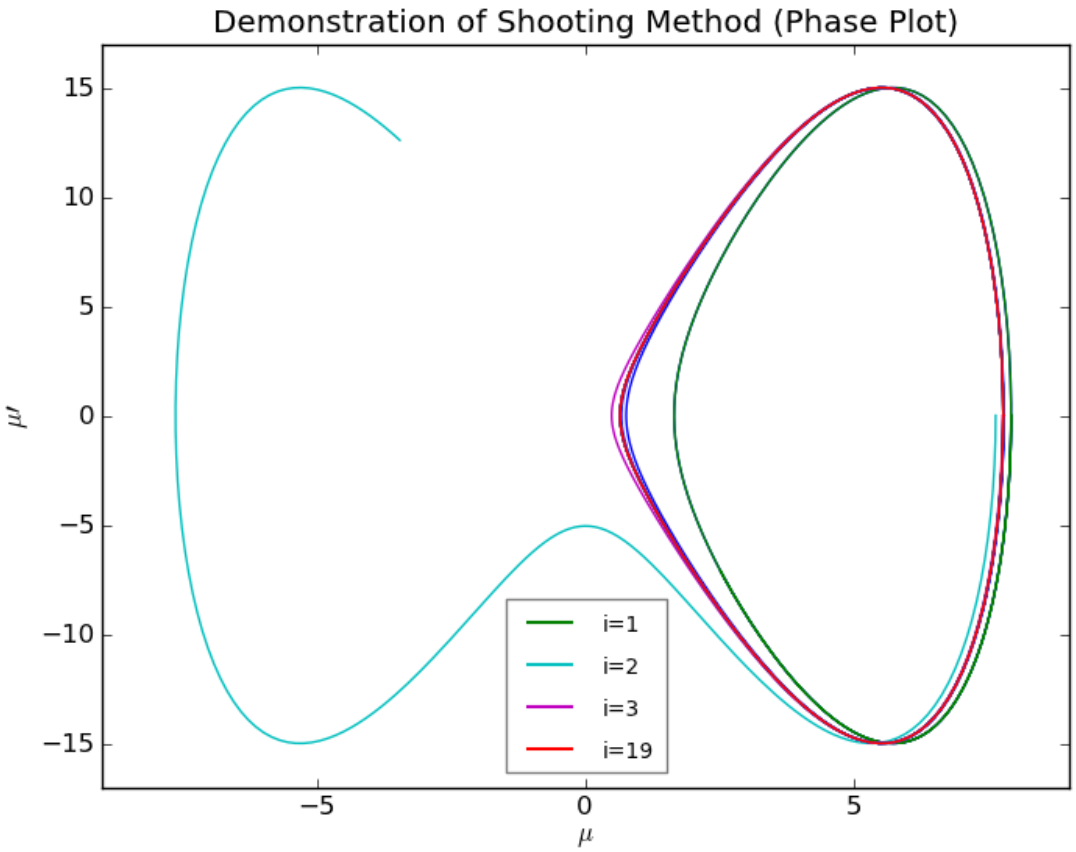

Figure 5.2: Phase plot of shooting iterations corresponding to Figure 5.1.

larger Δp, the faster the algorithm makes progress. We found that the best approach to solving this was simply to allow Δp to be adjusted based on a measure of how easily the algorithm was able to predict and correct at each iteration. As an example of why this was necessary, Figure 5.3 shows the convergence results for an early attempt to continue using a fixed Δp.

We adjust Δp indirectly by parameterizing the arc-length of the curve being discovered in $(p, \mu(-1))$ space, i.e., $s = \sqrt{\Delta p^2 + \mu(-1)^2}$, and then adapting this quantity. The method used is reminiscent of "psuedo arc-length" continuation due to Keller [8], though in this case we use no explicity Jacobian or, in fact, any information other than the current derivative of the curve $\frac{\Delta \mu(-1)}{\Delta p}$ itself to help us predict the next point on the curve. In this sense, we use a pure predictor-corrector scheme where the predictor is geometry-driven. The adaptation scheme used for Δp is heuristic

in nature, and takes the basic form expressed in Algorithm 5.5. In words, we define the "normal" number of iterations to be 3 and then increase or decrease our step size based on the number of iterations the shooting method takes at each step in the continuation. In addition, the number of iterations taken by the shooting method is normalized with a sensitivity input so that the user can tune the meaning of "normal" to the particularities of the continuation. For example, a sensitivity (multiplier) of 0.1 (meaning 30 is "normal") was often used for λ continuation, since iterations are computationally cheap and convergence was not hindered terribly by taking large steps along the curve. On the other hand, for γ-continuation, a typical value was 0.333 or even 0.5 (meaning 9 or 15 is "normal") since each iteration is extremely computaionally expensive and a large step can often break convergence (due to the extra $\mu(x)$ dependence described above).

The complete algorithm used for continuation is found as Algorithm 5.6. This algorithm is simple in the extreme, but we include details of arc-length calculations for clarity. Results of the both the shooting and continuation algorithms are presented in Chapters 3 and 4, so we defer to the plots there to display the effectiveness of the algorithms.

Algorithm 5.5 AdaptDS ($\Delta s, n, n_{prev}$)

Note that n and n_{prev} are the number of iterations normalized by a sensitivity parameter
if $n_{prev} \leq n$ **then**
  Set $\Delta s_{new} = 1.618 \cdot \Delta s$
else
  if $n = 1$ **then**
    Set $\Delta s_{new} = 2 \cdot \Delta s$
  else if $n = 2$ **then**
    Set $\Delta s_{new} = 1.618 \cdot \Delta s$
  else if $n = 3$ **then**
    Set $\Delta s_{new} = \Delta s$
  else
    Set $\Delta s_{new} = \frac{\Delta s}{1.618}$
  end if
end if
return Δs_{new}

Notes on Numerical Code

Except for the basic ODE solver, all algorithms were designed from scratch and implemented, first in Python, and finally in C++ for efficiency.

The core ODE solver was CVode, which is maintained and distributed as part of the SUNDIALS numerical library, `https://computation.llnl.gov/casc/sundials/main.html`.

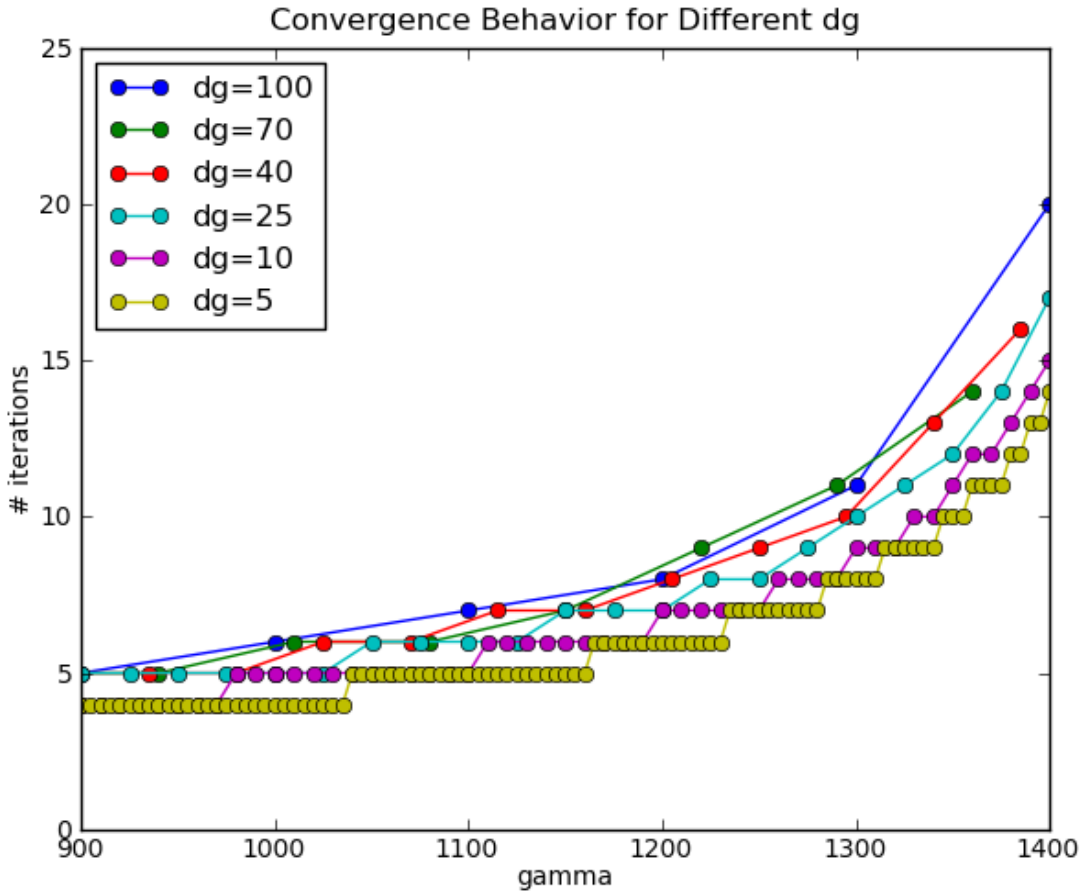

Figure 5.3: An early convergence result with fixed $\Delta\gamma$ (labeled *dg* in the graphic). Here we plot the number of iterations taken to predict/correct for each iteration for various values of $\Delta\gamma$ for increasing $\gamma \in [900, 1400]$. For these particular curves, final convergence was acheived (although barely in the $\Delta\gamma = 100$ case). The trade-off is clear: although $\Delta\gamma = 5$ produces high fidelity results, it takes an enormous number of iterations overall to reach the same goal as the other $\Delta\gamma$ values. On the other hand, as $\Delta\gamma$ increases, convergence takes longer at a given value of γ and eventualy, either for larger $\Delta\gamma$ or even for these $\Delta\gamma$ as γ gets even larger, convergence will fail. Striking a balance between these two tendencies is central to a good continuation algorithm.

Algorithm 5.6 Continue $(\mu_0(x), p, p_{min}, p_{max}, \Delta s, \Delta s_{min}, \Delta s_{max}, t_{max})$

Set total number of iterations $t = 1$
Set iteration $i = 1$, which increment by one each step of this algorithm
Set previous number of iterations returned by GridShoot to $n_{prev} = 3$, the normal case
Set prediction $\mu_{i,*} = \mu_* = 0$
Set $\Delta s = |\Delta s|, \Delta\mu_{0,*} = 0$
repeat
  if $t > t_{max}$ **then**
    return FAIL
  end if
  Set $\mu_i = \text{GridShoot}(\mu_{i,*}, m = 7, n_{max} = 25, \varepsilon = 10^{-5})$
  Set n = number of iterations taken by GridShoot, n_{max} on failure
  if $n < n_{max}$ **then**
    Set $\Delta s = \text{AdaptDP}\left(\sqrt{\Delta p^2 + \Delta\mu^2_{i-1,*}}, n, n_{prev}\right)$
    Set $\Delta\mu_{i,*} = \mu_i(-1) - \mu_{i-1}(-1)$
    $j = i$
    $d = 1$
    Update $i = i + 1$
  else
    Assume we stepped to far, adjust p and $\mu_{i,*}$ accordingly and retry i-th iteration
    Set $\Delta s = \frac{\Delta s}{2}$
    $j = i - 1$
    $d = -1$
  end if
  Ensure $\Delta s_{min} \le \Delta s \le \Delta s_{max}$
  Set $\Delta p = \text{sign}\,(\Delta p)\sqrt{\Delta s^2 - \Delta\mu^2_{i,*}}$,
  Set $p = p + d \cdot \Delta p$
  Set prediction $\mu_{j+1,*} = \mu_j(-1) + \text{sign}\,(\Delta\mu_{j,*})\sqrt{\Delta s^2 - \Delta p^2}$
  $t = t + n$
until $p < p_{min}$ or $p > p_{max}$

Chapter 6

Conclusions

In Chapter 2, we derived the equations of motion describing a thin, infinite plate conducting current along its length. One of the more interesting characteristics of these equations is the non-local nature of the body forces caused by a feedback between the electromagnetic field and the body itself as it deforms. These non-local terms are expressed as an integral operator on the solution function, while the basic dynamics are expressed as a PDE, as is typical in elasticity theory. Our focus is on the bifurcation and buckling behavior of the system, so that we ignored dynamical behavior in favor of searching for and characterizing the static equilibrium solutions. The equations in this case reduce to an integro-differential equation that we analyzed first without current (in Chapter 3) and then with the current turned on (in Chapter 4).

In all, our goal was to take a relatively complex problem in elasticity theory and form a realistic but simple model that would shed light on the bifurcation and buckling behavior resulting from the electromagnetic-field induced self-forces. We were able to show that an applied current can indeed produce multiple static equilibrium solutions and that the bifurcation structure predicted by Moon does indeed exists. Furthermore, we were able to exhibit how the resulting buckled shapes resulted from compressive body forces, confirming the intuitive notion of the attractive force between parallel extents of conducting material.

In the process of solving this problem, we developed a numerical solver for integro-differential boundary value problems. Although not completely generic, the ideas and code developed for this purposes could be applied to other similar problems without great effort.

Although the main goals of the research were fulfilled, there are never-the-less several points that could be improved upon. In particular, although the numerical code works and produced verifiable results, a more thorough theoretical treatment of the convergence behavior and optimization

of the overall algorithm would greatly increase the scope and breadth of any future work.

Besides improvements to the numerical code, there are further questions that follow immediately from this research. These include:

1. Are there odd μ solutions that can be found to satify the BVP? In this case, as discussed in the Chapter 4, there are additional constraints that need to be satisfied during the shooting process, which makes the convergence much more difficult. In particular, in the case when $\gamma > 0$, we already have to shoot for two quantities, $\mu(1) = \mu(-1)$ and $\mu_x(1) = 0$, and adding a third requires much more attention to be paid to what amounts to a very delicate optimization problem.

2. For the purposes of this thesis, it was sufficient to confirm the existence of branches bifurcating from both the trivial and "inverted circular" solutions, as it proves the notion that there are multiple buckled shapes for a given γ. However, probing larger values of γ would be very interesting to see if there are unexpected changes to the solutions for extreme γ.

3. Further work on the stability of the trivial solution is warranted, and would allow for a more careful description of the conditions under which buckling would occur.

4. Another avenue that could be pursued would be a relaxation of the assumptions in the context of more realistic application. It would be interesting to apply the basic ideas and techniques developed here to a "real" problem in an engineering setting. I can think of many problems to pursue, but this might first be as simple as running Moon's original experiment that conducted current along a thin sheet of aluminum foil in order to calibrate and verify the basic model in that context. Given success here, one could generalize the problem with respect to the geometry (a curved sheet, for example) and try to develop and apply a more general model to a less controlled situation, such as what might occur in a lightning strike to an airplane or an industrial structure.

Bibliography

[1] Stuart S. Antman, *Nonlinear Problems of Elasticity, Second Edition*, Springer Series in Applied Mathematical Sciences, v. 107, 2005.

[2] Chattopadhyay, S., and Moon, F. C. (1975). "Magnetoelastic buckling and Vibration of Rod Carrying Electric Current," J. Appl. Mech. 42, 809-914.

[3] Dolbin, N. I., and Morozov, A. I., *Elastic Bending Vibrations of a Rod Carrying Electric Current*, Zhurnal Prikladnoi Mekhaniki and Technicheskoi Fiziki (in translation), No. 3, 1966, pp. 97-103.

[4] Jerrold Franklin, *Classical Electromagnetism*, Pearson Education, Inc., 2005.

[5] Keith D. Hjelmstad, *Fundamentals of Structural Mechanics*, Second Edition, Springer Science + Business Media, LLC, 2005.

[6] Davresh J. Hasanyan, Liviu Librescu, Damodar R. Ambur, "Buckling and postbuckling of magnetoelastic flat plates carrying an electric current", International Journal of Solids and Structures **43**, 2006, 4971-4996.

[7] Keith D. Hjelmstad, *Fundamentals of Structural Mechanics*, Springer Science & Business Media, LLC, New York, 2005.

[8] H. B. Keller, "Numerical Solution of Bifurcation and Nonlinear Eigenvalue Problems", in "Applications of Bifurcation Theory", P. Rabinowitz ed., Academic Press, 1977.

[9] Leontovich, M.A., and Shafranov, V. D., *The Stability of a Flexible Conductor in a magnetic Field*, Plasma Physics and the Problem of Controlled Thermonuclear Reactions, Vol. 1, Pergamon Press, 1961.

[10] Francis C. Moon, *Magneto-Solid Mechanics*, John Wiley & Sons, New York, 1984.

[11] Robert C. Rogers, "Derivations of linear beam equations using nonlinear continuum mechanics", ZAMP **44**, 1993, 732-754.

[12] Michael Renardy, Robert C. Rogers, *An Introduction to Partial Differential Equations*, Second Edition, Springer-Verlag New York, Inc.,2004.

[13] Stephen P. Timoshenko and James M. Gere, *Theory of Elastic Stability*, Second Edition, Dover Publications, Mineola New York, reproduction of original 1961 edition.